BUREAU OF METEOROLOGY
Department of the Environment,
Sport and Territories

Meteorological Study No. 41

Downslope winds

Warwick Grace

April 1995

BUREAU OF METEOROLOGY
Department of the Environment,
Sport and Territories

Meteorological Study No. 41

Downslope winds

Warwick Grace

Australian Government Publishing Service
Canberra 1995

A thesis submitted to the School of Earth Sciences
of The Flinders University of South Australia
for the degree of Doctor of Philosophy.

Presented March 1992
Accepted July 1992

© Commonwealth of Australia 1995
ISBN 0 644 33417 7

This work is copyright. Apart from any use as permitted under the *Copyright Act 1968*, no part may be reproduced by any process without prior written permission from the Australian Government Publishing Service. Requests and inquiries concerning reproduction and rights should be directed to the Manager, Commonwealth Information Services, Australian Government Publishing Service, GPO Box 84, Canberra ACT 2601.

ACKNOWLEDGEMENTS

Many people have helped me during this study. I sincerely thank all. Dr Roly Byron-Scott of Flinders University provided encouragement, faith and advice of a mathematical, meteorological and general nature; and simply did all the things that a model supervisor would do. Colleagues at the Bureau of Meteorology and at the University's Earth Sciences School gave me moral, material and logistic support, and accommodated (usually cheerfully!) many impositions.

A lot of people generously gave personal time and energy in reviewing allied material, in gathering and presenting archived and real time data, in helping overcome computer problems, in doing extra observations, in word processing, in graphics, in drafting, and in general and specific meteorological discussions, and in many practical ways. I am lucky to be part of such a responsive network.

Some of these people were:– Dave Willes, Peter Webb, Andrew Watson, Tony Vaughan, Graeme Tepper, Peter Strickland, Dr Yaping Shao, Prof Peter Schwerdtfeger, Bob Schahinger, Brian Rowe, Andrew Porter, Bill Plant, Dr William Physick, Rick Millard, Peter Merchant, Jess McMahon, Bob Manson, Dr Peter Manins, Assoc Prof Tom Lyons, Judy Laing, Prof Helmut Kraus, Kris Kentwell, Ian Holton, Dr Jörg Hartmann, Dr Jörg Hacker, Dr Adrian Gordon, Richard Geytenbeek, Graeme Furler, John French, Kerrie Feirclough, Dr Rod Dingle, Hank Dewit, Phil Davill, Alan Cusworth, Beth Curran, Graham Crooks, Graham Cowan, John Corbett, Bett Charlesworth, Michelle Carrington, Roscoe Calver, Kevin Burrows, Jill and Paul Brooking, Alan Blakers, Peter Blake, Peter Betts, Ian Berechree, Dr John Bennett, Mark Bedson, Alan Beatty, Dr Lutz Bannehr, Nick Ball, Dr Peter Baines, and John Armstrong. Of special note were the discussions with Ian Holton and the programming assistance of Hank de Wit and Bob Schahinger. Discussions with other friends and colleagues were also valuable.

And mostly I thank Karen Grace, my wife, who quietly suggested I think about starting... ... and several years later, strongly suggested I think about finishing. Karen and Amanda, Damon and Adam became a single parent family for great lengths of time. Now it's about time that I rejoined them.

For the final three years I was in receipt of a Flinders University post graduate scholarship which pays the candidate's HECS fees. The Bureau, being a Commonwealth public service organization, has generous study leave provisions of up to five hours a week for approved coursework: I was significantly advantaged by these arrangements.

CONTENTS

Page

ACKNOWLEDGEMENTS iii

DECLARATION xi

SYMBOLS AND ABBREVIATIONS xiii

ABSTRACT xv

1. INTRODUCTION 1
   - 1.1 General 1
   - 1.2 The Adelaide gully-wind 3
   - 1.3 Philosophy of approach 5
   - 1.4 Outline of paper 6

2. THEORY AND CURRENT MODELS 7
   - 2.1 Background: wave theory 7
   - 2.2 Laboratory models 10
   - 2.3 Hydraulic mechanism 10
   - 2.4 Lee wave amplification – Klemp and Lilly 10
   - 2.5 Lee wave amplification – Peltier and Clark 11
   - 2.6 Smith's model 12
   - 2.7 The model of Baines and Granek 13

3. OBSERVATIONS OF ADELAIDE GULLY-WINDS 14
   - 3.1 General 14
   - 3.2 The case study of 6/7 February 1985 18
   - 3.3 The case study of 25/26 February 1991 18
   - 3.4 The case study of 6/7 February 1972 19
   - 3.5 Field observations 23
     - 3.5.1 Outline of measurements 23
     - 3.5.2 Analysis of study nights A and B 23
   - 3.6 The definition, description and use of ΔT 29
   - 3.7 Observations of a hydraulic jump in a fog bank 30

4. A QUASI $1^1/_2$-LAYER MODEL (Q$1^1/_2$) 32
   - 4.1 Development 32
     - 4.1.1 Assumptions and nomenclature 32
     - 4.1.2 Altitude of the splitting streamline 33
     - 4.1.3 Critical mountain height 34
     - 4.1.4 Leeward velocity 35
     - 4.1.5 The jump 37
     - 4.1.6 Wave drag 39

Page

4.2 Comparison with Smith's model 41
4.3 Topographic effects 42
4.4 Critical-layer effects 45
    4.4.1 Development 45
    4.4.2 Results 45
    4.4.3 Comparison with Durran & Klemps's numerical results 48
4.5 Summary 48

5. A MODEL OF GUST PERIODICITY 50
5.1 Background 50
5.2 Development 50
5.3 Results and discussion 52

6. THE TIME-DEPENDENT $1^1/_2$-LAYER MODEL (QT) 53
6.1 Background 53
6.2 Development 53
6.3 Comparison with other models 57
6.4 Simulations using the QT model 57
    6.4.1 Balanced synoptic flow – (Type I) 58
    6.4.2 Inertially unbalanced flow – (Type II) 62
6.5 Summary 67

7. DISCUSSION AND CONCLUSIONS 68
7.1 Hydraulics versus waves 68
7.2 Utility of the steady-state ($Q1^1/_2$) model 68
7.3 Utility of the time-dependent (QT) model 69

8. FINAL REMARKS AND FUTURE DIRECTIONS 71

REFERENCES 72

APPENDICES

Appendix

A Derivation of transitional flow conditions 76
B Derivation of steady-state jump conditions 79
C Derivation of steady-state mountain drag 81

FIGURES

Figure		Page
1	Comparison of isentropic 'streamlines' for; (a) bora (right-left flow), (b) chinook (left-right) and (c) Perth downslope winds (right-left). From Smith 1987, Brinkmann 1974, Pitts and Lyons 1989, respectively.	2
2	Composited upwind and downwind soundings for chinook windstorm events (after Brinkmann 1974).	3
3	Map of South Australia.	4
4	Map of Mount Lofty Ranges.	5
5	Map of Adelaide and surrounds.	6
6	Steady-state streamlines for stratified flow over a 'Witch of Agnesi' obstacle with $H = 500\ m$, $a = 3\ km$, $N_0 = 0.01\ s^{-1}$, and $u_0 = 5\ m/s$ (from Laprise and Peltier 1989a): (a) a linear solution, (b) a nonlinear solution, (c) a nonlinear and nonhydrostatic solution and (d) a nonlinear and nonhydrostatic solution with $a = 1\ km$.	9
7	Analogue of hydraulic flow as suggested by Küttner.	11
8	Schematic diagram of the splitting-streamline concept of S85.	12
9	Mean wind at Highbury (near Wattle Park) in January and February 1980 on a diurnal basis for west to southwesterly streams and for east to southeasterly streams (after Marsh 1987).	14
10	Mean sea level pressure chart for 0900 CSST 13 February 1980: typical for strong gully-winds.	15
11	Surface synoptic chart for 0900 CSST 7 February 1985.	15
12	Synoptic charts for 0900 CSST 7 February 1985 for; (a) gradient, (b) 850 *hPa*, (c) 7000 *feet*, (d) 700 *hPa*, (e) 14 000 *feet*, (f) 500 *hPa*.	16
13	Temperature profiles for Adelaide Airport and Mount Gambier at 0900 CSST on 7 February 1985. ML denotes Mount Lofty summit.	17
14	Charts for 0900 CSST 26 February 1991: (a) gradient level and (b) mean sea level pressure chart.	19
15	Temperature profiles for Adelaide Airport and Mount Gambier at 0900 CSST on 26 February 1991. When used in conjunction with Fig. 14, these show that there is a shallow layer of cool air crossing the ranges from the east to southeast.	20
16	Mean sea level pressure chart for 2100 CSST 6 February 1972.	20
17	Acoustic-sounding record of turbulent-layer depth, the vertical velocity at 100 *m* and the 100 *m*-layer mean wind for the period 2200 CSST on 6 February to 0200 CSST 7 February 1972 at Salisbury, South Australia.	21

Figures (continued)

Figure Page

18 Vertical temperature profile for 2100 CSST 6 February 1972 at Adelaide Airport. 21

19 Mean sea level pressure charts for 0900 CSST on; (a) 3 February 1988 and (b) 4 February 1988. There is weak gradient flow for (a) but a shallow cool-air intrusion occurs in the wake of the (dotted) trough in (b). 22

20 Three-hourly isentropic cross-sections (using virtual potential temperatures in °C) for night of 2/3 February 1988 along the true bearing 110°–290° through Mount Lofty. Faint lines show aircraft tracks and balloon trajectories. Offset winds are for Adelaide Airport (left) and Nairne (right). 24

21 As for Fig. 20 but for specific humidity in *gm/kgm*. 25

22 As for Fig. 20 but for the night of 3/4 February 1988. 26

23 As for Fig. 22 but for specific humidity in *gm/kgm*. 27

24 Three-hourly temperature profiles at Nairne (solid) and Adelaide Airport (broken) on the nights of the 2/3 and 3/4 February 1988 (identified as nights A and B, respectively). At 2330 CSST on the second night a sounding was completed at the crest of the ranges. The superadiabatic layers on the B3 profile have been double checked and therefore appear to be real. 28

25 Average ΔT as a function of Adelaide Airport wind direction at 736 *m*, above MSL (after Marsh 1987). 29

26 Scatterplot matrix of peak gust at Port Stanvac (between 1000 and 1200 CSST), ΔT and geostrophic wind speed at 1100 CSST. 30

27 Photographs (looking west out over Backstairs Passage) of hydraulic jump in fog bank on 2 May 1988 in Backstairs Passage, South Australia. Top sequence taken at 1420 CSST; lower one taken at about 1530. See Grace (1991) for further details. (Photographs courtesy of Mr Richard Geytenbeek) 31

28 Steady 2D flow over a mountain with upstream static stability N_0, and velocity, u_0. The streamline initially at altitude d_0 splits, so that above d_0 the flow is unchanged. Below the lower split streamline the flow is essentially hydraulic, and between the split streamlines the air is well-mixed and turbulent but with no mean motion. Stability and speed of the layer beneath the lower split streamline (θ_0) are constant with height. 32

29 Graphical solution of Eqn 18 showing $\hat{d}_0$ and higher order solutions as a function of $\hat{H}$. Also shown is the ratio d_0/H for $n = 1$. 35

30 Plots of $\hat{d}_0$, $\hat{d}_1$, $\hat{d}_2$, $\hat{d}_P$, $\hat{d}_{0s}$ and $\hat{d}_{1s}$ against $\hat{H}$. 36

31 Plots of jump strength β, wind-speed amplification $\hat{s}$ and turbulence intensity $\hat{j}$ against $\hat{H}$. 37

Figures (continued)

Figure Page

32 Nondimensional drag, $\hat{r}$, for S85 (labelled S), Q1½ model (labelled Q) and linear waves compared as functions of $\hat{H}$ with spot values from numerical experiments by Durran and Klemp (1987) (triangles) and Bacmeister and Pierrehumbert (1988) (circles). 40

33 Model solutions of $\hat{d}_0$ for Q1½ and S85/SS87 as a function of $\hat{H}^{-1}$ with spot values from tank experiments (unfilled circles) and numerical experiments (filled). The spot values and S85/SS87 curve are from Rottman and Smith (1989). 40

34 The defining sketch for *M*. The topography has been modified in such a way that the lee plains are lower than the windward ones. 42

35 Plots of (a) jump strength, β, (b) wind-speed amplification $\hat{s}$ and (c) turbulence intensity $\hat{j}$ against $\hat{H}$ for various values of *M*. 43

36 Plan view of a string of conical hills 'melded' together. Heavy solid lines are contours and dashed lines represent streamlines. Flow along VV represents flow through a valley while SS represents flow along the highest path or spur line. 44

37 Plots of (a) jump strength, β, (b) wind-speed amplification $\hat{s}$ and (c) turbulence intensity $\hat{j}$ against $\hat{H}$ for various values of γ. 46

38 Adaptation of the diagram of Houghton and Kasahara (1968) for transitional and nontransitional flow regimes to the Q1½ model. 47

39 Comparison of the results of Durran and Klemp (1987) for high drag (filled circles) and low drag (hollow circles) events with Q1½ predictions. 47

40 Plot of dual periods in minutes against H/u_0 and N_0. 52

Figures 41 to 49 – evolution of Type I flow with 'Witch of Agnesi' topography given by $H = 500\ m$, $a = 3\ km$, $b = 15\ km$, and preconditions of $u_0 = 10\ m/s$, $v_0 = 0\ m/s$, $d_0 = 1500\ m$, $g' = 0.2\ m/s^2$, $f = -83 \times 10^{-6} s^{-1}$, $C_D = 0.002$ and $E = 0.0$ unless noted otherwise.

41 The case $f = 0\ s^{-1}$, $C_D = 0$, in which transitional flow and downslope winds eventuate. 59

42 The case in which $C_D = 0$ but $f = -83 \times 10^{-6}\ s^{-1}$. In this, the leeward jump is further leeward but the upstream jump is weakened and retarded. 60

43 The 'reference' preconditions for Type I flow. 60

44 Non-transitional flow for the reference conditions except that $u = 5\ m/s$. 61

45 Non-transitional flow for the reference conditions except that $d_0 = 2000\ m$. 61

46 Flow results for the reference conditions except that $g' = 0.1\ m/s^2$. Note that the supercritical flow is more extensive than before, although maximum speeds are decreased. 63

Figures (continued)

Figure Page

47 Flow results for the reference conditions except that $g' = 0.3\ m/s^2$. Note that the transitional flow is much less extensive, although maximum speeds are increased. This is equivalent to very strong gully-winds about the foothills with much weaker winds a few kilometres downstream. 63

48 Flow results for the reference conditions except that C_D over the hills region is increased to 0.01 (though C_D over the plains is held at 0.002). Note that the leeward jump is held back. 64

49 Flow results for the reference conditions except that C_D over the hills region is increased to 0.005 (while C_D over the plains is held at 0.001). Note that the leeward jump is held back, but less so than in Fig. 48. 64

50 Type II flow with initial conditions of a southerly of 8 m/s, $d_0 = 400\ m$, $g' = 0.1\ m/s^2$ and $C_D = 0.002$. Note that this type of flow is associated with a sea-breeze from the Coorong area. 65

51 Type II flow under the same conditions as for Fig. 50, except that $v_0 = -4\ m/s$. 66

52 Type II flow under the same conditions as for Fig. 51, except that $E = 0.001$. 66

A1 Schematic diagram of transitional flow over an obstacle. 76

B1 Schematic diagram of an idealised hydraulic jump. 79

C1 Schematic diagram of homogeneous fluid crossing a two-dimensional obstacle. 81

DECLARATION

I certify that this thesis does not incorporate without acknowledgment any material previously submitted for a degree or diploma in any university; and that to the best of my knowledge and belief it does not contain any material previously published or written by another person except where due reference is made in the text.

WARWICK GRACE

SYMBOLS AND ABBREVIATIONS

^	denotes non-dimensionalised value
α	leeward position where $h = 0$
β	jump strength
Υ	measure of valley constriction
ΔT	temperature difference
ε	amount of perturbation
θ	potential temperature
κ	numerical diffusion coefficient
λ	numerical space-time grid ratio
μ	m times $u = udu$; a momentum flux
ρ	density
ϕ	n times $u = vdu$; a momentum flux
a,b	mountain half-widths
BP	Bacmeister and Pierrehumbert (1988)
c	horizontal gravity-wave speed
C_D	coefficient of surface friction
CST	Central Standard Time (= UTC + $9^1/_2$ hours)
CSST	Central Standard Summer Time (= UTC + $10^1/_2$ hours)
d	layer depth
DK	Durran and Klemp (1987)
e	energy loss at jump
E	coefficient of interfacial drag
F	Froude number
f	frequency, Coriolis force
g	gravity
g'	modified gravity
h	topographic height
H	mountain height (maximum)
HK	Houghton and Kasahara (1968)
j	turbulence intensity
m	cross-range flux (ud)
M	height difference of plains compared to H
MF	momentum flux

n	along range flux (vd), dummy index
N	Brunt-Väisälä frequency
p	pressure
P	period
PC	Peltier and Clark (1977) and subsequent papers
PF	pressure force
m	mass flux, specific humidity
$\mathrm{Q}1^1/_2$	steady-state quasi $1^1/_2$-layer model
QT	time-dependent version of $\mathrm{Q}1^1/_2$ model
r	mountain-wave drag
$\hat{s}$	ratio of windward to leeward wind
S85	Smith (1985)
SS87	Smith and Sun (1987)
T	temperature
u	cross-range wind speed
v	along-range wind speed
l	N/u
l_s	Scorer parameter

Subscripts

0	upstream, upper
1	before jump
2	after jump
A	aloft
c	crest
S	S85, or Scorer
T	threshold or transition

ABSTRACT

Downslope winds occur in the lee of all mountain ranges. Those occurring over the western flank of the Mount Lofty Ranges of South Australia are known locally, but slightly misleadingly, as gully-winds. Case and field analyses of several gully-wind events are presented. Within the framework of hydraulic theory, downslope winds and, in particular, the Adelaide gully-wind are investigated and modelled. A steady-state model for continuously stratified flow perturbed by an obstacle is developed and compared with other models. Comparison with the results of numerical model and tank experiments shows good agreement. A useful result of this steady-state model is that it is apparently reasonable to approximate a continuously stratified layer by an equivalent homogeneous layer.

With this approximation, and with some findings from the field and case events as to the scale depth of the gully-winds, the time-dependent shallow-water equations are used to model two proposed archetypes of Adelaide gully-wind situation: a Type I, where a synoptic stream is perturbed by topography; Type II, where a density current flowing initially parallel to a mountain range is subject to inertial forcing. A surprising feature of Type II is that Coriolis turning is sufficient to force the density current to spill over the range as a supercritical leeslope flow. Surface drag is found to be important. Results of Type I and II simulations compare favourably with case studies compiled from synoptic data, with field studies and with sophisticated numerical models.

Using the results of the steady-state model, a resonance mechanism for gustiness is proposed and developed. The susceptibility of supercritical (single-layer) flow to perturbations is investigated and it is shown that supercritical flow would tend to jump near the lee foot. It is concluded the relatively simple hydraulic theory developed herein can explain most of the features of the Adelaide gully-wind.

The time-dependent model has been developed for operational use in a forecasting office. Rigorous and objective testing is precluded because of inadequate upstream observations and continuously changing synoptic features. Nevertheless, predictions tend to be consistent with forecasters' subjective assessments. The software package is included with the thesis. Three published papers (one co-authored) are also presented as part of this thesis.

CHAPTER 1

INTRODUCTION

1.1 General

Downslope winds occur in the lee of mountains all over the world. Well-known downslope winds include the Föhn of Alpine Europe, the Mistral of the northern Mediterranean coast, the bora of Yugoslavia, the chinook of North America and the zonda of Argentina. Less widely known are the Norwegian fallwind (Humphreys 1929), the helm wind of the British Pennines (Manley 1945), the strong 'katabatics' off the coastal iceshelves of Antarctica and Greenland (Ball 1956) and those down the eastern flank of the Western Cordillera of Colombia (Lopez and Howell 1967), the hiroto-kaze of Japan (Suzuki and Yabuki 1956), the chinook arch of the Canadian Rockies (Ash 1987), the scarp wind of Perth (Van Burgel 1986; Pitts and Lyons 1989,1990) and the Adelaide gully-wind (Bureau of Meteorology 1971; Holton 1985; Marsh 1987; Grace and Holton 1988,1990). One of the most spectacular and most studied downslope winds is that of Boulder, Colorado (e.g. Colson 1954; Lilly and Zipser 1972; Brinkman 1974; Klemp and Lilly 1975; Peltier and Clark 1979; Bower and Durran 1986; Durran 1986).

In some locations, downslope winds may gust to more than 50 *m/s*, creating a hazard to aviation in particular and damage to buildings and trees. The bora has even overturned streetcars in Trieste! In one famous incident, the hangar of the research aircraft, that was on a sortie studying the chinook, was severely damaged (Lilly and Zipser 1972)! Typical, but not universal, features of such winds are a night-time speed enhancement, sudden onset, a threshold speed to windward (Nicholls 1973; Brown 1986), marked variability in strength but not in direction, and a stable layer or inversion near or just above hilltop level (Atkinson 1981). Generally the cross section of the mountain range is ramp shaped – that is, gently sloping to windward with a much steeper slope to leeward.

Much investigative effort has gone into compiling a quantitative description of downslope winds. Although the bora is famous as a cold wind and the chinook as a relatively warm wind, the mechanism for each is probably the same and the relative warmth of the chinook is due to the displacement of a very cold shallow layer over the lee plains. There are also many counter-examples of warm bora and cold chinooks. Boras and chinooks have been known to contain gusts as high as 50–60 *m/s*. Downslope winds are usually more pronounced at night. Typically they are very gusty yet very steady in direction. For climatologies of chinooks and boras see Brinkmann (1974) and Yoshino (1976).

Isentropic cross-sections from a bora (Smith 1987), a chinook (Brinkmann 1974) and Perth's downslope wind (Pitts and Lyons 1989) are compared in Fig. 1. (In passing, note that Smith (1987) provides a series of magnificent colour photographs of bora effects). All three, and many others in the literature, have in common a single large amplitude (forced) wave with or without secondary lee waves further downstream. Turbulence and vertical motion are most pronounced in association with the large trough. Most of the 'action' is within the lowest 2–3 *km*, although this is not always so: Lilly and Zipser's (1972) famous example, featured in many text books, shows that the whole tropopause descended to within about 2 *km* of the leeside surface.

Brinkmann (1974) composited upwind and downwind soundings associated with Boulder chinook windstorms and the results are shown in Fig. 2. Referring to the latter, it can be seen that

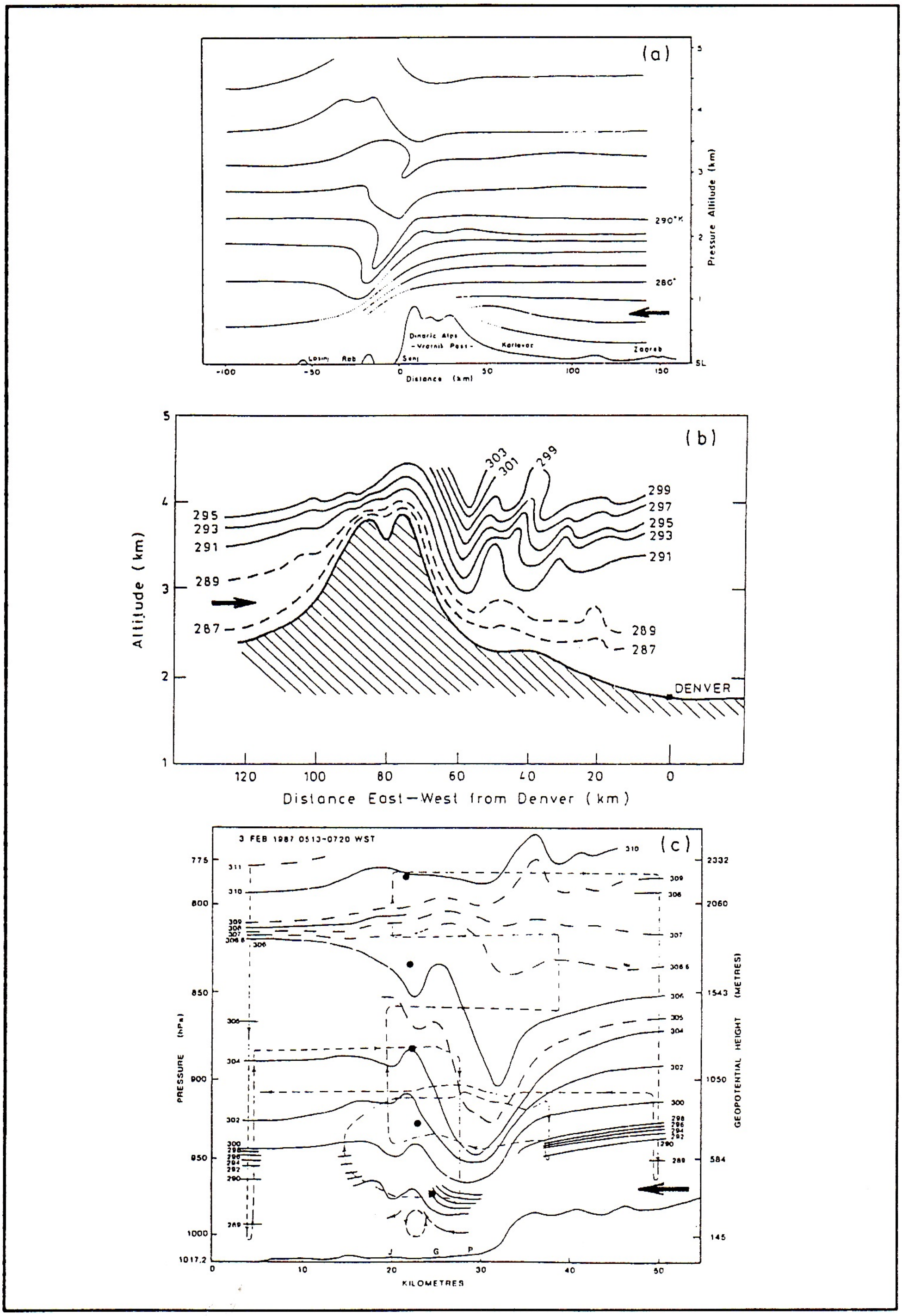

Fig. 1 Comparison of isentropic 'streamlines' for; (a) bora (right-left flow), (b) chinook (left-right) and (c) Perth downslope winds (right-left). From Smith 1987, Brinkmann 1974, Pitts and Lyons 1989, respectively.

the inversion is consistently lower to leeward. For the bora, it is known that a windward inversion occurs somewhere between 1500 and 2000 *m* (AMSL), whereas to leeward the inversion is usually some 500 to 100 *m* lower (Yoshimura 1976). This is very similar to Suzuki and Yabuki's (1956) findings for a hiroto-kaze (a downslope wind event accentuated by valley effects). They presented a transect of soundings for five stations, showing a pronounced inversion decreasing from an altitude of 3000 *m* on the windward side to 1600 *m* on the leeward side of the ranges.

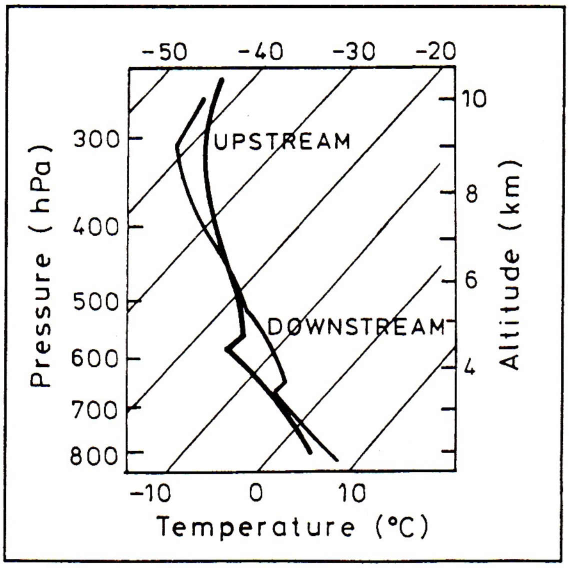

Fig. 2 Composited upwind and downwind soundings for chinook windstorm events (after Brinkmann 1974).

1.2 The Adelaide gully-wind

The Mount Lofty Ranges of South Australia have a ramp shape with respect to easterly flow. These ranges extend northeastward from Cape Jervis to Myponga, then approximately northwards on past Adelaide. The ranges are 40 to 50 *km* wide with the highest point being Mount Lofty itself which is 736 *m* AMSL. The average height of the ridge is about 500 *m*, however. To the east, the countryside is generally flat and open and about 100 *m* AMSL; to the west, the land falls steeply over a horizontal distance of 3 to 5 *km*, but then slopes gently across a coastal plain of varying width. (Figures 3, 4 and 5 show locations and topography.) Further north, the northern Flinders Ranges have a ramp shape to westerly flow.

Easterly downslope winds commonly occur on the western flank of the Mount Lofty Ranges and often extend several kilometres further westward. It is possible that, on occasion, they blow right across Gulf St Vincent although this conjecture is based on undocumented evidence from local fishermen. In the Adelaide region, these winds are known as gully-winds and a common observation is of moderate easterly winds at the mountain top with strong gusty easterly winds about the lee foothills, while a few kilometres further downstream the wind is light and may even be weakly reversed. Frequently the wind above 1500–2000 *m* on a synoptic scale is westerly. In extreme cases trees have been uprooted and houses damaged.

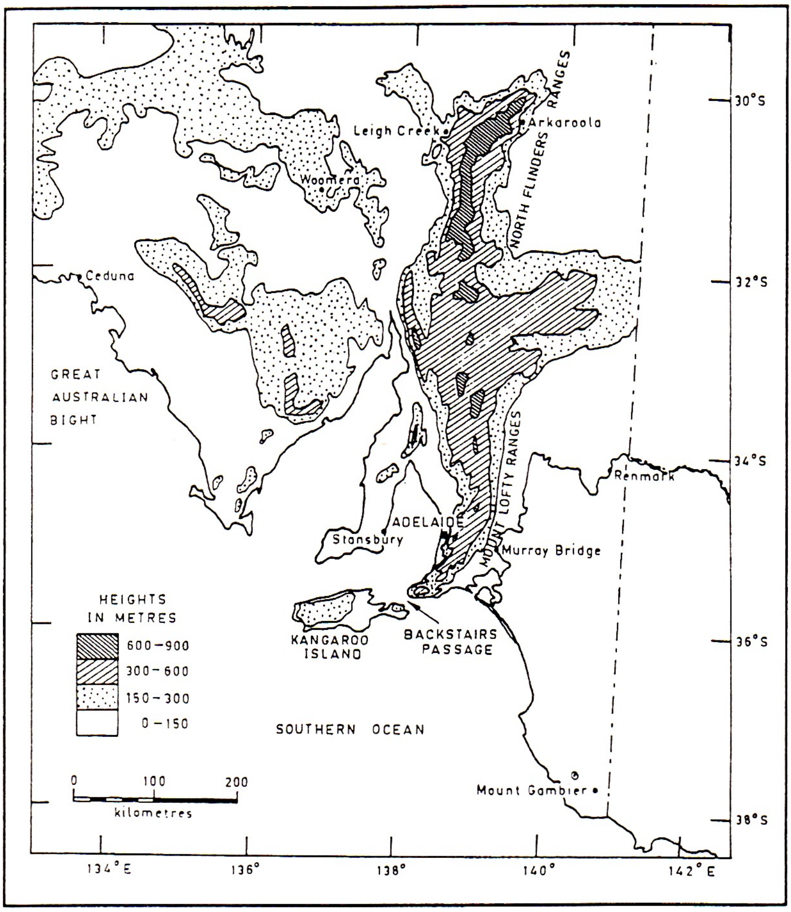

Fig. 3 Map of South Australia.

The winds may seriously hamper fire-fighting operations in the Mount Lofty Ranges. Marsh (1987) reported a gust of 30 *m/s* at a wind energy monitoring site at Myponga Beach which is located about 40 *km* south of Adelaide. Holton (1985) documented aircraft reports of turbulence at Adelaide Airport and found that 74 per cent of all reports rated as severe occurred during gully-wind events. Major errors (> 5°C) in summertime minimum temperature forecasts for Adelaide are mainly attributed to the unpredictable nature of the gully-winds (Furler private communication). Late last century, during the era of Adelaide's horse-drawn trams, extra horses were required for trams travelling from Parkside (a suburb on the southern edge of the Adelaide city centre) to Glen Osmond into the face of strong gully-winds (Kingsborough 1967). Typically, they occur if the synoptic stream is a stable and vigorous east to southeasterly. These conditions correspond well with the pre-conditions generally accepted for forecasting large-amplitude mountain waves. Durran (1986a) lists these as being stability at lower levels, wind speed of at least 7 *m/s* (for mountains of 1 *km*) and asymmetric mountains with gentle windward and steep leeward slopes.

The Adelaide region downslope winds are more pronounced in gully sites, hence the local term 'gully-wind'. On occasion, despite apparently favourable pre-conditions, downslope winds in the lee of the highest part of the ranges around Mount Lofty are weak or non-existent, yet 10 to

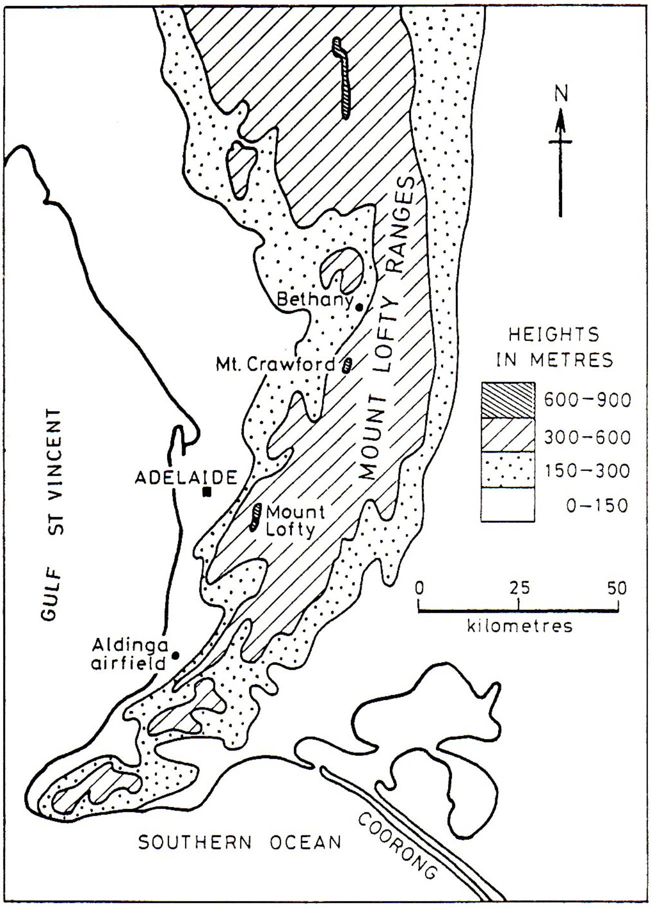

Fig. 4 Map of Mount Lofty Ranges.

50 *km* north or south, where the ranges are about 200 *m* lower, strong downslope winds are observed. Little is documented of downslope winds elsewhere in South Australia: during an environmental impact study (Holmes 1981) in the northern Flinders Ranges, westerly downslope winds of 28 *m/s* (mean) were recorded: this compares to 30 *m/s* for the hangar-damaging chinook incident.

1.3 Philosophy of approach

In keeping with Occam's Razor, this thesis pursues the simplest and least abstract (in the author's opinion) of the postulated mechanisms of downslope winds, and extends it to include more realistic model atmospheres. Extremely simple models have the advantage that if the 'correct' behaviour is observed or obtained then it is likely that the underlying physics has been captured. Most mesoscale models include elaborate parametrisations of physical processes (that is, boundary-layer formulation, boundary conditions, humidity and drag) and highly complex model structure; it is sometimes difficult to distinguish between physical and non-physical aspects of the model results (Hoinka 1985). The particular theory applied here has much in common with

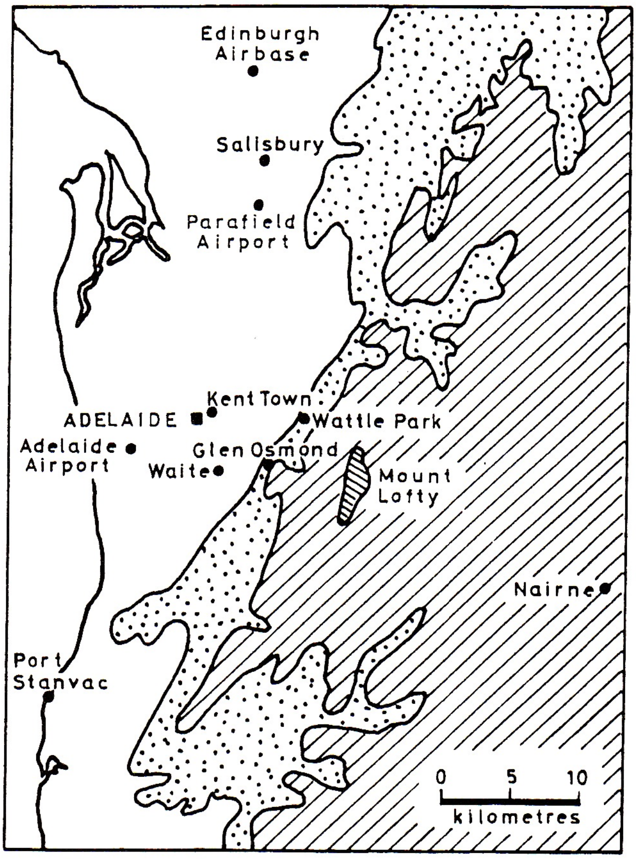

Fig. 5 Map of Adelaide and surrounds

observations of water flow both in the laboratory and in nature and is therefore easily visualised. An associated aim of this work is to produce a workable model on a modest desktop computer for real-time use by operational forecasters.

1.4 Outline of paper

Chapter 2 summarises current models and theories of downslope winds. Chapter 3 presents case and field studies of the Adelaide gully-wind, and shows photographic evidence of a hydraulic jump in a bank of sea fog at the southern end of the Mount Lofty Ranges. Chapter 4 develops a steady-state 'layer-and-a-half' model and compares its results with those of other models in the literature. A possible cause for the quasi-periodic gustiness of downslope winds is presented in Chapter 5. Chapter 6 develops a time-dependent model of downslope winds. Results are compared to available observations. The importance of drag is examined. The discussion of Chapter 7 draws together the literature, the data presented, and the model results. Chapter 8 points to some avenues for further research. Figures 1 to 3 show relevant topography and all South Australian locations as mentioned in the text. Because the Adelaide gully-wind is a markedly diurnal summertime feature it is natural to use CSST (Central Standard Summer Time). CSST = UTC+10½ hours. On one or two occasions Central Standard Time is used, where CST = UTC+9½ hours.

CHAPTER 2

THEORY AND CURRENT MODELS

Although the *mechanism* for downslope winds is still not established (Scorer 1978; Atkinson 1981 and Durran 1986 a,b), it is well-established that their ultimate *cause* is the buoyancy force in conjunction with topography. Currently several different mechanisms are invoked to explain the development of downslope winds. The review contributions of Durran (*ibid.*) are particularly lucid and comprehensive. Corroboration of each of the theories is mainly attempted through the use of numerical models incorporating the fundamental equations and these in turn have been validated against a few well-documented case studies, or the analytic solution of idealised atmospheres, or laboratory tank models. The tank model experiments have also been used to test implications of the postulated mechanisms, as have the available observational data.

2.1 Background: wave theory

The perturbation of incident hydrostatic flow by the gravity waves launched by a ridge was investigated by Queney (1948). Two types of wave are induced by a ridge – a *forced* wave which is collocated with the topography and *lee* waves which propagate downstream (Pielke 1984). Trapped lee waves are, of course, a common sight. Scorer (1949) showed that the lee waves would be well developed if the Scorer parameter, l_s, decreased with height where

$$l_s = \sqrt{\frac{N^2}{u^2} - \frac{1}{u}\frac{\partial^2 u}{\partial z^2}} \tag{1}$$

where N is the Brunt-Väisälä frequency, u is the cross-ridge component of the wind speed and z is altitude. Nevertheless, observational experience (e.g. Vergeiner 1971; Brinkmann 1974; Pitts and Lyons 1989) and numerical simulations (e.g. Hoinka and Rosler 1987) show that the trapped lee waves are not directly relevant to downslope winds. Downslope winds are associated with an amplification of the forced wave. Most of the numerical models used have been hydrostatic but this is not a serious limitation, as they do simulate the forced wave quite well, although they do not properly simulate the trapped lee waves (Pielke 1984).

For a nonhydrostatic regime, Long (1953) showed that if the upstream profiles of stability and speed (N_0 and u_0) are constant with height then the streamline deflection δ satisfies the linear equation (Long's equation)

$$\frac{\partial^2 \delta}{\partial x^2} + \frac{\partial^2 \delta}{\partial z^2} + l^2 \delta = 0 \tag{2}$$

where x is the direction of stream flow and l is a specialised form of Scorer's parameter; namely,

$$l = \frac{N_0}{u_0} \; . \tag{3}$$

If the hydrostatic approximation is made – which is equivalent to assuming that

$$\frac{\partial \delta}{\partial x} \ll \frac{\partial \delta}{\partial z} , \qquad (4)$$

then Eqn 2 becomes

$$\frac{\partial^2 \delta}{\partial z^2} + l^2 \delta = 0 . \qquad (5)$$

This linear perturbation equation has a solution

$$\delta = \bar{h} e^{ilz} \qquad (6)$$

where $\bar{h}$ is a complex function whose real part defines the surface topography, $h(x)$. (That is, $R(\bar{h} = h)$. For a bell-shaped ('Witch of Agnesi')[1] mountain of the form

$$\bar{h} = \frac{H}{1 + \frac{x^2}{a^2}} \qquad (7)$$

with H and a being mountain height and 'half-width' respectively, then the solution is given by

$$\delta = \frac{He^{ilz}}{1 - \frac{ix}{a}} . \qquad (8)$$

The form of Eqn 7 was originally chosen by Queney because it is simple, realistic and has a convenient Fourier integral of the form

$$h = Ha \int_0^{\infty} e^{-ka} \cos(kx)\, dk \qquad (9)$$

where k is wave number. The use of the 'Witch of Agnesi' profile has since become traditional in downslope wind models.

It turns out that for a symmetrical Witch-shaped mountain critical steepening of the streamlines occurs if $lH = 1$ (see Fig. 6(a)). By critical steepening, we mean that streamlines become vertical, on the verge of overturning. The lower boundary condition used is that $\delta = h$ on $z = 0$ (not on $z = h$, the actual surface) and this effectively assumes that the mountain is a 'small' perturbation[2]. This leads to a linear theory, in that the amplitude of the forced wave is linear, and hence the term 'linear' waves. The lower boundary condition is clearly not realistic and results in the lowermost streamlines going through the mountain. Note that the dashed line in Fig. 6(a) represents the ground surface.

---

[1] *In the theory of radiation, this function is sometimes known as the Lorentz function, so it could be described as a 'Lorentz-shape'.*

[2] *This condition is sometimes known as the slender-body approximation in aerodynamics.*

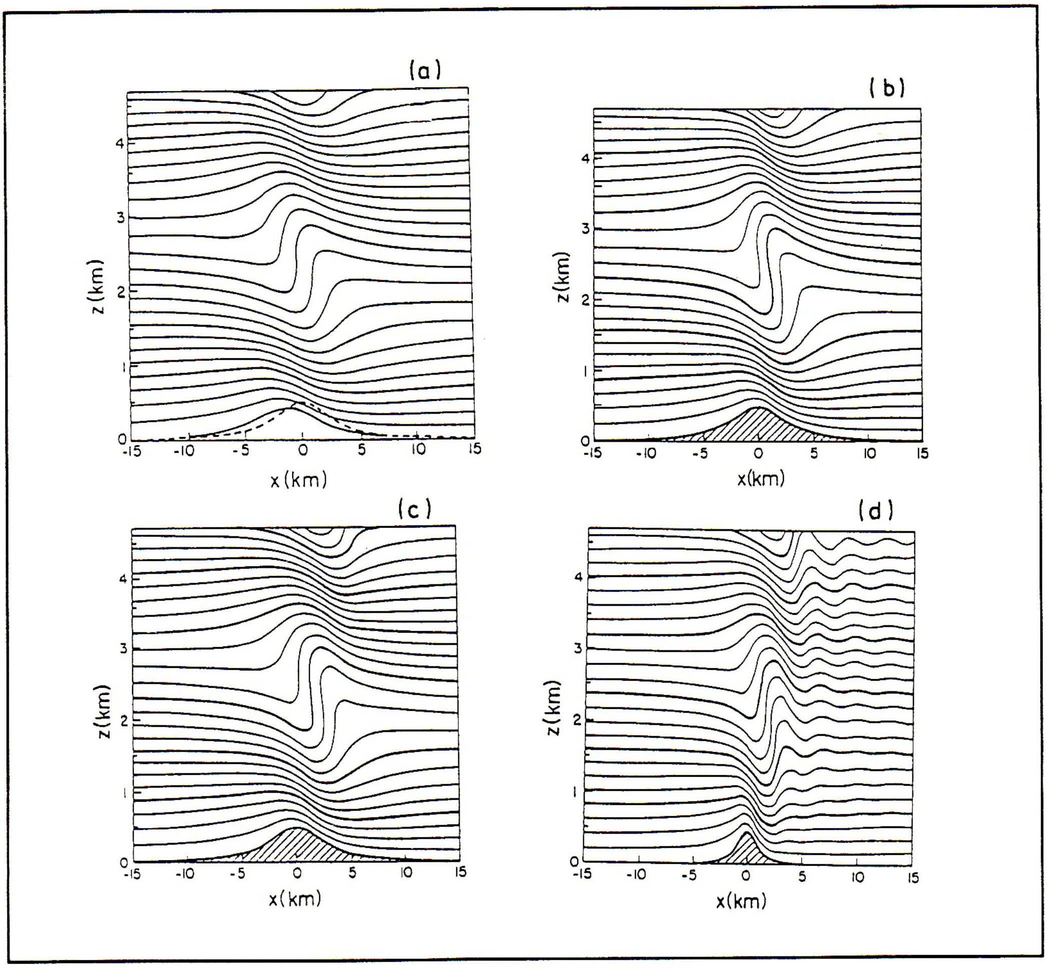

Fig. 6 Steady-state streamlines for stratified flow over a ‘Witch of Agnesi’ obstacle with $H = 500\ m$, $a = 3\ km$, $N_0 = 0.01\ s^{-1}$, and $u_0 = 5\ m/s$ (from Laprise and Peltier 1989a): (a) a linear solution, (b) a nonlinear solution, (c) a nonlinear and nonhydrostatic solution and (d) a nonlinear and nonhydrostatic solution but $a = 1\ km$.

A non-linear theory requires Eq. 5 to be solved subject to the non-linear boundary condition that $\delta = h$ at $z = h$. For detailed discussions of the linear and nonlinear theories, the reader is referred to Gill (1982) or Laprise and Peltier (1989a). In the nonlinear case, critical steepening occurs if $lH = 0.85$ (see Fig. 6(b)). Baines and Granek (1990) have shown that critical steepening occurs for $0.5 < lH < 1$ where the lower (higher) value applies to ramp- (backward ramp-) shaped ‘Witch of Agnesi’ mountains.

In the linear theory, critical steepening first occurs at an altitude of $(n+3/4)$ of a vertical wavelength, where $n = 0,1,2...$, and is directly above the crest. An implication of having the maximum steepening over the crest is that the strongest winds would occur halfway along the lee slope; whereas, in fact, they usually occur near the foot.

In the nonlinear theory, the altitude of maximum steepening remains at about the same height and is displaced downstream (with some dependence on the half-width of the mountain). Laprise and Peltier (1989a) have investigated the nonlinear nonhydrostatic case and the essential features of their solutions compare closely (Fig. 6(c)). For narrower hills, the hydrostatic approximation is coarser and secondary lee waves become more prominent (Fig. 6(d)).

2.2 Laboratory models

These are usually tank models of saline water in which the density decreases linearly with height. A model mountain is towed from a standing start and a camera travelling alongside records the fluid motion made visible by dye streaks or neutrally buoyant polystyrene balls. Experiments with tank models (e.g. Baines and Hoinka 1985; Boyer and Tao 1987; Rottman and Smith 1989) have shown conclusively that the flow is dominated by lee waves for small *Hl* but for larger *Hl* the flow evolves to one of hydraulic character.

The advantages of the tank models are that they show the extreme complexity of the phenomena and they can be used as a check on numerical models directly and to test implications of the mechanisms postulated. A disadvantage is that some effects such as boundary-layer drag may be disproportionately more or less important in the atmosphere. Currently, there are three mechanisms postulated to explain downslope winds.

2.3 Hydraulic mechanism

The first mechanism is often referred to as that of the hydraulic jump (Küttner 1939, 1958; Long 1953, 1954; Ball 1956; Lopez and Howell 1967; Houghton and Kasahara 1968; Arakawa 1968), where an inversion (usually) above ridgetop height is regarded as analogous to the upper surface of a shallow layer of water.

The hydraulic jump model of downslope winds is based on the premise of a transition from subcritical windward flow to supercritical leeward flow which then dissipates its energy within a hydraulic jump. On both windward and leeward sides, the flow accelerates (prior to the jump). Küttner's idea is represented in Fig. 7. This approach has the merit of explicitly accounting for the nonlinearities in the system; however, unlike the atmosphere, all the models considered have an upper boundary consisting of either a free surface or a rigid lid. In this type of model, no upward energy transport can occur across the upper boundary, and so vertically propagating atmospheric waves cannot be properly represented. Because many of the hydraulic models have been limited to homogeneous layers, any comparison of results with waves in a (more realistic) continuously stratified atmosphere must be primarily qualitative. *This thesis seeks to explain much of the associated observations by applying and extending the hydraulic theory.*

2.4 Lee wave amplification – Klemp and Lilly

A second mechanism for downslope winds is based on an extension of Scorer's *linear* lee wave theory by Klemp and Lilly (1975, 1978), who proposed that amplification of lee waves (primarily the forced wave) could be accomplished by the resonant partial reflections of wave energy propagating vertically between the surface and an upper reflecting level, or levels. This mechanism is sometimes referred to as linear lee wave amplification.

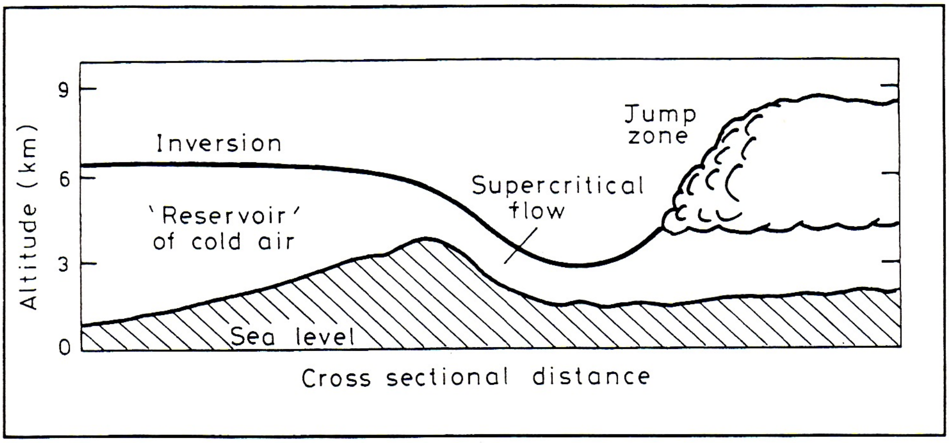

Fig. 7 Analogue of hydraulic flow as suggested by Küttner.

The upper reflection occurs at a discontinuity in l. Strictly speaking, the reflection occurs at discontinuity in Scorer's parameter, l_s, where l_s is given by

$$l_s^2 = \frac{N^2}{u^2} - \frac{\delta^2 u}{u \delta z}. \tag{10}$$

Such a discontinuity is often termed an Environmental Critical-Layer (ECL) which is usually modelled by a wind-shear layer one or two kilometres deep; less commonly, a strong inversion layer is used. The implication is that if the upstream atmosphere is 'tuned' in such a way that, for example, the tropopause is located at an altitude equal to a half wavelength (or some integral multiple thereof) of the internal (vertical) waves, then downslope winds will occur.

However, since this is a linear model, it must be applied with caution to the case of large-amplitude waves, because the perturbation fields associated with these waves are comparable in magnitude to the mean flow. Predictions from linear multilayer models are sometimes rather misleading ((Durran 1986a,b); and Durran and Klemp (1987) and Bacmeister and Pierrehumbert (1988), (hereafter DK and BP respectively)) found little support for this mechanism.

2.5 Lee wave amplification – Peltier and Clark

A third mechanism for the generation of large-amplitude waves has been suggested by Peltier and Clark (Clark and Peltier 1977, 1984; Peltier and Clark 1979; Laprise and Peltier 1989a,b,c). They examined the behaviour of large-amplitude mountain waves with a numerical nonlinear non-hydrostatic model which gave a detailed representation of the atmospheric flow. They observed that a substantial increase in the strength of the wave occurs once the streamlines overturn and the wave 'breaks'. The wave-breaking region is characterised by strong mixing and a local reversal of the horizontal wind. They postulated that the energy in the upward-propagating wave is trapped below this *self-induced critical-layer* (the region where the wind reverses direction), thereby producing large-amplitude waves. This critical-layer developed if the local Richardson number decreased below 0.25.

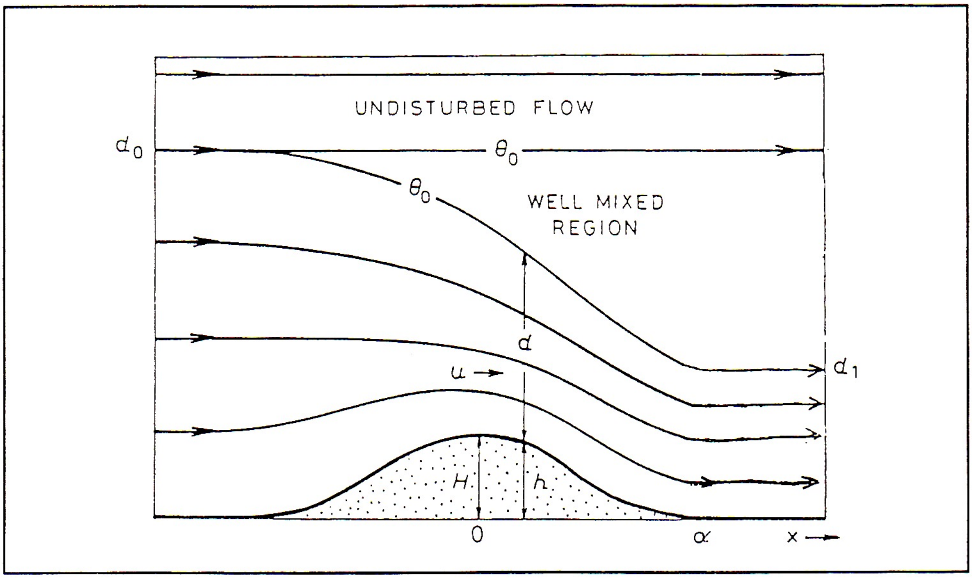

Fig. 8 Schematic diagram of the splitting-streamline concept of S85.

At present, there is still some controversy about the role played by self-induced critical-layers on the subsequent amplification of the wave. An atmosphere 'primed' with an environmental critical-layer at an altitude equal to (n+3/4) of the vertical wavelength should, by this theory, produce downslope winds. Though some numerical and tank experiments support this prediction, many others do not. Smith (1987) has suggested that the data from such experiments support an internal hydraulic mechanism, rather than a mechanism based on vertically propagating waves. However, more recently, Laprise and Peltier (1989a,b,c) have concluded that the 'linear instability of the nonlinear wave field' explains the transition of the flow to one with large amplitude waves.

2.6 Smith's model

In a landmark paper, Smith (1985), (hereafter S85), and subsequently Smith and Sun (1987), (hereafter SS87), noted that the atmosphere above large amplitude waves remains relatively undisturbed and used this idea to extend Long's model to *continuously stratified* fluid. On the assumption that there exists a decoupling of the low-level accelerated flow (termed the hydraulically active layer by him) S85 developed a steady-state model in which the wave energy is trapped within the low-level flow (Fig. 8). The height of the initial decoupling, ld_0, is dependent on the non-dimensional mountain height lH.

Numerical experiments by DK and BP showed that in the presence of an environmental critical-layer near or below Smith's d_0, lee-wave amplification occurred, and the overall flow was remarkably similar to hydraulic flow. For an environmental critical-layer located above d_0, they found that similar transitional flow could occur provided $lH > 0.85$ – which is the well established condition of Miles and Huppert (1969) for wave breaking in an unbounded medium. However, even with $lH <$ 0.85 and with an environmental critical-layer located well above d_0, but close to $d_0 + 2n\pi/l$, transitional flow could occur, although the resonance was considerably weaker and required 'tuning'.

BP found that the character of the high-drag states compared well with the hydraulic analysis of S85 and could not be explained in terms of linear resonance (Klemp and Lilly's postulated mechanism); and further concluded that regardless of the appropriate upper-boundary condition (that is, whether the environmental critical-layer is reflective or absorptive in nature), it is clear that nonlinear effects captured by hydraulic theory are the key element. Only partial support for the validity of PC's mechanism was found; for example, flow with an environmental critical-layer at the resonance altitude of Clark and Peltier (1984) did not necessarily develop to transitional flow as expected. Pitts and Lyons (1990) found partial support for PC's proposed mechanism by comparing numerical model results with their observations of Perth's downslope winds. Consistent with BP, DK concluded that their results suggested that 'the strong lee slope winds associated with wave-overturning are caused by a continuously stratified analog to the transition from subcritical to super-critical flow in conventional hydraulic theory' and, further, that their results did not appear to be consistent with the amplification mechanism of PC. Rottman and Smith (1989) state explicitly that only the model of S85 (as extended by SS87) is consistent with all published results of numerical model and tank experiments.

2.7 The model of Baines and Granek

S85 assumes pre-existing decoupling between hydraulically active and passive layers and that the decoupling is due to either the wave-breaking effect of PC or, for subcritical mountains, an environmental critical-layer positioned 'near'$d_0 + 2n\pi/l$ $(n = 0,1,2,...)$ although the exact meaning of 'near' is not specified. Baines and Granek (1990) have extended this concept and formulated a unifying, comprehensive and quantitative steady-state model.

They provide nonlinear wave-field solutions of Long's equation for asymmetric 'Witch of Agnesi' mountains up to the nondimensional height of $\hat{H}_T$, which they show to be a function of asymmetry. (For convenience, the nondimensionalised height is denoted as $\hat{H}$ and defined as lH; and $\hat{H}_T$ denotes the threshold value of $\hat{H}$ at which streamline overturning first occurs.) For $\hat{H} = \hat{H}_T$, the solution is that of S85. They assume that as $\hat{H}$ is increased beyond $\hat{H}_T$, the upper surface streamline remains unchanged: this assumption being supported by the experiments of Baines and Hoinka (1985). For the region $\hat{H} > \hat{H}_T$, a multilayer (64 level) steady-state hydraulic model based upon the numerical solution of the shallow-water equations is used. Beyond about $\hat{H} \sim 1.5$, blocking of lower-level fluid occurs and the effective value of $\hat{H}$ is changed. This overall approach accords with suggestions by Smith (1987) and Rottman and Smith (1989).

CHAPTER 3

OBSERVATIONS OF ADELAIDE GULLY-WINDS

3.1 General

Adelaide gully-wind events occur mostly in the warmer months of November to March and during the night (Bureau of Meteorology 1971). Marsh (1987) analysed 8 days of west to southwesterly airstream and 18 days of east to southeasterly airstream for January and February of 1980. Using data from a Woelfle anemometer at a quarry site in Highbury (where an Environmental Impact Study was conducted), mean diurnal winds for each stream type were compiled (Fig. 9) and the difference between them was found to be quite remarkable: at Highbury southwesterly streams decayed nocturnally, as one might expect, whereas east-southeasterly streams *freshened* nocturnally to 8 to 9 *m/s*.

Marsh (1987) identified the most common synoptic situation for gully-wind events: namely, a high centred at 40°S between 125° and 140°E, with a cold front moving across or east of Tasmania and extending a weak northern portion into the southeast of South Australia. This northernmost portion tends to become quasistationary and decay. An example is given at Fig. 10, which shows the synoptic situation at 0900 CSST on 13 February 1980. Of course, local forecasters have been aware of the significance of these patterns for many years.

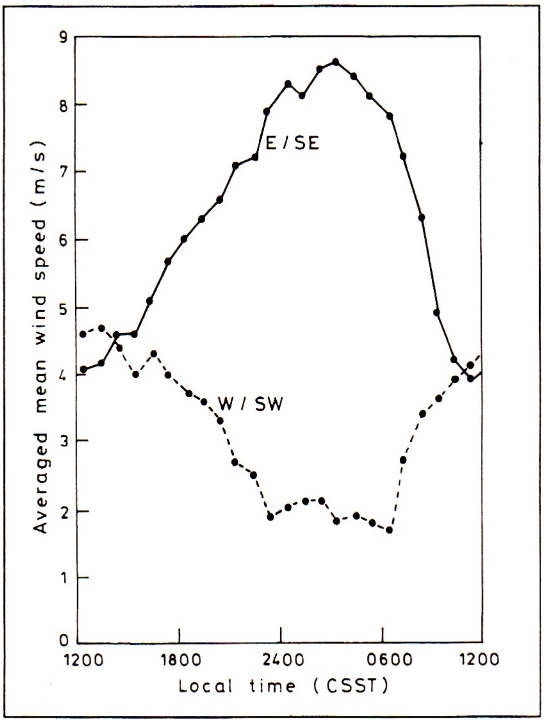

Fig. 9 Mean wind at Highbury (near Wattle Park) in January and February 1980 on a diurnal basis for west to southwesterly streams and for east to southeasterly streams (after Marsh 1987).

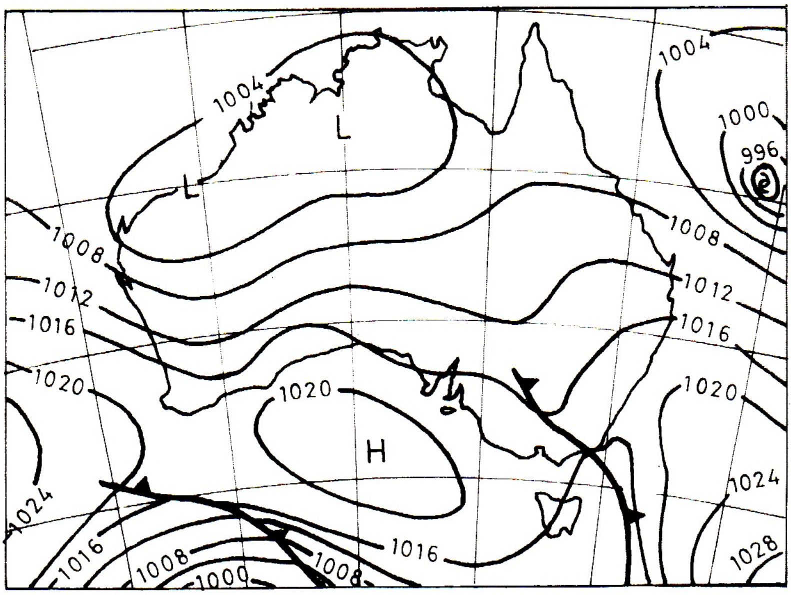

Fig. 10 Mean sea level pressure chart for 0900 CSST 13 February 1980: typical for strong gully-winds.

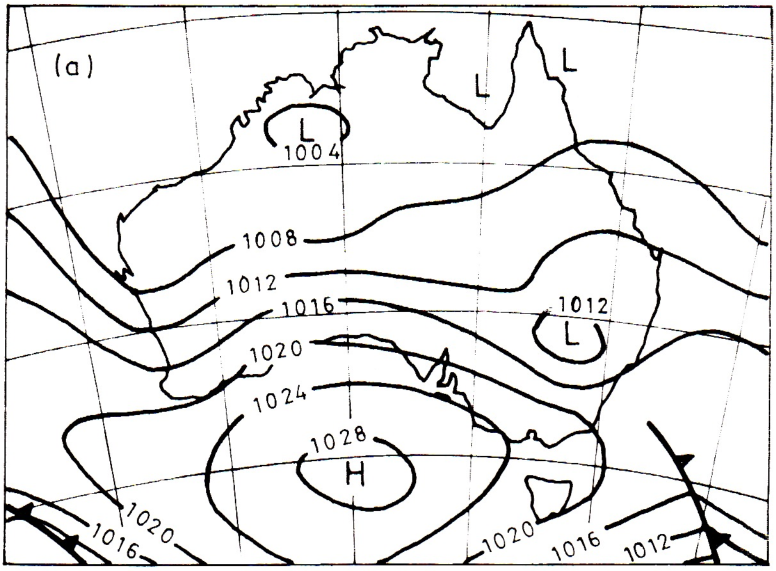

Fig. 11 Surface synoptic chart for 0900 CSST on 7 February 1985.

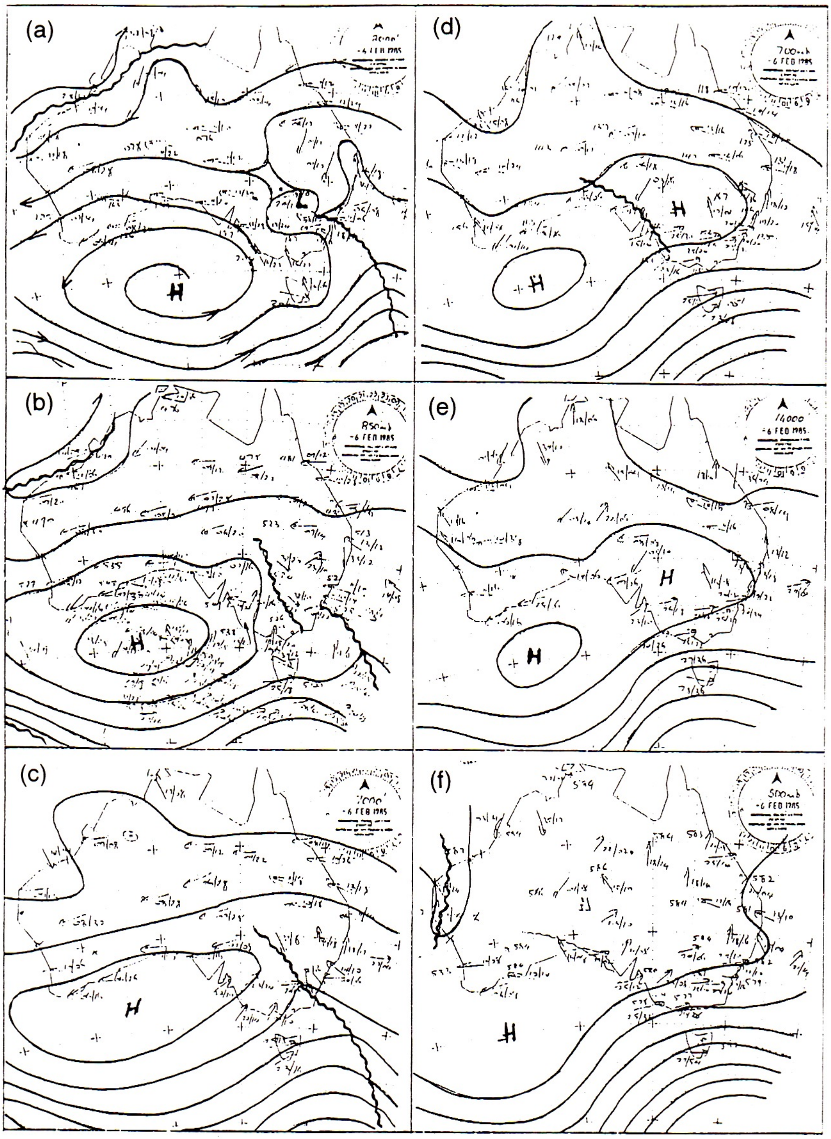

Fig. 12 Synoptic charts for 0900 CSST on 7 February 1985 for; (a) gradient, (b) 850 *hPa*, (c) 7000 *feet*, (d) 700 *hPa*, (e) 14 000 *feet* and (f) 500 *hPa*.

Grace and Holton (1988) examined 52 easterly events (geostrophic flow from the northeast to southeast quadrant at night time over Adelaide) occurring between 1986 and 1987. Thirty of these were gully-wind events – defined in that study as occurring if the overnight maximum wind (averaged over ten minutes) at Wattle Park was greater than that at Mount Lofty. Grace and Holton (1988) showed that the gully-wind often had an easily identified onset and cessation. Namely, the wind regime switched sharply from light and variable to fast and fairly steady in direction, or vice versa. For Wattle Park, the average onset was at 1815 CSST with the average cessation time being 1045 CSST. The mean maximum winds at Wattle Park and Mount Lofty were 10.2 *m/s* and

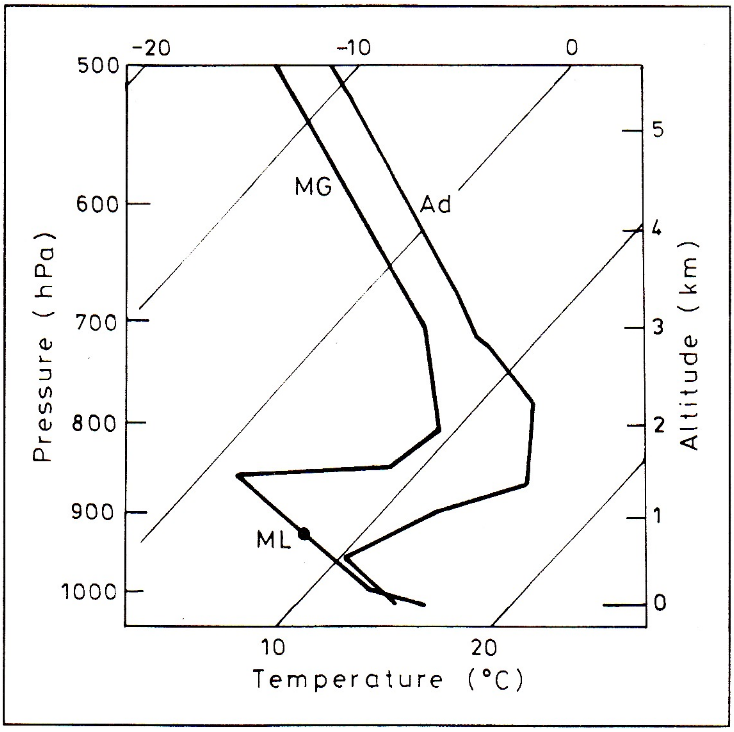

Fig. 13 Temperature profiles for Adelaide Airport and Mount Gambier at 0900 CSST on 7 February 1985. ML denotes Mount Lofty summit.

7.1 *m/s*, respectively, whereas the mean geostrophic wind was 6.8 *m/s*. Nineteen out of the thirty gully-wind events were associated with moderate to severe turbulence as reported by aircraft operating out of Adelaide Airport.

For 29 of the 30 events, low-level winds from Adelaide Airport were used to determine the altitude of any low level easterly jet. The wind reports have a nominal vertical resolution of 150 *m* based on an assumed balloon ascent rate of 300 *m/min* and $^1/_2$ minute readings. Marsh (1987) checked all February 1985 ascents and found that at 0300 CSST the average ascent rate during the first few minutes was 310 *m/min* but with extremes of 240 and 450 *m/min*. On this basis, Grace and Holton (1988) showed that a typical altitude of the low-level jet would have been about 300 to 400 *m*. About half of these events had westerly 1000-*m* winds, and about a quarter had westerly or light (less than 3 *m/s*) winds at 600 *m*. These results emphasise the shallow nature of the gully-wind.

The author has examined many Adelaide Airport vertical temperature profiles for 2100 CSST on the night of significant gully-winds. There is no obvious general feature: this is probably because on many occasions 2100 CSST is too early and on others, the balloon ascent could be either well within the downslope wind layer or in the rebound zone. The nature of this rebound zone will be clarified later. Grace and Holton (1988) found that the presence of a subsidence inversion on the Adelaide Airport sounding was a poor indicator of a subsequent or simultaneous gully-wind. Nevertheless, the most damaging gully-wind events appear to be associated with a marked subsidence inversion or a post-frontal inversion.

3.2 The case study of 6/7 February 1985

This subsection is based on the findings of Marsh (1987). On the nights of 6/7 and 7/8 of February 1985, gully-winds damaged trees and property in many foothill suburbs. Whilst winds were strong enough to fell large trees at locations 5 *km* from the crest, winds at Kent Town, 10 *km* from the crest, were light and variable. Gusts up to 23 *m/s* occurred at Waite Institute, although about 40 *km* further south, at a wind energy monitoring site, gusts to 30 *m/s* were recorded. At Adelaide Airport the maximum wind at 0900 CSST was 110/22 *m/s* at 400 *m* AMSL.

Synoptic charts for 0900 CSST 7 February are shown in Figs. 11 and 12, it should be noted that the surface chart therein is very similar to that in Fig. 10. Note that at 0900 CSST the wind at 1500 *m* was 100°/02 *m/s* and at 2100 *m* was 230°/05 *m/s*, with westerlies aloft; which again emphasises the shallow nature of the gully-wind. On a synoptic scale, the easterly flow over the Mount Lofty ranges ceases at about three times the height of those ranges.

Vertical temperature profiles for 0900 CSST at Adelaide and Mount Gambier are compared at Fig. 13. Immediately noteworthy are the 1400 *m* subsidence inversion at Mount Gambier and the inversion layer between 600 and 1200 *m* at Adelaide. It is likely that the Mount Gambier trace was representative of the stream in general, or possibly a little cooler (being further south), but that descent of the sharp inversion occurred over the ranges and to their lee. Shear-induced mixing would then act to 'smear out' such a sharp inversion.

3.3 The case study of 25/26 February 1991

This case is essentially similar to, although not as pronounced as, that in section 3.2. The 0900 CSST 26 February MSL chart with pertinent 600 *m* winds is shown at Fig. 14. Contemporaneous temperature traces from Adelaide and Mount Gambier Airports in Fig. 15 show a post-trough inversion indicative of a cool change penetrating into the southern part of South Australia. The air mass which produced the cool change at Mount Gambier is obviously cooler and deeper than at Adelaide.

At 0800 CSST an aircraft at Cleve, about 200 *km* downstream of Adelaide, reported an inversion at '1500 to 2000 *feet* AMSL', which would be about 550 *m* AMSL. At Port Stanvac, south of Adelaide, the mean wind at 0750 CSST was 14 *m/s* from the southeast.

At 0600 CSST, the conditions recorded by the Mount Lofty Automatic Weather Station (AWS) were an easterly wind of 8*m/s* with temperature of 22.5° and dew-point of 2.2°C; yet at 0728 CSST, they had changed dramatically – to an easterly of 4 *m/s* with temperature of 12.3° and dew-point of 12.0°C! This implies that a 10°C inversion rose through the AWS at 736 *m* between 0600 and 0728 CSST. (This 'convenient' occurrence was brought to the author's attention by his colleague, Mr Ian Holton). On a few apparently similar occasions, the Mount Lofty AWS records have revealed rapid fluctuations of up to 10° in both dry bulb and dew-point temperatures, though at Mount Crawford, at a lower altitude to the north, the sampled air was continuously cool and moist. It is evident that on 25/26 February 1991, a reservoir of cold air gradually increasing in depth formed a decoupled single-layer flowing across the ranges – very much as proposed by Küttner over 50 years ago.

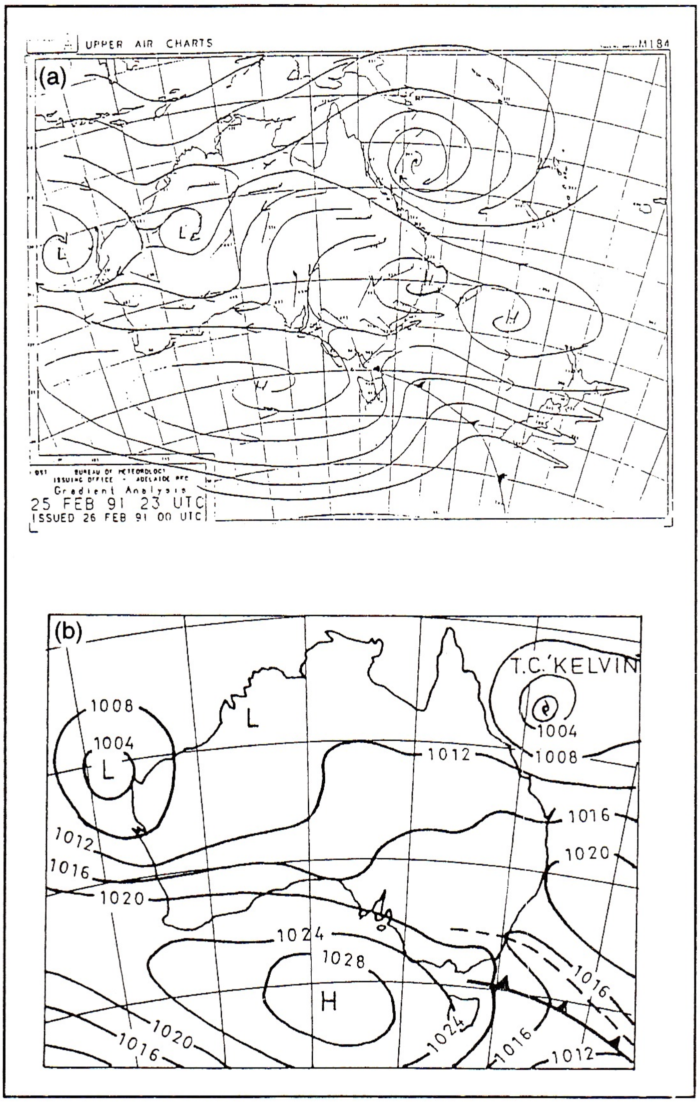

Fig. 14 Charts for 0900 CSST 26 February 1991: (a) gradient level and (b) mean sea level pressure chart.

3.4 The case study of 6/7 February 1972

On a night without any obvious strong synoptic stream (see Fig. 16), gully-winds were recorded by an experimental acoustic sounder at Salisbury by Mahoney et al. (1973). The Salisbury data for the four hours from 2200 CSST on 6 February 1972 are presented at Fig. 17 and show the height of the turbulent-layer, the vertical velocity at 100 *m*, and the 100-*m* layer mean wind speed. A measure of consistency is provided by the balloon-derived mean wind to 300 *m* (the lowest available) at 2100 CSST at Adelaide Airport, which was 127°/12 *m/s*. From the aerological profile at 2100 CSST at Adelaide Airport (Fig. 18), it is seen that the height of the base of

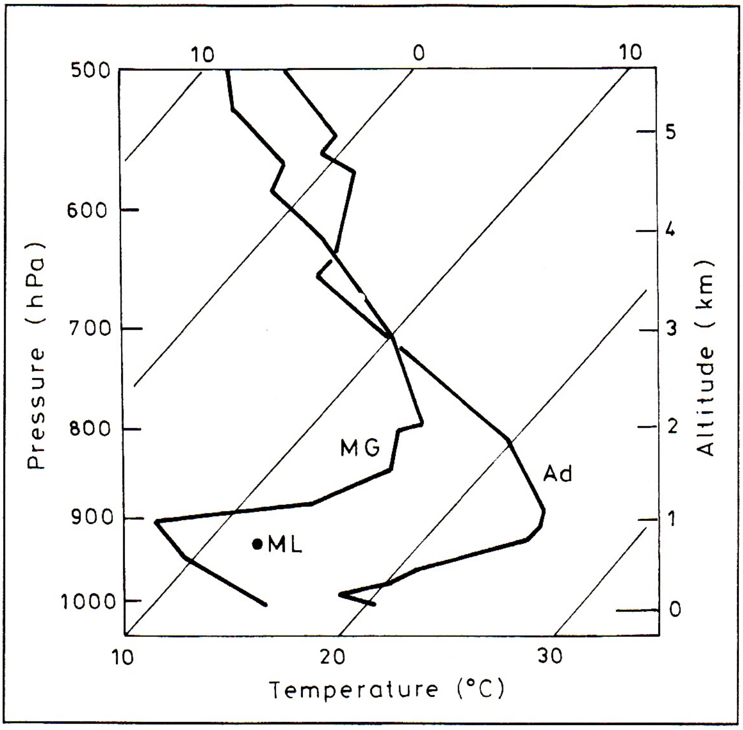

Fig. 15 Temperature profiles for Adelaide Airport and Mount Gambier at 0900 CSST on 26 February 1991. When used in conjunction with Fig. 14, these show that there is a shallow layer of cool air crossing the ranges from the east to southeast.

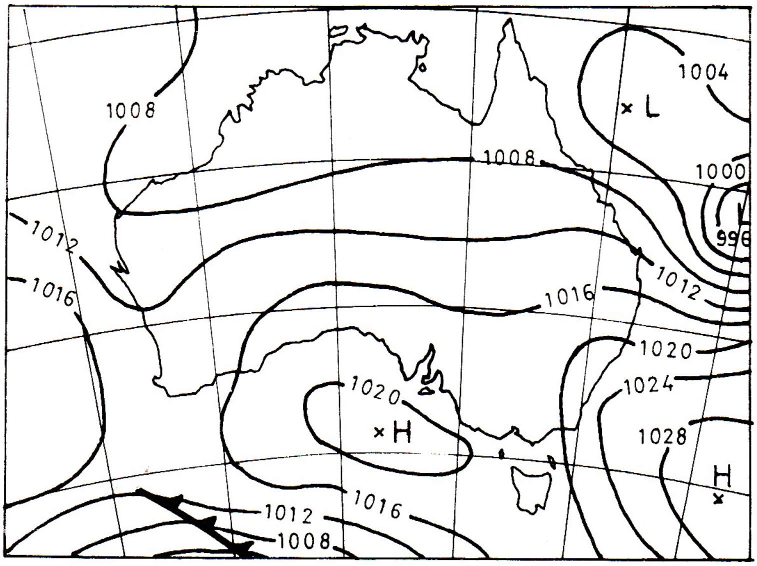

Fig. 16 Mean sea level pressure chart for 2100 CSST 6 February 1972.

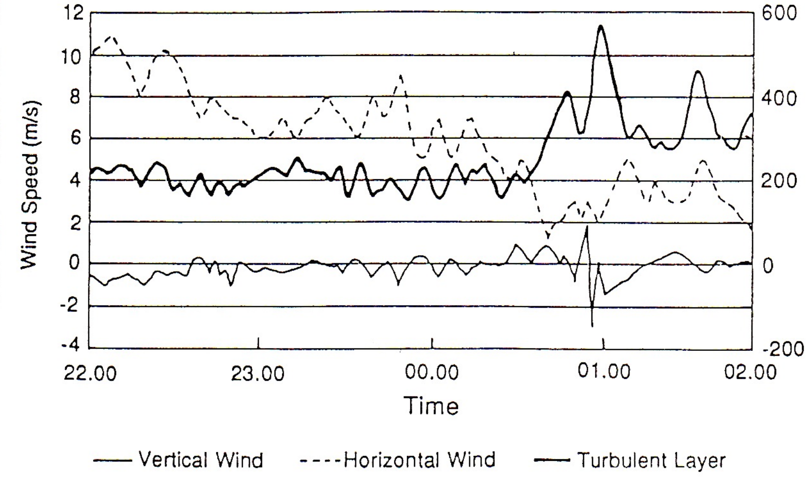

Fig. 17 Acoustic-sounding record of turbulent-layer depth, the vertical velocity at 100 *m* and the 100 *m*-layer mean wind for the period 2200 on 6 February to 0200 CSST 7 February 1972 at Salisbury, South Australia.

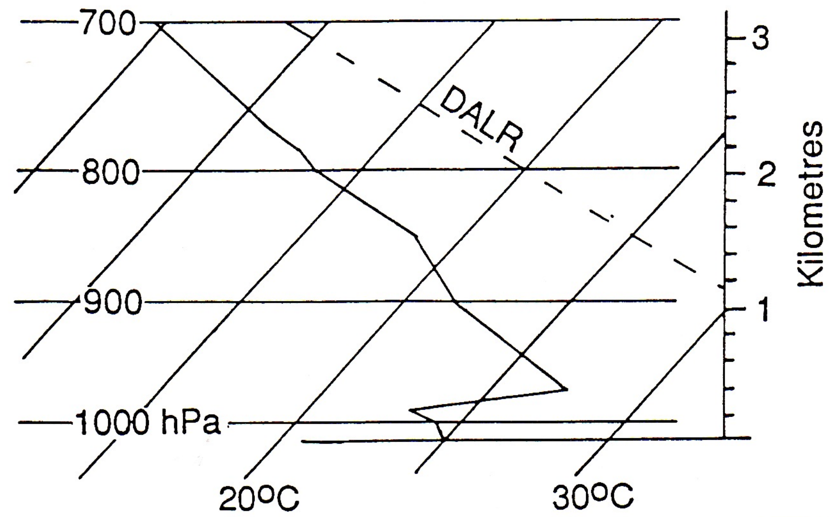

Fig. 18 Vertical temperature profile for 2100 CSST 6 February 1972 at Adelaide Airport.

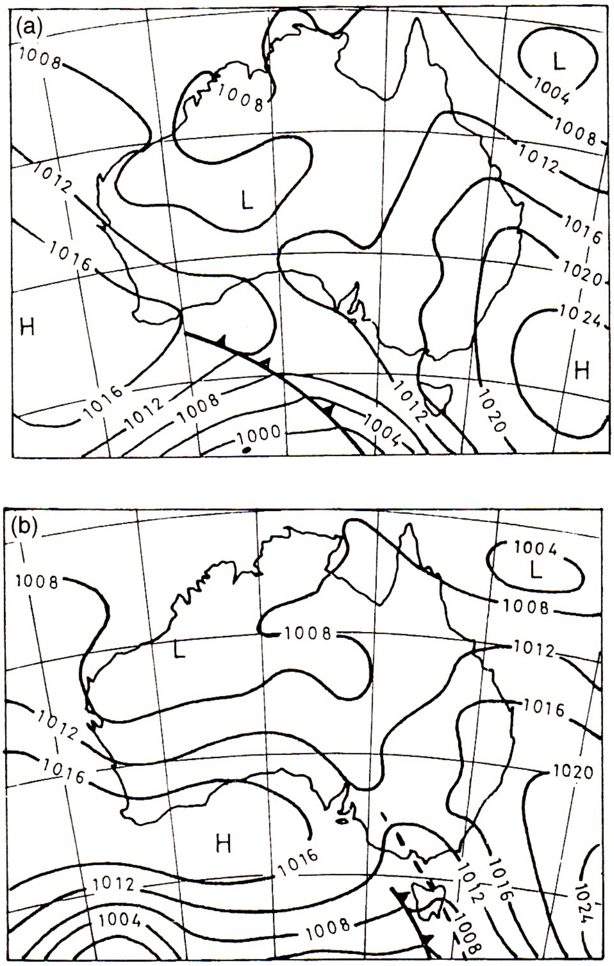

Fig. 19 Mean sea level pressure charts for 0900 CSST on; (a) 3 February 1988 and (b) 4 February 1988. There is weak gradient flow for (a) but a shallow cool-air intrusion occurs in the wake of the (dotted) trough in (b).

the inversion (210 *m*) was consistent with the Salisbury acoustic sounder data relating to the height of the turbulent-layer (about 200 *m*). The inversion itself was only 10 to 20 *m* thick.

Prior to the jump at about 0050 the layer depth was about 200 *m*. It is less clear what the value after the jump was, but a reasonable value would have been about 350 *m* (Fig. 17). (More details of this event are provided by Grace and Holton (1990), of which a copy is included with this thesis.) The remarkable feature is the shallowness of the layer. Corroboration that this is common comes from Mr Alan Shore, a hot-air balloon pilot who operates in the Barossa Valley mostly during early morning and late afternoon. (Mr Shore lives near Bethany in the Barossa Valley and maintained an anemometer at his property for the author.) According to him, the air aloft during gully-winds is calm, yet the surface wind is strong, gusty and noisy. The transition is usually quite sharp and occurs at about 200 *feet* (60 *m*) above ground level.

3.5 Field observations

3.5.1 Outline of measurements.

At Adelaide the most common gully-wind direction is from the east-southeast presumably because the ranges nearby are oriented north-northeast/south-southwest so that the gully-wind is generally perpendicular to the line of the ranges. To utilise Mount Lofty AWS, a 110°–290° transect was selected as a reference cross-range line. Nairne was selected as a windward aerological and surface observation site. Other sites marked in Figs 20–23 were fitted with available instruments.

On the nights of 2/3 and 3/4 February 1988, designated as nights 'A' and 'B' respectively, Adelaide Airport meteorological radar staff carried out three-hourly sonde and radar-wind flights and, at Nairne, Flinders University and Bureau of Meteorology staff carried out three-hourly radiosonde and visually-tracked balloon flights.

At approximately coincident times, the Flinders University 'GROB' aircraft flew out and back along the transect, with several shorter sorties to the lee of Mount Lofty. Because of Air Traffic Control requirements, the GROB was unable to fly sufficiently low over the lee foothills, and passed about a kilometre south of Mount Lofty (over a well-lit freeway interchange). Instrumentation available on the GROB allowed the acquisition at 13 Hz of air speed, temperature, humidity, pressure, altitude, and radar height above ground. Navigation and position fixes were coordinated by a co-pilot. Horizontal wind was measured, but these measurements were later discarded as unreliable (the aircraft's position finding equipment has since been upgraded to the satellite-based Global Positioning System (GPS), which obviates this problem).

Generally, the air/ground coordination was such that the aircraft flew over the balloon sites within a few minutes of each balloon release. This high degree of coordination was mainly due to the skilled flight-planning of the pilots, for radio transmissions from the aircraft had to be minimised, as this 'spiked' the data from most of the aircraft's sensors.

At 2330 CSST on the second night, an additional sonde was released from near Mount Lofty AWS (actually about 500 *m* south of the AWS in order to avoid trees, transmission towers and wires), but no wind flight was done. Some other unsuccessful attempts were made.

Other than the aircraft data, all data were processed using standard techniques and procedures. The aircraft data were managed by the pilots, analysed with the package described in Hacker and Schwerdtfeger (1988) and presented as a file containing directly-measured and derived parameters with x,y,z,t coordinates. Consistency was found between aircraft and balloon data with temperature and dew-point data from various sources differing by less than $^1/_2$ to 1°C.

3.5.2 Analysis of study nights A and B.

Surface charts for 0900 CSST (at the 'end' of each night) are shown at Fig. 19. For each three-hourly set of data, cross-sections of virtual potential temperature, θ_v, and specific humidity were analysed. These are shown as a series of panels for both nights at Figs 20 to 23. Some subjectivity was obviously necessary in the analyses, especially over the lee foothills. The balloon winds were also superimposed on these cross-sections. To aid in assimilating the data, the radiosonde flights are also presented on conventional aerological diagrams in Fig. 24. These emphasise the strength of the inversions on these occasions.

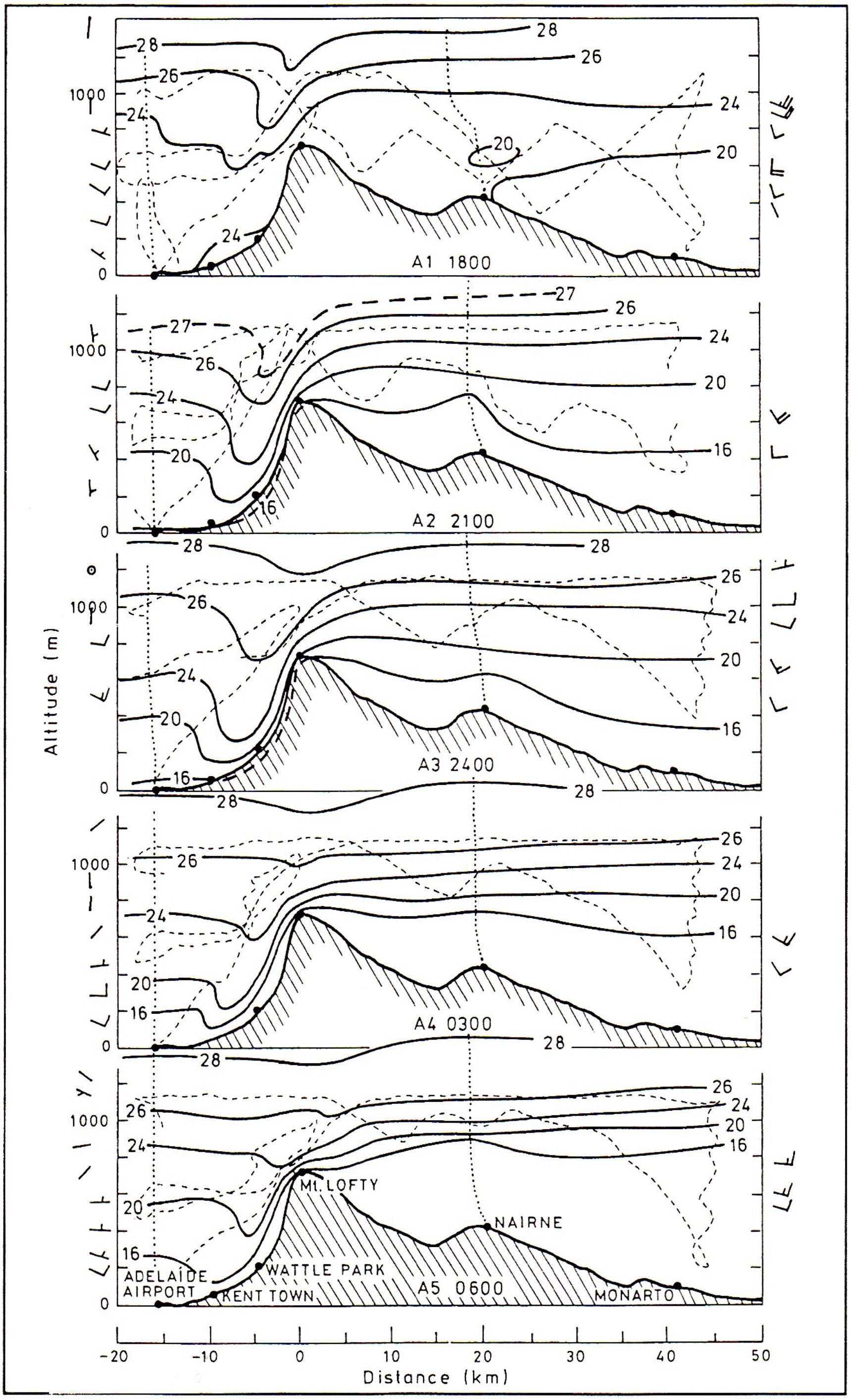

Fig. 20 Three-hourly isentropic cross-sections (using virtual potential temperatures in °C) for night of 2/3 February 1988 along the true bearing 110°–290° through Mount Lofty. Faint lines show aircraft tracks and balloon trajectories. Offset winds are for Adelaide Airport (left) and Nairne (right).

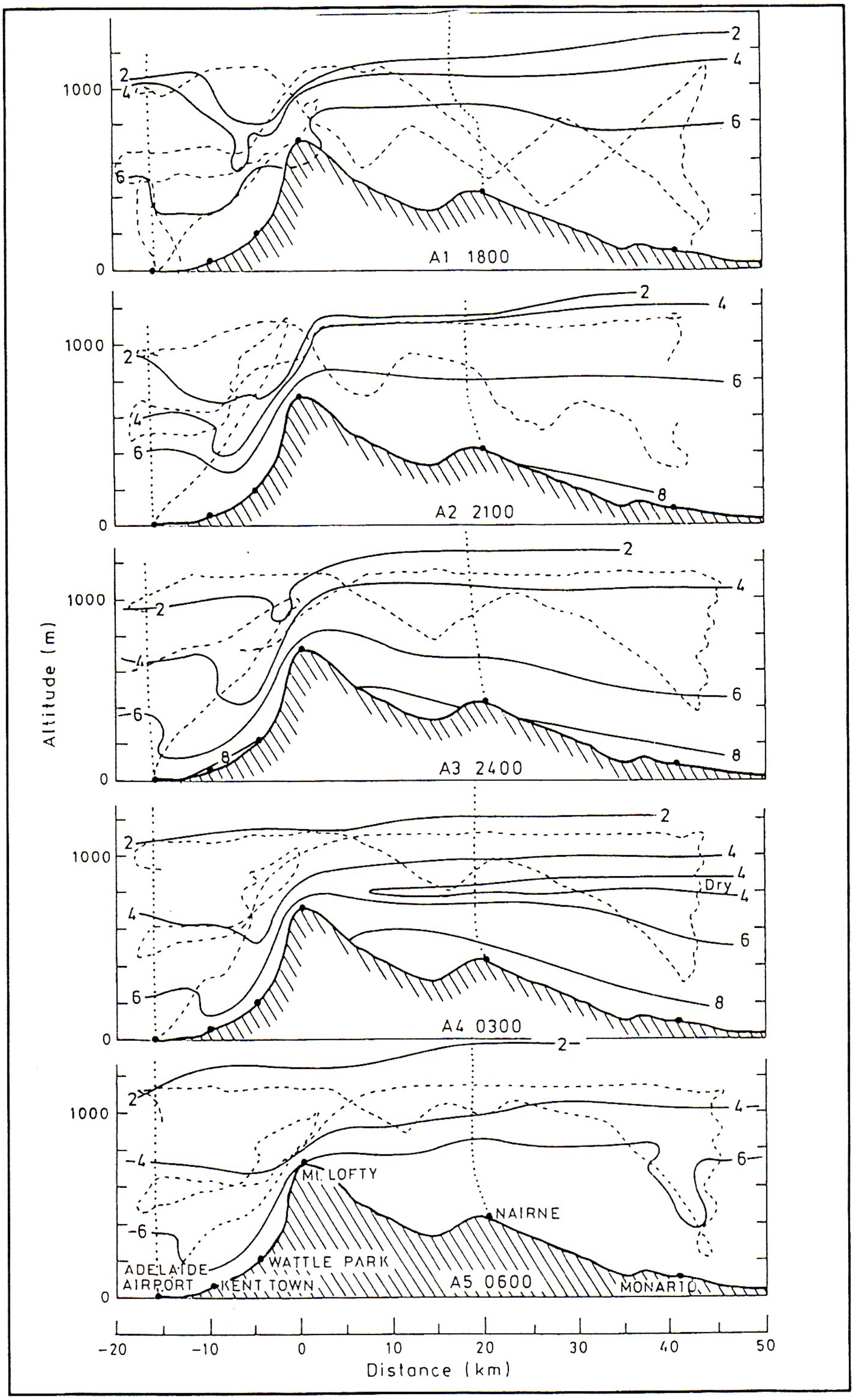

Fig. 21 As for Fig. 20 but for specific humidity in *gm/kgm.*

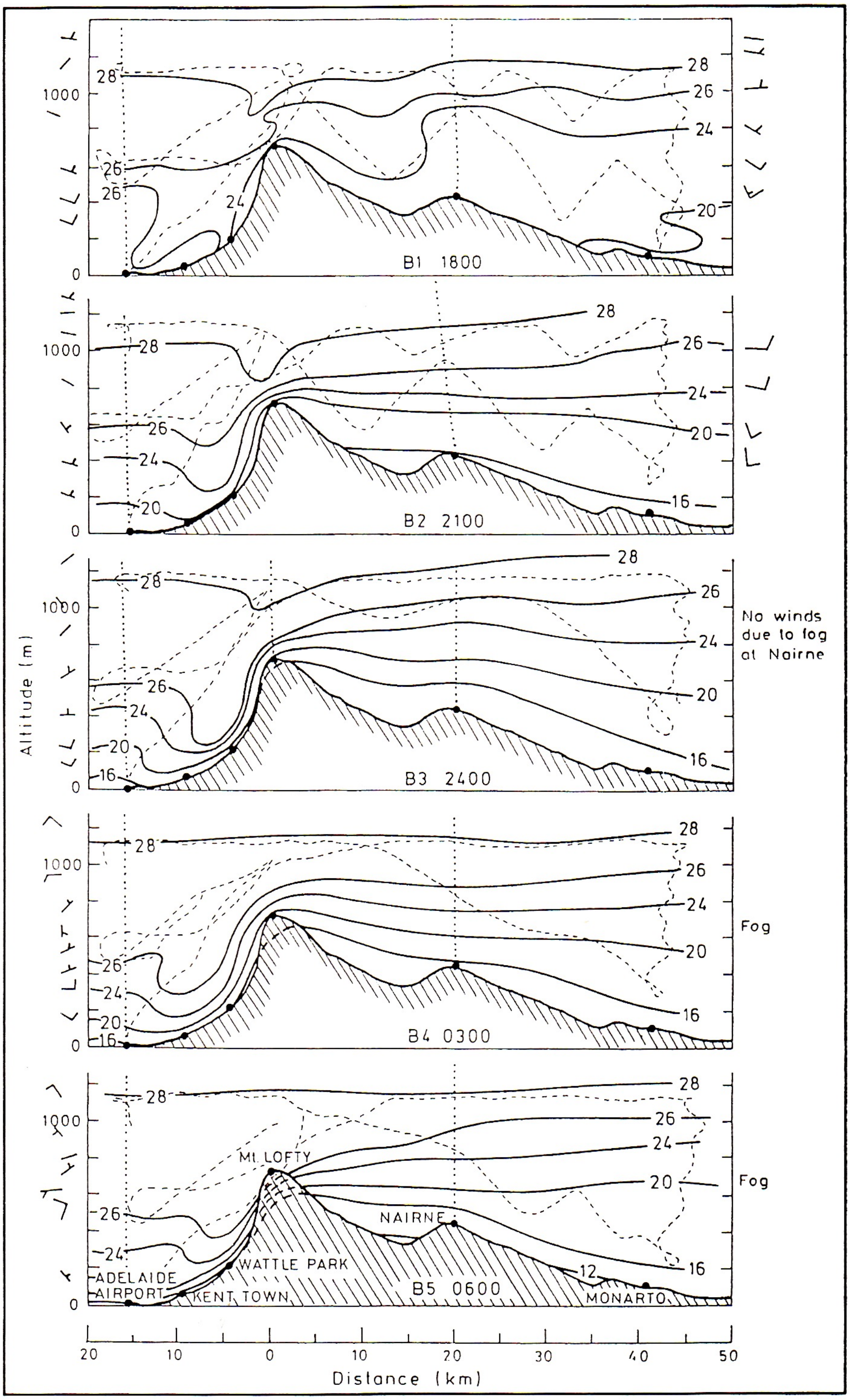

Fig. 22 As for Fig. 20 but for the night of 3/4 February 1988.

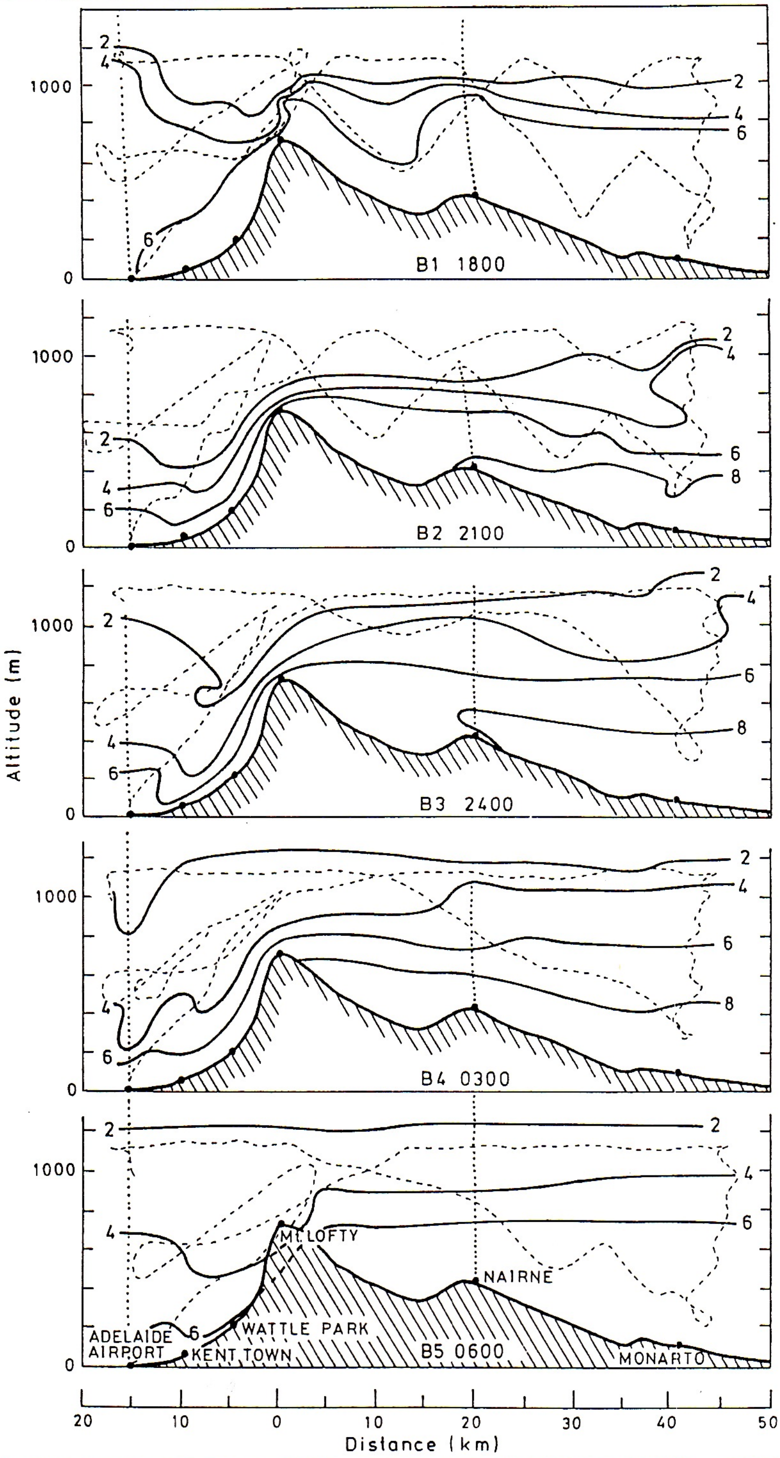

Fig. 23 As for Fig. 22 but for specific humidity in *gm/kgm*.

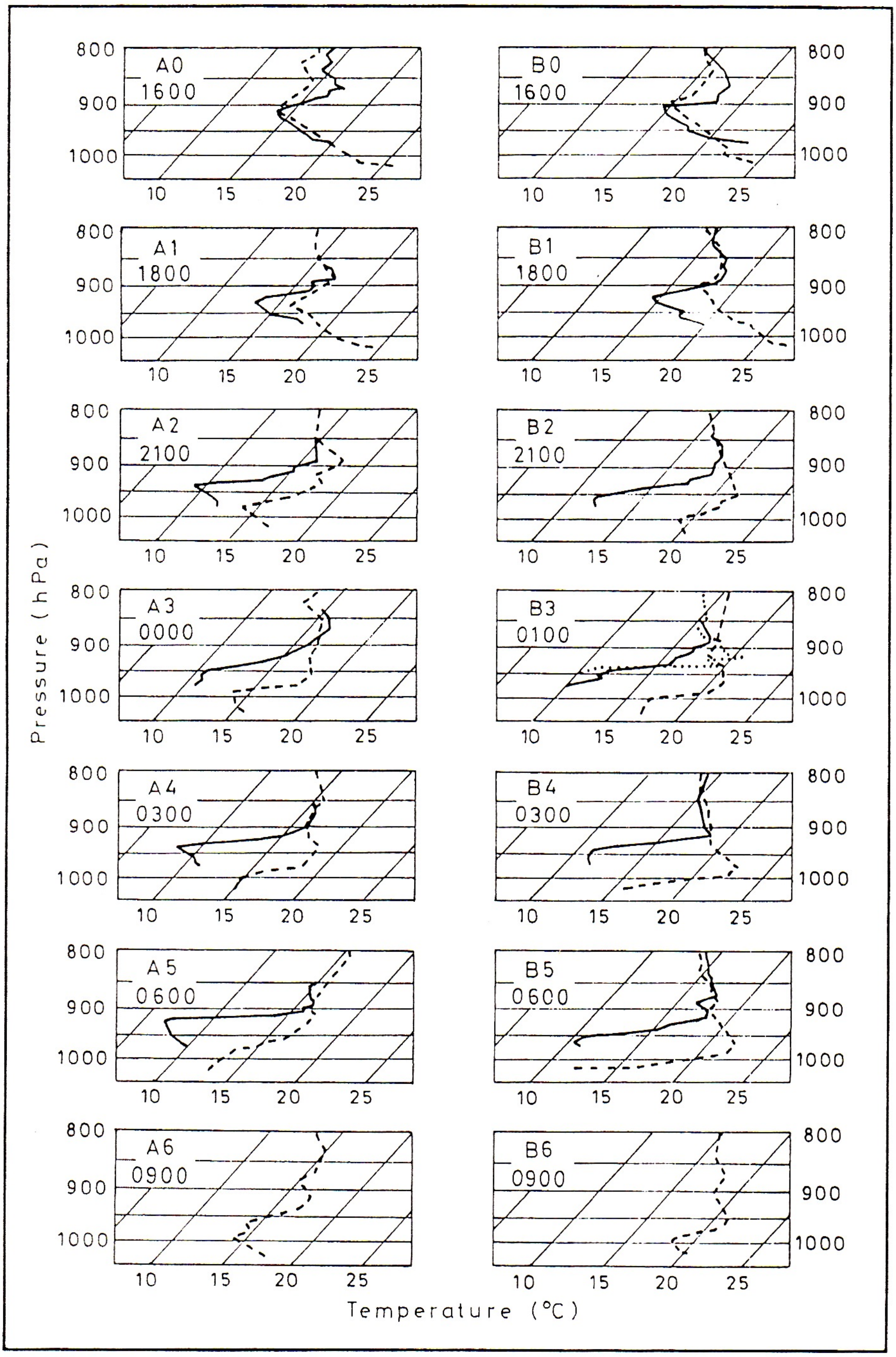

Fig. 24 Three-hourly temperature profiles at Nairne (solid) and Adelaide Airport (broken) on the nights of the 2/3 and 3/4 February 1988 (identified as nights A and B, respectively). At 2330 CSST on the second night a sounding was completed at the crest of the ranges. The superadiabatic layers on the B3 profile have been double checked and therefore appear to be real.

The striking features were that above 1200 *m* there was apparently little disturbance. After either 1800 or 2100 CSST decoupling was generally evident between the stable lower layer and the fairly unstable upper layer. The top streamline (usually $\theta_v \approx 27$ °C) of the stable layer was typically 1000 *m* above ground to windward. Near the ridge line, it was drawn down rapidly to a minimum of about 300 *m* over the lee foothills and then passed through a jump-like feature and exited at an altitude of 600 *m*. Wattle Park (10-minute mean) winds varied from 3 to 15 *m/s* indicating that the jump zone was certainly in the vicinity. The specific-humidity analyses and provide a consistency check with the isentropic analyses.

Directly in the lee of Mount Lofty itself, e.g. at Waite Institute, Kent Town and at Adelaide Airport, the surface winds were mostly only moderate. However, sites at Port Stanvac and Bethany recorded lengthy periods (several hours) of 12–15 *m/s* and 15 *m/s* mean winds, respectively. At Wattle Park, occasional periods of 15*m/s* mean wind were recorded. From the author's friends and colleagues, there were many reports that strong gusty gully-winds occurred in the southern and northern foothill suburbs. Apparently much of the flow is *around* the Mount Lofty summit and the final panels of Fig. 22 show this effect. This type of effect was noted before in section 3.3.

3.6 The definition, description and use of ΔT

In analyses of actual gully-wind events in the Adelaide region, one of the most important parameters turned out to be the temperature difference, ΔT, which is defined to be the environmental temperature at 736 *m* above Adelaide Airport minus the temperature at the Mount Lofty AWS (which is of course also situated at 736 *m* AMSL). Marsh (1987) used 0900 CSST radiosonde data from the months of December 1985 to April 1986 and determined the average ΔT, classified according to wind direction at Adelaide Airport (See Fig. 25). It is strikingly evident that in easterly streams, the average ΔT is about 4°C, whereas in others, it is close to zero.

A somewhat similar relationship is shown by a scatterplot matrix of ΔT, geostrophic wind and *peak* gust speed at Port Stanvac. The first two variables were determined at 2100 CSST and the peak gust used was that occurring within one hour of that time. The scatterplot matrix (Fig. 26) shows the dependence of gust speed on ΔT and on geostrophic wind but *little dependence* of ΔT

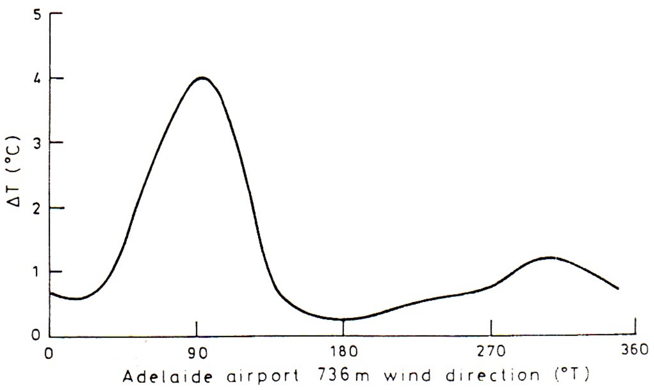

Fig. 25 Average ΔT as a function of Adelaide Airport wind direction at 736 *m*, above MSL (after Marsh 1987).

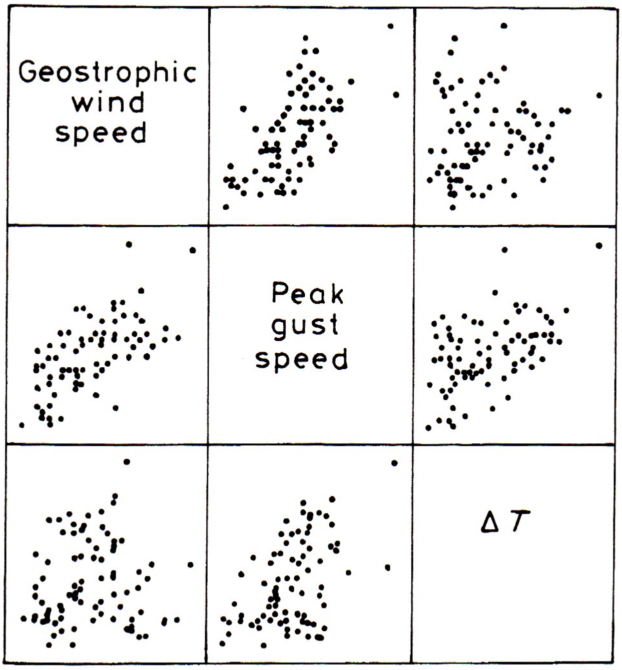

Fig. 26 Scatterplot matrix of peak gust at Port Stanvac (between 1000 and 1200 CSST), *ΔT* and geostrophic wind speed at 1100 CSST.

on geostrophic wind. So *ΔT* and geostrophic wind are quasi-independent predictors of gust speed. It is relatively easy to devise a best-fit quadratic plot of gust speed as a function of *ΔT* and geostrophic wind, although this is not shown.

The greater the amplitude of the forced lee-wave trough then the greater will be *ΔT*. In this sense, *ΔT* may be regarded as a proxy measure (albeit very crude) of the amplitude of the trough, and hence of the downslope wind speeds. Grace and Holton (1988) investigated this effect and found that, on average, gully-wind speed is a function of *ΔT*. Holton and Grace (1989a,b) were then able to produce gully-wind nowcasting aids.

3.7 Observations of a hydraulic jump in a fog bank

It is well known in hydraulics that transitional flow may occur due to a lateral constriction instead of a vertical obstacle (or, indeed, due to both together). An interesting example of this occurred in Backstairs Passage at the southern end of the Mount Lofty Ranges on 2 May 1988. More detail of this instance is provided in Grace (1991), of which a copy is provided with this thesis.

In this instance, a shallow cool, moist layer of fog of the order of 200 *m* deep transitioned from subcritical to supercritical flow, and eventually back to subcritical *via* a well defined hydraulic jump. To the author's knowledge, this is the only published photograph to show clearly an atmospheric hydraulic jump caused by a constriction. One of the photographs from Grace (1991) is shown in Fig. 27. Such striking evidence of this type of event leads to the conjecture that the actual gully-winds are induced by a combination of lateral constriction and vertical obstacle.

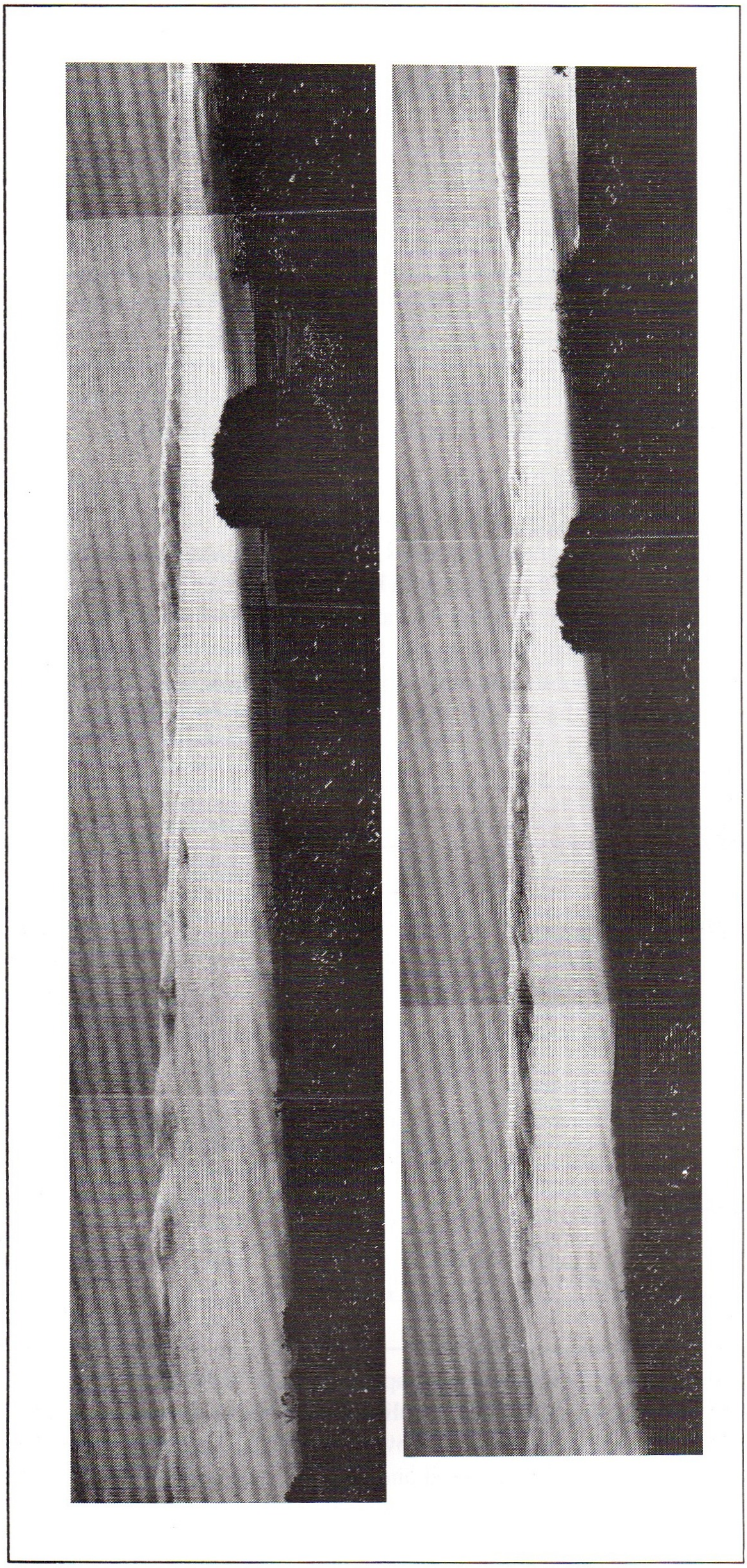

Fig. 27 Photographs (looking west out over Backstairs Passage) of hydraulic jump in fog bank on 2 May 1988 in Backstairs Passage, South Australia. Top sequence taken at 1420 CSST; lower one taken at about 1530. See Grace (1991) for further details. (Photographs courtesy of Mr Richard Geytenbeek).

CHAPTER 4

A QUASI $1^1/_2$-LAYER MODEL ($Q1^1/_2$)

4.1 Development

4.1.1 Assumptions and nomenclature

Hydraulic models with a single homogeneous layer are naturally termed single-layer models. Models with a shallow homogeneous layer overlain by an infinitely deep homogeneous layer are formally equivalent to the single-layer models (through the Boussinesq approximation) and so are often referred to as single-layer models, even though there are two separate layers in the model. To avoid confusion Baines (1987) has used the term 'one and a half layer' with the 'half' applying to the deep passive layer, and this terminology is followed in this paper.

Consider steady-state 2-dimensional, infinitely-deep, continuously-stratified flow across a mountain range as in Fig. 28. The flow is from left to right. The terrain height, $h(x)$, reaches a maximum of H at $x = 0$ and is exactly zero for $x \geq \alpha$. Far upstream h is effectively zero, and the flow velocity, u_0, and stability, N_0, are constant with height. The streamline, or potential temperature surface, θ_0, originating at level, d_0 splits on the windward approach to the mountain with the lower branch descending rapidly. Above d_0, the flow is assumed to be unchanged. Between the split streamlines the air is turbulent and well mixed with constant potential temperature, θ_0, but with no mean motion. Other than at the jump, the flow in the layer below the lower split streamline is regarded as smooth, non-dissipative, steady, hydrostatic and Boussinesq.

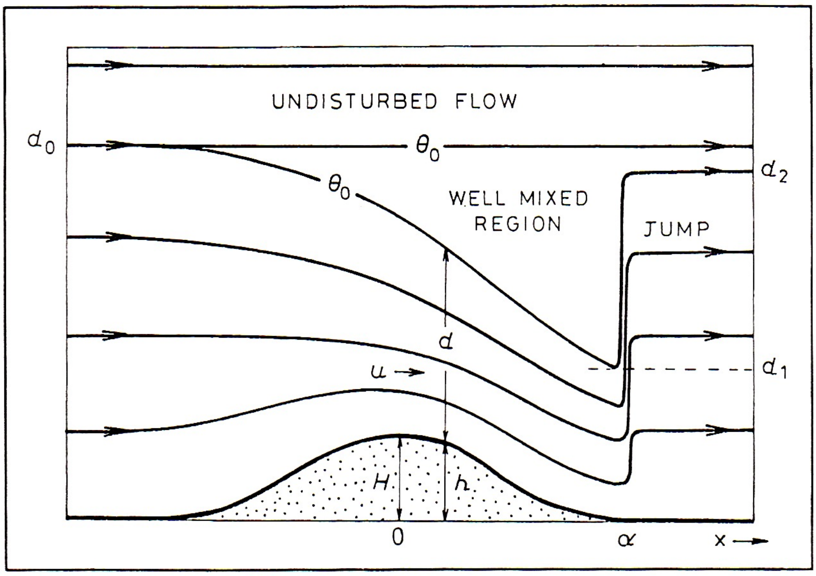

Fig. 28 Steady 2D flow over a mountain with upstream static stability N_0, and velocity, u_0. The streamline initially at altitude d_0 splits, so that above d_0 the flow is unchanged. Below the lower split streamline the flow is essentially hydraulic, and between the split steamlines the air is well-mixed and turbulent but with no mean motion. Stability and speed of the layer beneath the lower split streamline (θ_0) are constant with height.

The continuously-stratified lower layer is assumed to be approximated by an equivalent homogenous layer (of constant density and with velocity independent of height – hence the term 'quasi $1^1/_2$-layer', or $Q1^1/_2$). No *a priori* justification for this assumption is attempted other than observing that it must be plausible in view of the conclusions of DK and BP; however, it is anticipated that the realism of the model results will support its validity. Within the hydraulically-active, lower layer, the streamlines will remain equidistant and therefore both u and N remain independent of height. The infinitely-deep stratified layer above d_0 is 'replaced' by an infinitely deep layer of constant potential temperature, θ_0. It is reasonable to do this since it has already been assumed that there are no changes to the flow above d_0. A hydraulic jump is assumed to occur in the lee of the mountain. Subscripts apply to the active layer in such a way that '0' = far upstream, 'c' = crest, '1' and '2' = immediately before and after the jump, respectively, and 'T'= transition threshold.

4.1.2 Altitude of the splitting streamline

For an isentropic layer of velocity, u, and of depth, d, overlaid by a deeper isentropic layer, the shallow-water gravity-wave speed, c, is given by

$$c = u \pm \sqrt{g' d} \tag{11}$$

$$\text{where } g' = g\frac{\delta\theta}{\theta_0} \tag{12}$$

and g is acceleration of gravity, θ_0 is the upper-layer temperature and $\delta\theta$ is the temperature difference between the layers. For a layer of *continuously* stratified fluid of depth, d, and constant Brunt-Väisälä frequency, N, overlaid by an infinitely-deep isentropic layer with temperature equal to that at the top of the lower layer, it is known that the gravity waves have a speed given by

$$c = u \pm \frac{2Nd}{(2n-1)\pi}, \quad \text{where} \quad n = 1,2,3,0\ldots \tag{13}$$

Equating Eqn 11 and 13 gives an equivalent modified gravity for a continuously stratified layer of

$$g' = \frac{4N^2 d}{(2n-1)^2\pi^2}. \tag{14}$$

The layer Froude Number, F, is commonly defined as

$$F \equiv \frac{u}{\sqrt{g' d}} \tag{15}$$

although there are several other definitions in the literature. Combining Eqns 14 and 15, we therefore find that

$$F = \frac{(2n-1)\pi u}{2Nd}. \tag{16}$$

For a shallow homogenous layer overlaid by a deep layer, the condition for transitional flow (having $F < 1$ on the windward side and $F > 1$ on the leeward) is known to be

$$F_0^2 - 3F_0^{2/3} + 2\left(1 - \frac{H}{d_0}\right) = 0. \tag{17}$$

(A derivation of Eqn 17 is included at Appendix A.) Parameters d, H and h are non-dimensionalised by setting $\hat{d} \equiv dl$ and $\hat{H} = Hl$ where $l = N_0/u_0$. (Generally carats will indicate non-dimensional values.) The Q1½ (Quasi 1½-layer) model then has as the condition for transitional flow

$$\left(\frac{(2n-1)\pi}{2\hat{d}_0}\right)^2 - 3\left(\frac{(2n-1)\pi}{2\hat{d}_0}\right)^{2/3} + 2\left(1 - \frac{\hat{H}}{\hat{d}_0}\right) = 0\,. \tag{18}$$

Equation 18 shows that $\hat{d}_0$ is an analytic function of $\hat{H}$ and n and the graph of this function in Fig. 29 shows that $\hat{d}_0$ increases with $\hat{H}$ and n. For later discussion the ratio $\hat{d}_0/\hat{H}$ (which is of course identical to d_0/H) is also plotted thereon. $\hat{H}$ has only been graphed over the domain (0,1) although there is no upper limit imposed by the model. For $n=1$ (this effectively confines the discussion to the lower troposphere), $\hat{d}_0$ can be well approximated (using a best-fit power curve) by the explicit expression

$$\hat{d}_0 = 2.27\hat{H}^{0.633} + \frac{\pi}{2} \tag{19}$$

while the more general Eqn 18 has a family of solutions for $\hat{d}_0$ with a quasi-period in $\hat{d}_0$ of π (this compares to S85 which has multiple solutions with period 2π). A more convenient but less accurate form of Eqn 19 is

$$\hat{d}_0 \approx 2.3\hat{H}^{2/3} + \frac{\pi}{2} \tag{20}$$

and so

$$d_0 \approx 2.3H^{2/3} + \left(\frac{u_0}{N_0}\right)^{1/3} + \pi\frac{u_0}{2N_0} \tag{21}$$

showing that d_0 increases with H and u_0 but decreases with N_0. That is, d_0 is decreased for a low obstacle or if the stream is light and/or stable. A typical value of l is $10^{-3}m^{-1}$ (with $N_0 = 10^{-2}s^{-1}$ and $u_0 = 10\ m/s$). So for a 1 km high mountain, $d_0 \sim 4$ km and, for a 500 m mountain, $d_0 \sim 3\ km$. The ratio, $\hat{d}_0/\hat{H}$, or d_0/H, is about five for $\hat{H} \sim 0.7$.

4.1.3 Critical mountain height

For continuously stratified flow there is a critical or threshold value ($\hat{H}_T$) such that if $\hat{H} \geq \hat{H}_T$ then the flow will adopt the transitional steady-state configuration of Fig. 28. In Chapter 2 it was noted that the value of $\hat{H}_T$ is 0.85 for symmetrical bell-shaped hills (Miles and Huppert 1969; Lilly and Klemp 1979). For asymmetric bell-shaped obstacles, Baines and Granek (1990) have shown that $0.5 \leq \hat{H}_T \leq 1$: with the lower (higher) values applying as the approach (lee) slope decreases.

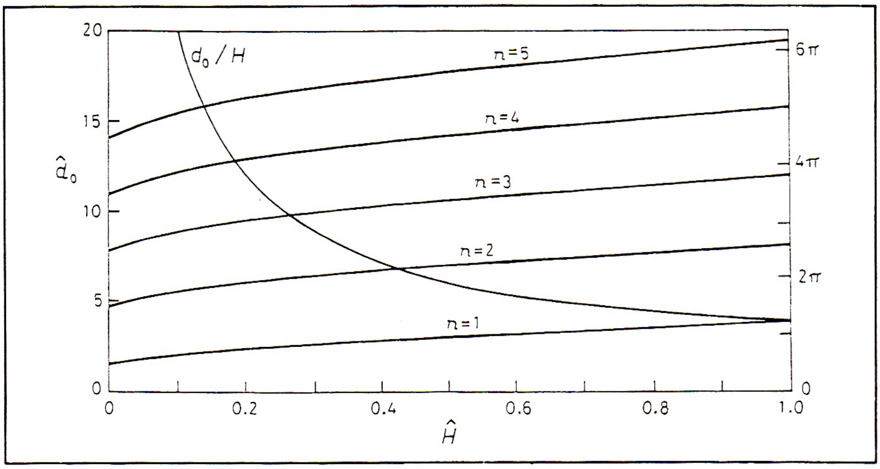

Fig. 29 Graphical solution of Eqn 18 showing $\hat{d}_0$ and higher order solutions as a function of $\hat{H}$. Also shown is the ratio d_0/H for $n = 1$.

4.1.4 Leeward velocity

Application of Bernoulli's equation along the uppermost streamline of the active layer (implicitly assuming constant pressure along this streamline) prior to the jump gives

$$\frac{u^2}{2g'} + d + h = \frac{u_0^2}{2g'} + d_0 \tag{22}$$

and, on substitution for g' from Eqn 14 (with $n = 1$), this yields

$$\frac{\pi^2 u^2}{8N_0^2 d_0} + d + h = \frac{\pi^2 u_0^2}{8N_0^2 d_0} + d_0 \tag{23}$$

$$= k_0$$

where k_0, say, is a constant. By continuity it follows that the volume flux *(ud)* is constant so that after some manipulation, Eqn 23 reduces to

$$\frac{\pi^2 d_0}{8l^2 d^2} + d + h = k_0. \tag{24}$$

Equation 24 is a cubic in d and has two real positive roots which correspond to the sub and supercritical flow. Thus, the altitude *(d+h)* of the uppermost streamline is known at any point and, since the layer streamlines maintain their initial relative spacing, the subsequent position of a streamline passing through any given height far upstream is determinable.

Assuming that no rebound, or jump, occurs before $x = \alpha$, then, setting $d = d_1$ and noting that $h = 0$, Eqn 24 yields

$$\frac{1}{2}\left(\frac{\pi}{2\hat{d}_1}\right)^2 + \frac{\hat{d}_1}{\hat{d}_0} = \frac{1}{2}\left(\frac{\pi}{2\hat{d}_0}\right)^2 + 1 \tag{25}$$

which shows that $\hat{d}_1$, being closely related to $\hat{d}_0$, is also a function of $\hat{H}$ (see Fig. 30). The so-called speed-up ratio, $\hat{s}$, defined as

$$\hat{s} \equiv \frac{u_1}{u_0} = \frac{d_0}{d_1} = \frac{\hat{d}_0}{\hat{d}_1} \tag{26}$$

increases with $\hat{H}$ (Fig. 31). Figure 31 shows that the leeward velocity is typically 2 to 3 times the upstream velocity! Later, it will be shown that $\hat{s}$ can be even greater, with favourable topography. Under the circumstances, it is not surprising that downslope wind gusts of up to 60 *m/s* have been recorded (Durran, 1986b). Since $\hat{s}$ is evidently well approximated by

$$\hat{s} = 2\hat{H}^{2/3} + 1 \tag{27}$$

and therefore

$$\begin{aligned} u_1 &= u_0 + 2u_0\hat{H}^{2/3} \\ &= u_0 + 2N_0^{2/3}H^{2/3}u_0^{1/3} \, . \end{aligned} \tag{28}$$

Thus, for a high-drag regime, u_1 increases with each of N_0, u_0 and H. For example, with $u_0 = 20$ *m/s*, $N_0 = 0.01s^{-1}$ and $h = 1.2$ *km*, then $u_1 = 48$ *m/s*. These are plausible values for the well-known chinook windstorms of Boulder, Colorado.

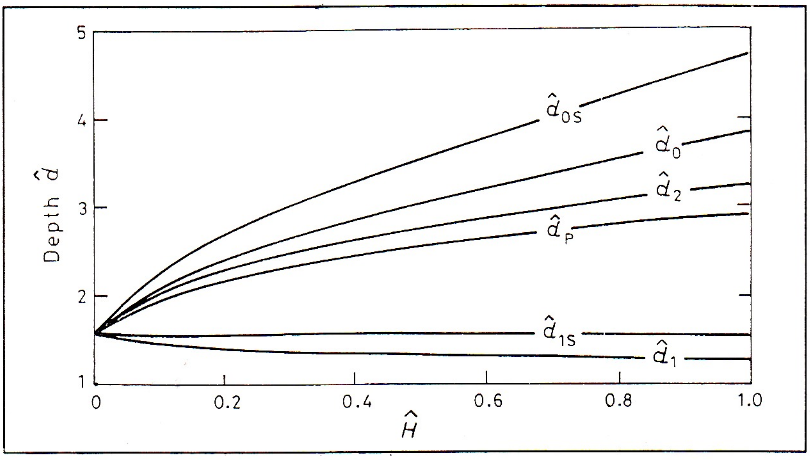

Fig. 30 Plots of $\hat{d}_0$, $\hat{d}_1$, $\hat{d}_2$, $\hat{d}_p$, $\hat{d}_{0s}$ and $\hat{d}_{1s}$ against $\hat{H}$.

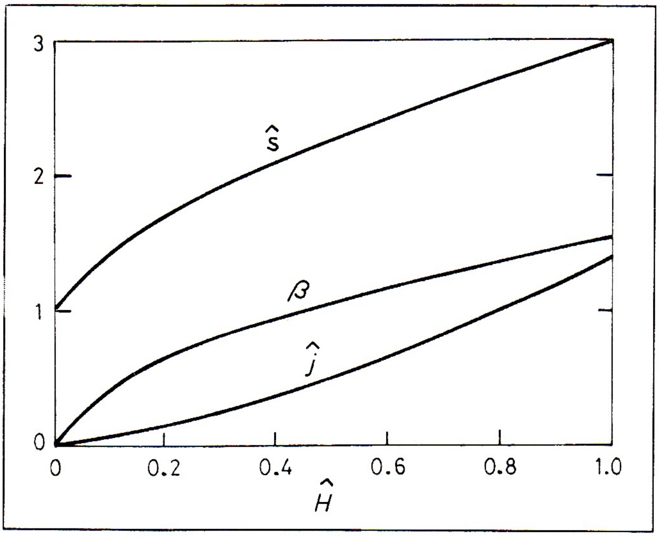

Fig. 31 Plots of jump strength β, wind-speed amplification $\hat{s}$ and turbulence intensity $\hat{j}$ against $\hat{H}$.

4.1.5 The jump

If it is assumed that the jump is stationary at $x = \alpha$ and that the leeward and windward plains are at the same altitude, then the characteristics of the jump in terms of the upstream parameters are easily determined. The basis for the assumption that the jump associated with self-initiating transitional flow is located at the point $x = \alpha$ is that that point is the first leeward point where $h = 0$. The strongest possible stationary jump occurs at this point: stronger jumps propagate downstream; weaker jumps are stationary on the leeward slopes. Thus this discussion on jumps in steady-state flow configuration relates only to the strongest (that is, biggest) jumps. This restriction is applicable only to the results of subsections 4.1.5 and 4.1.6. From conventional single-layer theory it is known that

$$\frac{d_2}{d_1} = \frac{1}{2}\sqrt{1 + 8F_1^2} - \frac{1}{2} \qquad (29)$$

where F_1 is the Froude Number immediately before the jump. A derivation of Eqn 29 is provided in Appendix B. Adapting Eqn 29 to the Q1$^1/_2$ model, we then find (after some manipulation) that

$$\frac{\hat{d}_2}{\hat{d}_1} = \frac{1}{2}\sqrt{1 + 2\pi^2\frac{\hat{d}_0}{\hat{d}_1^3}} - \frac{1}{2}\,. \qquad (30)$$

Thus, $\hat{d}_2$ is seen to be a function of $\hat{H}$ and is also graphed in Fig. 30. Note that $\hat{d}_2$ is always less than $\hat{d}_0$, because energy is lost in the jump. Following Lighthill (1978), the strength of the jump, β, is defined by

$$\beta \equiv \frac{d_2 - d_1}{d_1} = \frac{\hat{d}_2 - \hat{d}_1}{\hat{d}_1} \tag{31}$$

and β is therefore also a function of $\hat{H}$ (as shown in Fig. 31) and can be approximated by

$$\beta = 1.5\sqrt{\hat{H}} \tag{32}$$

showing that it increases with either of N_0 or H but decreases with u_0. Of course, if the jump is positioned at some point up the hill, the energy losses, $\hat{s}$ and β are decreased. The energy is dissipated by either dispersive short waves downstream from the jump or by turbulence at the jump face. It is of course the turbulent type of jump which is of especial relevance to aircraft. For $\beta > 0.75$ turbulence is the main agency of energy loss for water flow. The corresponding value of β for two-layer flow is probably significantly greater but not yet established accurately (Rottman and Simpson 1989). It is speculated here that for stratified flow the threshold value of β is 1.38 which from Eqn 32 would imply that $\hat{H} = 0.85$. That is, possibly $\hat{H}_T$ turns out to be 0.85 *because* β_T is 1.38. Once β_T is ≥ 1.38 then sufficient turbulent mixing would sustain the decoupling between the hydraulically-active lower layer and the well-mixed passive layer (passive in the hydraulic sense).

The energy dissipation rate per unit breadth of the jump, e, at either type of jump is given by Lighthill (1978) as

$$e = \rho u_1 g' \frac{(d_2 - d_1)^3}{4d_2} \tag{33}$$

where ρ is density. For a turbulent jump, the dissipation rate *per square metre of jump face* is defined here as the turbulent intensity, j such that

$$j \equiv \frac{e}{d_2 - d_1}. \tag{34}$$

Therefore, after some algebraic manipulation, we find that

$$j = \frac{\rho u_0 N_0^2 d_0^2 (d_2 - d_1)^3}{\pi^2 d_1 d_2}. \tag{35}$$

Define normalised turbulent intensity, $\hat{j}$, by

$$\hat{j} \equiv \frac{j}{\rho u_0^3} \tag{36}$$

then

$$\hat{j} = \frac{\hat{d}_0^2 (\hat{d}_2 - \hat{d}_1)^2}{\pi^2 \hat{d}_1 \hat{d}_2}, \tag{37}$$

$\hat{j}$ is a function of $\hat{H}$ (see Fig. 31) and is approximated by

$$\hat{j} = 1.4\hat{H}^{3/2}, \tag{38}$$

and thus,

$$j = 1.4\rho\,(N_0 H u_0)^{3/2}. \tag{39}$$

It is therefore expected that as any of N_0, H, or u_0 increase, then the intensity of turbulence at the jump face increases; this result is certainly intuitively reasonable. Of course, if the jump remains undular then it is the amplitude of the undularities which will increase.

4.1.6 Wave drag

It is convenient to define a normalised wave drag, $\hat{r}$, as

$$\hat{r} \equiv \frac{rN_0}{\rho u_0^3} \tag{40}$$

where r denotes wave drag. Other common terms used to describe this quantity are mountain drag, mountain wave drag, pressure drag and gravity-wave drag. The wave drag, r_L, associated with linear waves over a symmetric mountain is given by (e.g. Gill 1982)

$$r_L = \frac{1}{4}\rho\pi N_0 u_0 H^2, \tag{41}$$

so that

$$\hat{r}_L = \frac{1}{4}\rho\hat{H}^2. \tag{42}$$

Assuming that any jump on the lee side is stationary and located at $x \geq \alpha$, then, for the Q1$\frac{1}{2}$ model, the normalised drag, $\hat{r}$, is (see Appendix C)

$$\hat{r} = \frac{2\hat{d}_0^3}{\pi^2}\left(1 - \frac{1}{\hat{s}^2}\right) - \hat{d}_0(\hat{s} - 1) \tag{43}$$

The graphical comparison in Fig. 32 shows that this drag is more than three times the linear drag. Values from BP and DK are also plotted, and it is clear that these compare quite well with the Q1$\frac{1}{2}$ model drag. Since $\hat{r}$ can be approximated closely by the curve $26\hat{H}^{1.95}$ and the latter exponent can be rounded to 2.0, it follows that

$$r \approx 3.3r_L. \tag{44}$$

Thus $\hat{r}$ increases with any of N_0, u_0 or H.

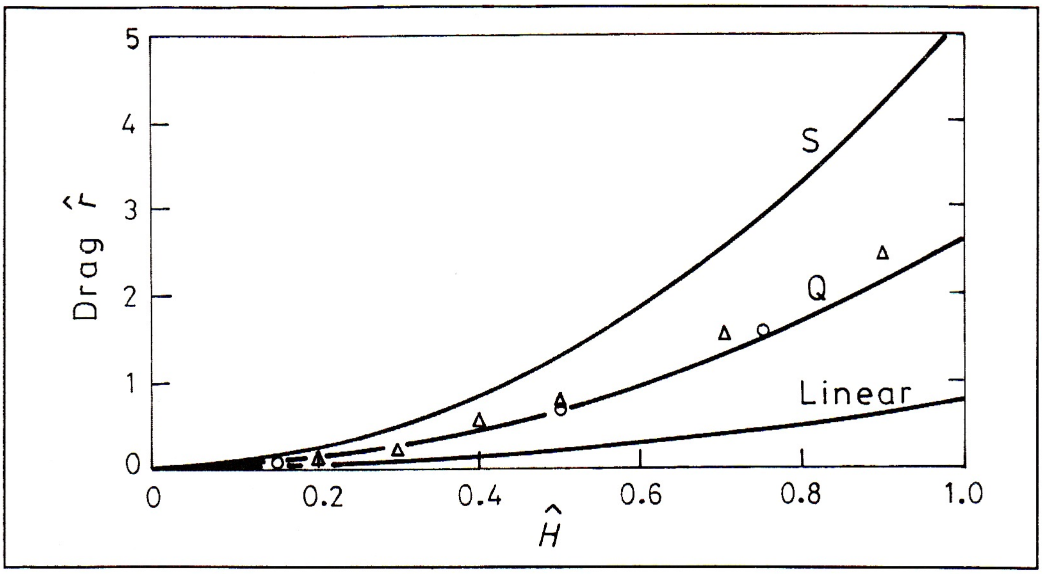

Fig. 32 Nondimensional drag, $\hat{r}$, for S85 (labelled S), Q1½ model (labelled Q) and linear waves compared as functions of $\hat{H}$ with spot values from numerical experiments by Durran and Klemp (1987) (triangles) and Bacmeister and Pierrehumbert (1988) (circles).

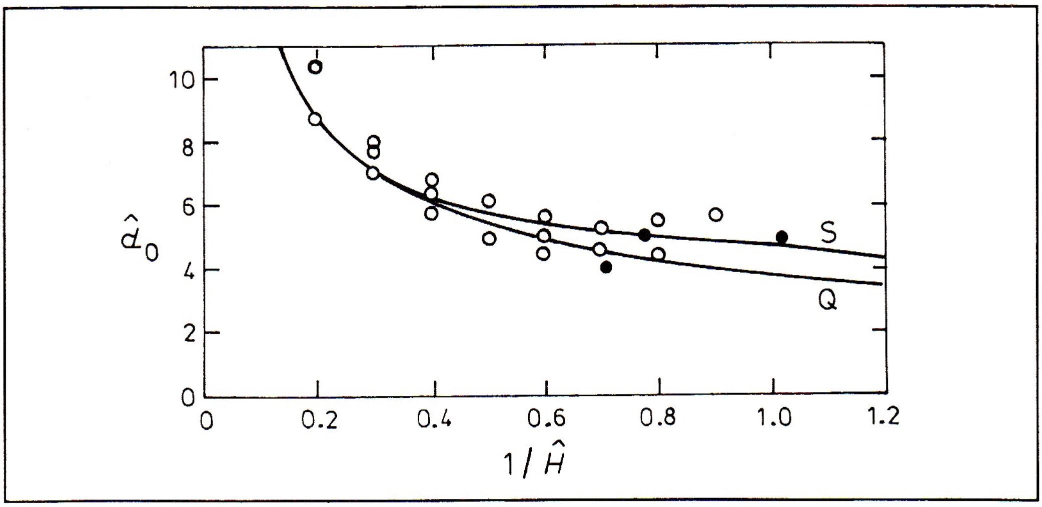

Fig. 33 Model solutions of $\hat{d}_0$ for Q1½ and S85/SS87 as a function of $\hat{H}^{-1}$ with spot values from tank experiments (unfilled circles) and numerical experiments (filled). The spot values and S85/SS87 curve are from Rottman and Smith (1989).

4.2 Comparison with Smith's model

The main difference between the assumptions of S85 and Q$1^{1}/_{2}$ is that S85 does not assume that the velocity in the hydraulically active layer is constant with height. Partly because of this, S85 makes no comment regarding any eventual rebound of the accelerated flow. The predictions of S85 and Q$1^{1}/_{2}$ for both $\hat{d}_0$ and $\hat{d}_1$ are fairly close (see Fig. 30) with the Q$1^{1}/_{2}$ values being up to 10-20% lower. From data provided in S85, it is easily shown that, at least to good approximation,

$$\hat{d}_{os} = \pi \hat{H}^{2/3} + \frac{\pi}{2} \tag{45}$$

where the subscript 's' denotes S85 model. This is similar to the Q$1^{1}/_{2}$ approximation at Eqn 20 and its simple form suggests that an alternative derivation to that given by S85 and SS87 is possible. However, this has not been attempted herein.

Values for d_0 from the numerical models are known to accord fairly well with S85 values, which in turn are about 10-15% higher than the Q$1^{1}/_{2}$ values (see Fig. 30). However, the vertical resolution in the models is usually about 200 to 350 *m* and this is too coarse to determine clearly whether S85 or Q$1^{1}/_{2}$ gives the better estimate. Rottman and Smith (1989) compared predictions of $\hat{d}_0$ from the model of S85 and SS87 with their tank experiment results and with some numerical model results from the literature. Figure 33 shows the S85 $\hat{d}_0$ value, the tank results, the numerical model results (adapted from Rottman and Smith) and the Q$1^{1}/_{2}$ model predictions for $\hat{d}_0$. Obviously, the Q$1^{1}/_{2}$ values compare extremely well with the experimental data; but S85 ones are equally as good.

Interestingly, the speed-up factor, $\hat{s}$, is effectively identical for both models. For example, at $\hat{H} = 1$ the S85 value is 3.017 (from SS87) compared to 3.022 for the Q$1^{1}/_{2}$ model. This implies that the layer mean wind $\hat{s}u_0$ over the lee foot of the hill is virtually identical in each case.

S85 has multiple higher-order solutions of the form $\hat{d}_0 + 2n\pi$, where $n = 0,1,2,...,$ and these appear to correspond approximately to the well-elevated but narrow bands of environmental critical-layer positions associated with a weak tendency to initiate transitional flow. Q$1^{1}/_{2}$ has multiple higher-order solutions of the very approximate form $\hat{d}_0 + n\pi$ where $n = 0,1,2,...$ Compared to S85, Q$1^{1}/_{2}$ has too many solutions in as much as those for odd n are invalid. More importantly, this points to a specific area in which to test Q$1^{1}/_{2}$ against S85 using numerical and tank models. Even so, it seems that at least for the Adelaide gully-winds where, as shown in Chapter 3, d_0 is less than about $2h$, then the higher terms are not of practical significance.

For S85, the drag, r_s, is given by

$$r_s = \frac{\rho}{6} N_0^2 (d_0 - d_1)^3 \tag{46}$$

or, equivalently,

$$\hat{r}_s = \frac{1}{6}(\hat{d}_0 - \hat{d}_1)^3 = \frac{1}{6}\left(\hat{d}_0 - \frac{\pi}{2}\right)^3 \tag{47}$$

where the subscript S denotes S85 values. $\hat{r}_S$ is graphed as a function of $\hat{H}$ in Fig. 32, where it is seen to be significantly greater than that of the Q1½ model. In comparison with the numerical model results, S85 overpredicts the drag by a factor of 2, and this indicates, through Eqn 47, that it overestimates $\hat{d}_0$ by about 15%. As mentioned, the vertical resolution of the numerical models is such that this is not easily verifiable, at least from results in the literature.

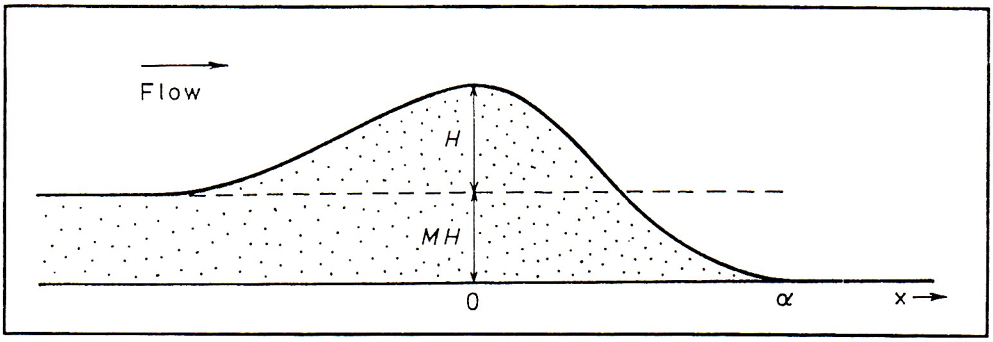

Fig. 34 The defining sketch for M. The topography has been modified in such a way that the lee plains are lower than the windward ones.

4.3 Topographic effects

Now let us consider the topographic case in which the lee plains are lower than the windward plains by an amount MH, where M is defined as $(h_{-\infty} - h_{+\infty})/H$, as in Fig. 34. In such a case, $h = -MH$ and $d = d_1$ at $x = \alpha$, so that Eqn 23 yields

$$\frac{\pi^2 u_1^2}{8N_0^2 d_0} + d_1 - MH = k_0 \qquad (48)$$

so in similar fashion to the derivation of Eqn 25, we can find that

$$\frac{1}{2}\left(\frac{\pi}{2\hat{d}_1}\right)^2 + \frac{\hat{d}_1}{\hat{d}_0} - \frac{M\hat{H}}{\hat{d}_0} = \frac{1}{2}\left(\frac{\pi}{2\hat{d}_0}\right)^2 + 1\ . \qquad (49)$$

In this case, $\hat{d}_1$ and hence, $\hat{s}$, β and $\hat{j}$ are functions of $(M,\hat{H})$ (see Fig. 35). In particular it is evident that u_1, β, and $\hat{j}$ increase with M, that is, with a 'dropped' lee plain. This result is intuitively reasonable and consistent with the occurrence of chinook windstorms along the Front Range in Colorado.

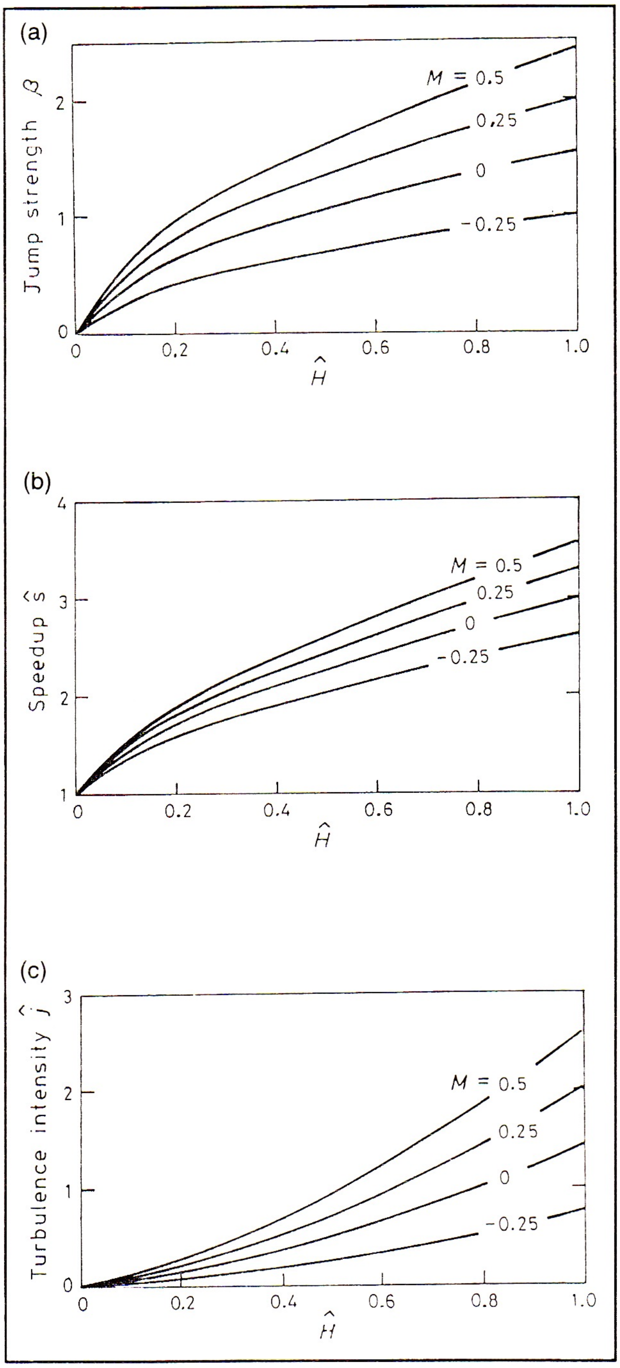

Fig. 35 Plots of (a) jump strength, β, (b) wind-speed amplification $\hat{s}$ and (c) turbulence intensity $\hat{j}$ against $\hat{H}$ for various values of M.

Now consider a symmetric range comprising a string of linked conical hills as in Fig. 36. The relevant feature of cross-range flow is that there are two extreme possibilities, namely, valley-valley (VV) flow or spur-spur (SS) flow. For valley-valley flow, Arakawa (1969) extended the conventional hydraulic theory and this extension may be applied to the $Q1^1/_2$ model. Consequently, Eqn 18 (with $n = 1$) becomes

$$\left(\frac{\pi}{2\hat{d}_0}\right)^2 - 3\left(\frac{\gamma\pi}{2\hat{d}_0}\right)^{2/3} + 2\left(1 - \frac{\hat{H}}{\hat{d}_0}\right) = 0 \qquad (50)$$

where $\gamma \equiv m_c/m_0$ and is greater than one, and m_c is the (two dimensional) mass flux at the crest. The parameter, γ, may be regarded as a valley funnelling factor. Sufficiently far downstream, the flux, m, again equals m_0. Arakawa has shown that the windward convergence/leeward divergence in such flow implies that the valleys experience more violent downslope winds than the spurs. More recently, Pettre (1982) has used the concept to model successfully the Rhone Valley winds, and Grace (1991) used a similar idea to model transitional flow through Backstairs Passage (see section 3.7). Strictly speaking, Arakawa's model applies to an homogeneous layer bounded by vertical valley walls. However, it seems reasonable to apply it qualitatively to the $Q1^1/_2$ model. The concept may be extended to SS flow ($\gamma < 1$) where windward divergence/leeward convergence is expected. It is reasonable to assume that all other flows normal to the range will lie between the VV and SS cases. Equation 50 shows $\hat{d}_0$ to be a function of $\hat{H}$ and γ. Interestingly enough, transitional flow may occur with $\hat{H} = 0$. The fact that $\hat{d}_0$ increases with γ, is a result consistent with Arakawa's findings relating to F_0 in the homogeneous layer case.

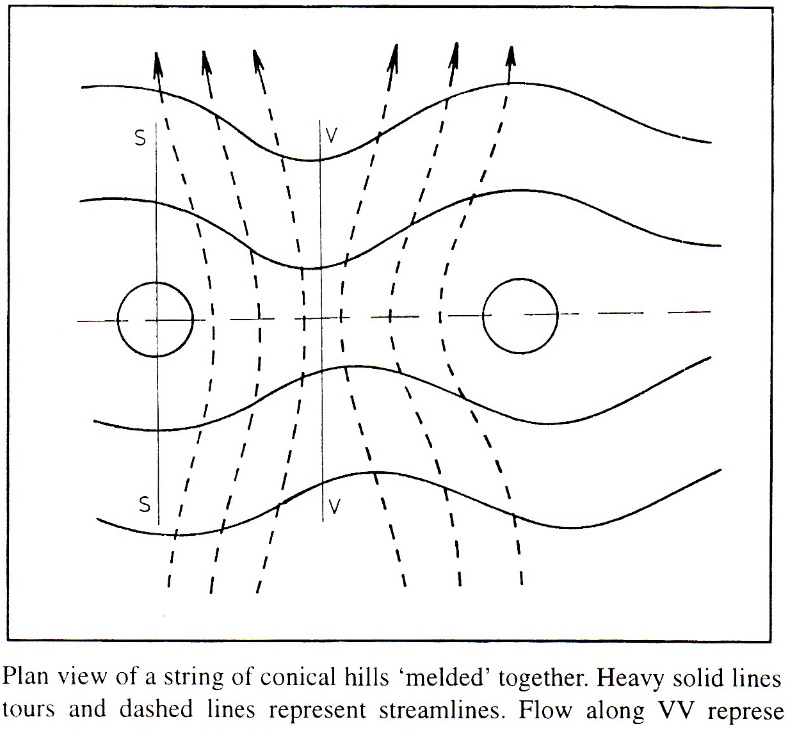

Fig. 36 Plan view of a string of conical hills 'melded' together. Heavy solid lines are contours and dashed lines represent streamlines. Flow along VV represents flow through a valley while SS represents flow along the highest path or spur line.

If the valley mouth, the jump, and the point where m again equals m_0, are all collocated at $x = \alpha$ then, as with the lower lee-plain effect, each of $\hat{d}_1, \hat{s}, \beta$ and $\hat{j}$ may be determined as functions of $\hat{H}$ and γ (see Fig. 37 - but note that $\hat{d}_1$ not shown). Of special interest is the fact that u_1, β and $\hat{j}$ increase with γ, that is, with valley-valley flow. This is a similar effect to that found with lower leeside plains – again, an intuitively expected result. The occurrence of Antarctic 'katabatics' is also consistent with this result.

4.4 Critical-layer effects

4.4.1 Development

The numerical experiments of DK and BP show that even for subcritical mountains (those with $\hat{H} \leq \hat{H}_T$), the high-drag regime may occur if the model atmosphere has an environmental critical-layer. For conventional single-layer hydraulic flow, Houghton and Kasahara (1968) (hereafter HK) have shown that, in reference to their diagram (see Fig. 38), transitional flow occurs when Domain IIa or IIb applies, but does not occur for Domain I. In Domain IIb, propagating jumps are expected whereas, in IIa, the jumps are stationary above a point on the lee slope at which h/H corresponds to the dashed isopleth value. An advantage of the Q1$^1/_2$ model is that this diagram may be adapted by assuming that the environmental critical-layer is analogous to the free surface in the single-layer model of HK and that the appropriate g' for the layer is given by Eqn 14 with $n = 1$. By way of precedent, it is noted that Klemp and Durran (1987) successfully applied HK's diagram to the case of a strong inversion layer embedded in an otherwise continuously stratified atmosphere in order to demonstrate the hydraulic-like character of the flow simulated by their numerical model. They did, however, use a modified gravity calculated by setting the mid-layer θ value to the average θ value for the layer. This led to

$$g' = \frac{1}{2}N_0^2 d_E \qquad (51)$$

in contrast to that of the Q1$^1/_2$ model, in which (from Eqn 14)

$$g' \approx \frac{4}{\pi^2}N_0^2 d_E = 0.4N_0^2 d_E \qquad (52)$$

where d_E is the environmental critical-layer height far upstream. The vertical axis of Fig. 38 in the HK model is the Froude number of the single-layer far upstream, and this is equivalent to $^1/_2\pi/\hat{d}_E$ in the Q1$^1/_2$ model. The horizontal axis is the ratio of the mountain height to the single-layer depth far upstream and this becomes H/d_E or $\hat{H}/\hat{d}_E$. The special case $\hat{d}_E = \hat{d}_0$ coincides with the jump/no jump boundary between Domains I and IIa. Defining d_P to be that value of d_E for which the jump is stationary at $x = \alpha$ (where $h = 0$) corresponding to the boundary of IIa/IIb, it can be mapped from HK's diagram (Fig. 38) and may therefore be regarded as a function of $\hat{H}$ (Figs 30 and 39).

4.4.2 Results

There are three situations for a subcritical mountain height. The first is that there is no transitional flow if $\hat{d}_E > \hat{d}_0$. Otherwise, if $\hat{d}_E < \hat{d}_0$ then upstream adjustment occurs with a bore propagating indefinitely upstream. The values of d_E, N_0, u_0 (but notably *not* g', which is unchanged) are thus effectively modified by the flow itself to set up transitional flow with a leeside hydraulic jump. The second situation is that if $\hat{d}_P < \hat{d}_E < \hat{d}_0$, then stationary jumps occur on the lee slope. Thirdly, if $\hat{d}_E < \hat{d}_P$ then jumps propagate downstream over the lee plain. This compares well with

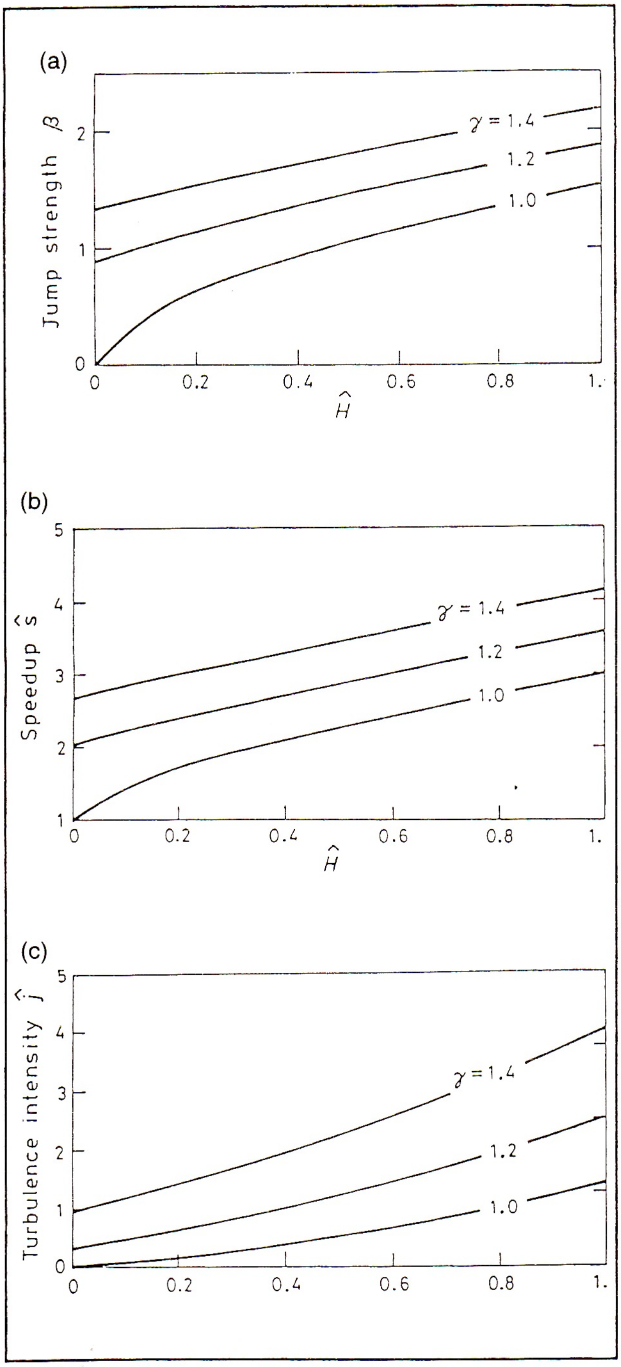

Fig. 37 Plots of (a) jump strength, β, (b) wind-speed amplification $\hat{s}$ and (c) turbulence intensity $\hat{j}$ against $\hat{H}$ for various values of γ.

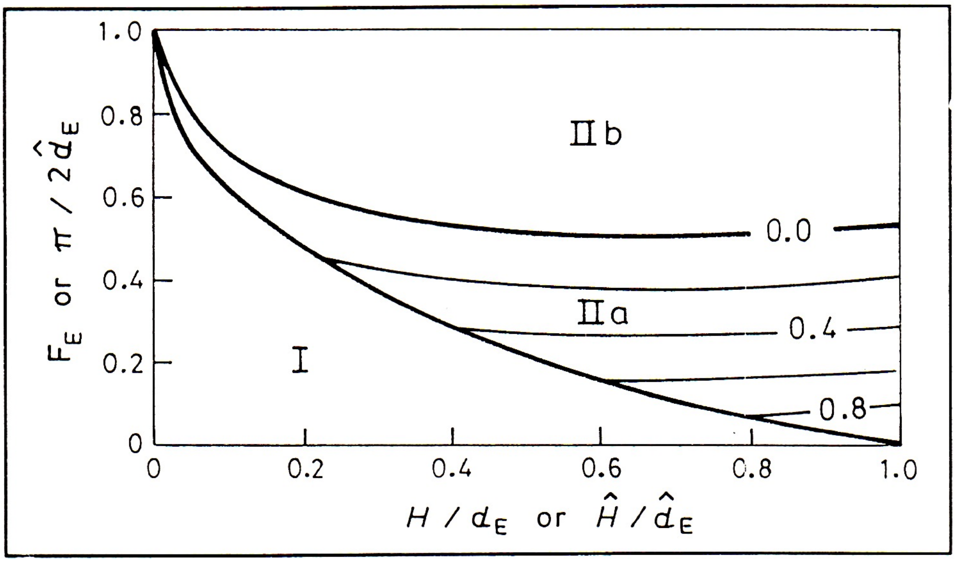

Fig. 38 Adaptation of the diagram of Houghton and Kasahara (1968) for transitional and nontransitional flow regimes to the Q$1^1/_2$ model.

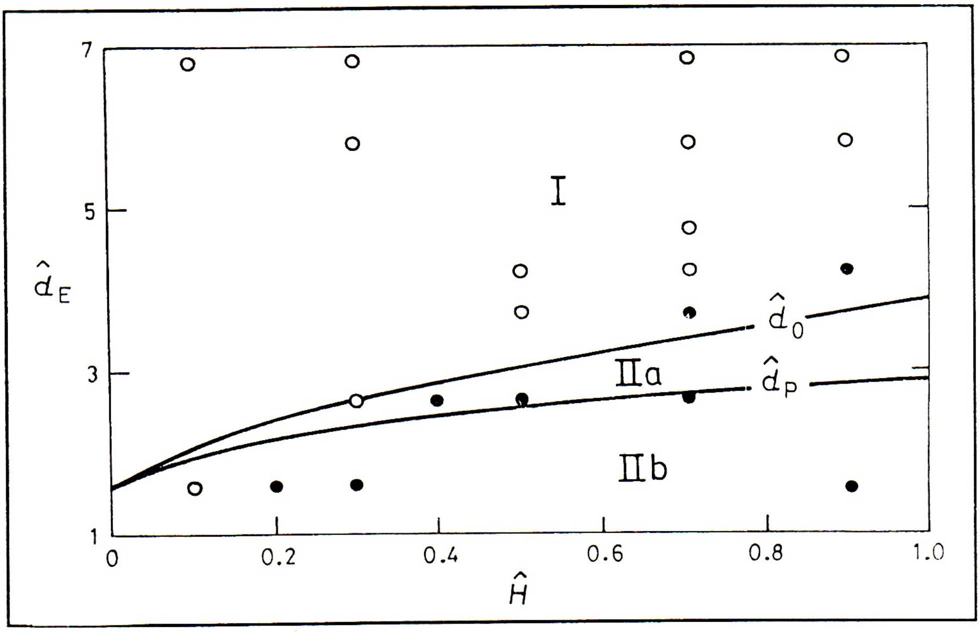

Fig. 39 Comparison of the results of Durran and Klemp (1987) for high drag (filled circles) and low drag (hollow circles) events with Q$1^1/_2$ predictions.

the numerical model results. Unfortunately, there is some ambiguity in the precise definition of d_E, as we do not know whether it should be taken to be at the top, bottom, or some mid-point of an environmental critical-layer. If the bottom is selected, however, there is then reasonable agreement between the numerical and $Q1^1/_2$ models.

4.4.3 Comparison with Durran & Klemps's numerical results

The agreement between $Q1^1/_2$ and other models is illustrated by the plot of high-and low-drag regimes from DK's simulations given in Fig. 39. There is a one-to-one correspondence between high-drag regimes and downslope wind events (DK). The $Q1^1/_2$ model predicts that if $\hat{H} < \hat{H}_T$ then the curve $\hat{d}_E = \hat{d}_0$ separates the two drag regimes (low drag above, high drag below), and assumes that if $\hat{H} \geq \hat{H}_T$ then high drag occurs regardless of $\hat{d}_E$. From this point of view, the $Q1^1/_2$ predictions are therefore quite good.

The lowest plot at $\hat{H} = 0.1$ showing a low-drag regime is an apparent discrepancy, but is arguably a high-drag regime on the grounds that BP's simulated outcome for $\hat{H} = 0.08$ was one of high drag. BP suggested that their different result was because their simulated run time was significantly greater. In BP's simulations, an hyperbolic-tangent wind profile was used and so any selection of a bottom point in the environmental critical-layer would have been quite arbitrary. A detailed comparison with their results has therefore not been attempted herein. The numerical models indicate that there are also well-elevated but narrow bands for d_E (above 13 *km*) which have a weak tendency to initiate transitional flow.

4.5 Summary

An important assumption in the model is that the hydraulically active layer can be approximated by a single homogeneous layer; in effect, the flow velocity is assumed uniform with height. This assumption allows the application of a comprehensive body of well-established single-homogeneous-layer hydraulics. It appears justified *a posteriori*, since the model results compare reasonably well with S85 and quite well with sophisticated numerical models.

It was shown that as each of N_0, H and u_0 increases, so too does u_1. For turbulent jumps, increasing N_0, H or u_0 increases j, the intensity of turbulence at the jump face. For undular jumps, increasing N_0, H, or u_0 increases the amplitude of the dispersive short wave undularities associated with a jump. In a speculative vein, since jump strength, β, was shown to be a monotonically increasing function of normalised mountain height, $\hat{H}$, it appears that increasing $\hat{H}$ increases the likelihood that β will exceed a threshold value, β_T, and therefore that the jump will become turbulent. In this respect, β_T could be linked to $\hat{H}_T$in such a way that self-sustaining decoupling occurs – a concept similar to that of PC.

Consideration of the relative elevation of the lee-side plain showed that turbulence intensity, the jump strength and u_1 increased with a lower lee-side plain. A similar effect was found for funnelling due to valley-valley flow. It is therefore expected that valley-valley topography with lower lee-side plains (relative to the windward plains) will be especially prone to strong downslope winds.

In comparison with S85, $Q1^1/_2$ underpredicts $\hat{d}_0$ by up to 10-20% although, within resolution limitations, both compare well with numerical and tank-model results. Drag estimates from the $Q1^1/_2$ model are 50-60% of the S85 estimates. The $Q1^1/_2$ drag compares very well with the numerical models. Compared to S85, $Q1^1/_2$ has 'twice too many' higher-order solutions for $\hat{d}_0$. Interestingly, the speed up factor, $\hat{s} = d_0/d_1$ is effectively identical for both models, implying the same layer-mean speed over the lee plains.

In the model, a high-drag regime is assumed to self-initiate if $\hat{H} \geq \hat{H}_T$. However, if $\hat{H} < \hat{H}_T$, then the model predicts that a high-drag regime is initiated if an environmental critical-layer is located below or at d_0 (that is, $d_E \leq d_0$). Overall, the very simple Q$1^1/_2$ model therefore yields results similar to those of the sophisticated numerical models when simple upstream profiles are specified.

CHAPTER 5

A MODEL OF GUST PERIODICITY

5.1 Background

A feature of downslope winds is their directional steadiness and the gusty nature of the speed. A striking exception is the Antarctic 'katabatic', which is renowned for its steadiness of both direction and speed. Boras of Yugoslavia tend to have a quasi-periodicity of 3 to 4 minutes, although periods of 3 to 11 minutes have been reported. Lidar observations by Nieman et al. (1988) of a Boulder windstorm showed a tendency for gusts and surges to occur with periods of 3 to 4 minutes and of 14 minutes. Scinocca and Peltier (1989) performed experiments on Peltier and Clark's numerical model using a much larger domain than in previous experiments. They were able to demonstrate quasi-periodic transience in the wind speed in the 5 to 15 minute range, and attributed it to the breaking of the topographically forced internal waves.

5.2 Development

For stratified fluid the vertically propagating internal gravity waves have a frequency of oscillation (in the vertical) of $\frac{1}{2}N/\pi$. Horizontally propagating waves in otherwise still fluid have a speed, c, given by

$$c = 2N\frac{d}{\pi} \qquad (53)$$

and a frequency of oscillation f (in hertz) of oscillation in the vertical given by

$$\left.\begin{aligned} f &= \frac{c}{\lambda} \\ &= \frac{2Nd}{\pi\lambda} \end{aligned}\right\} \qquad (54)$$

where λ is the wavelength. We assume that topographic irregularities induce internal gravity-waves in the continuously-stratified fluid. If we further assume that an (unspecified) mechanism due to resonance causes the vertically-propagating waves to feed energy to the horizontally-propagating waves, then, of all the possible combinations of frequencies, the one where the two types of waves have the same frequency is the most important. So suppose that the horizontal waves somehow 'tune' to the same frequency as the internal waves: after all, they are both oscillating in the vertical; then

$$\lambda = 4d. \qquad (55)$$

Superimposing a flow speed of u, then the local frequency becomes

$$\left.\begin{aligned} f &= \frac{u \pm c}{\lambda} \\ &= \frac{u}{4d} \pm \frac{N}{2\pi} \\ &= \frac{\pi u \pm 2Nd}{4\pi d} \; . \end{aligned}\right\} \qquad (56)$$

The dual values of *f* are positive when

$$\left.\begin{aligned} &\pi u > 2Nd \\ &\frac{\pi u}{2Nd} > 1\mu \end{aligned}\right\} \qquad (57)$$

that is, when $F > 1$ (see Eqn 16); which (as expected) states that waves in the supercritical region of the fluid cannot travel upstream. Denoting leeside parameters by the subscript 1, a special case of Eqn 56 is

$$f = \frac{u_1}{4d_1} \pm \frac{N_1}{2\pi} \; . \qquad (58)$$

A property of the Q1$^1/_2$ model is that

$$\left.\begin{aligned} \hat{s} &\equiv \frac{u_1}{u_0} \\ &= \frac{d_0}{d_1} \\ &= \frac{N_1^2}{N_0^2} \; . \end{aligned}\right\} \qquad (59)$$

Multiplying Eqn 58 by $2\pi/N_0$ and using Eqn 59 then

$$\frac{2\pi f}{N_0} = \frac{\pi \hat{s}^2}{2\hat{d}_0} \pm \sqrt{\hat{s}} \qquad (60)$$

and hence

$$f = N_0\left(\frac{\hat{s}^2}{4\hat{d}_0} \pm \frac{\sqrt{\hat{s}}}{2\pi}\right) . \qquad (61)$$

5.3 Results and discussion

From Fig. 31, values of $\hat{s}$ are in the range 2 to 3 and $\hat{d}_0$ is in the range 2.5 to 4. Choosing as typical, $\hat{s} = 2$ and $\hat{d}_0 = 3$ and $N_0 = 0.01s^{-1}$ then $f = (0.56 \pm 0.10)\,10^{-2}s^{-1}$ corresponding to periods of 3 min and 17 min.

By using Eqns 20 and 27, namely,

$$\hat{d}_0 \approx 2.3\hat{H}^{2/3} + \frac{\pi}{2} \qquad (62)$$

and

$$\hat{s} = 2H^{2/3} + 1 \qquad (63)$$

it is evident that f is a function of $(N_0, \hat{H})$ which may be expressed as a plot. More conveniently, if we define the period by $P = f^{-1}$ and then plot P against H/u_0 for selected values of N_0, we obtain the diagram shown in Fig. 40. It is apparent that for $\hat{H} = 0.5$ and $N_0 = 0.01s^{-1}$, the leeside periodicities expected are 3 and 17 minutes. In view of the periods actually observed, these are very reasonable values. It is also apparent that the shorter (longer) period decreases (increases) with increasing mountain height.

Such reasonable results indicate the plausibility, at least, of the hypothesised resonance interaction, whereby internal gravity-waves, induced by topographic irregularities, feed energy to the horizontal waves. The fact that the Antarctic downslope winds are exceptional in their steadiness could be due to the presence of a relatively smooth and friction-free ice surface.

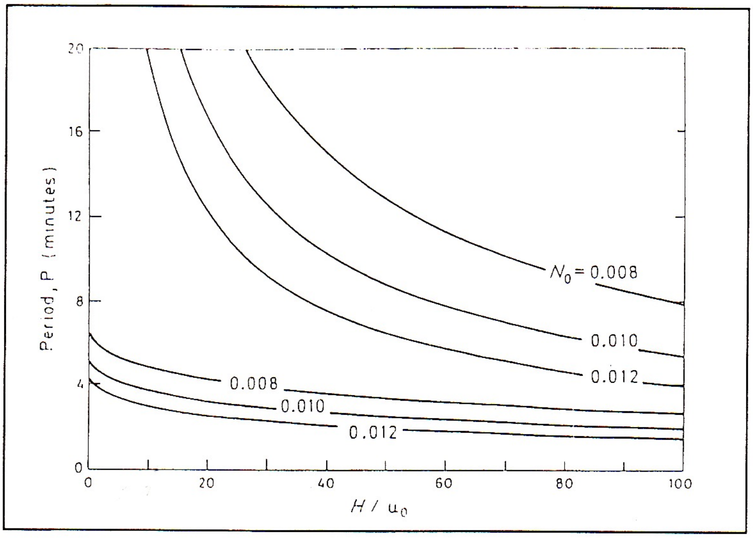

Fig. 40 Plot of the dual periods in minutes against H/u_0 and N_0.

CHAPTER 6

THE TIME-DEPENDENT 1½-LAYER MODEL (QT)

6.1 Background

For continuously-stratified flow with an environmental critical-layer positioned below $\hat{d}_0$, the flow is hydraulic in nature (BP). For many downslope winds (e.g. the bora and the Adelaide gully-wind especially), the height of the environmental critical-layer, or discontinuity, is well below $\hat{d}_0$, so that it is unlikely that PC's mechanism is important therein. To clarify this point, it is noted that Peltier and Clark's mechanism predicts a decoupling height, $\hat{d}_0$, close to that of S85 and Q1½, so the predicted value of d_0/H is about 5 (see Fig. 29). However, observations of several events (see Figs 4, 20 and 22) show that the decoupling heights are much lower.

In these circumstances, it is natural to ask whether the steady-state Q1½ model can be extended to include frictional and Coriolis forces and temporal variations. The answer is in the affirmative and the model developed herein (for convenience hereafter referred to as the QT model) is a variant of those presented by Houghton and Kasahara (1968), Parrett and Cullen (1984) and Baines and Leonard (1989). In this model, the value of g' is determined as appropriate from either Eqn 12 (for a homogeneous layer) or Eqn 14 (for a continuously-stratified layer). At relatively low resolution, say 100 to 200 grid-points, it is capable of running in an interactive mode on a desktop computer. A floppy-disk version suitable for a '386' PC with a numeric coprocessor is included with this thesis.

Typically all three models above consider an obstacle of height H perturbing the otherwise uniform flow of a homogeneous layer of initial height d_0. The fluid is impulsively started with an initially free-standing surface and in all cases (to the author's knowledge, at least) $d_0 > H$.

The model developed here will be used to investigate two 'archetypal' situations: first, a geostrophic flow perturbed by topography (Type I) and second, a very shallow layer (where $d_0 < H$) initially flowing parallel to a mountain range and not in geostrophic balance (Type II). The simulations are relevant to the case studies of Chapter 3.

6.2 Development

The appropriate starting equations are the shallow-water equations as presented by, for example, Pedlosky (1987) with additional quadratic drag terms. These are the two horizontal momentum equations and the mass conservation equation, namely:

$$u_t + uu_x + vu_y + gh_x + gd_x - fv + \frac{C_D U u}{d} - P_x - EV(u_A - u) = 0 \qquad (64)$$

$$v_t + uv_x + vv_y + gh_y + gd_y + fu + \frac{C_D U v}{d} - P_y - EV(V_A - v) = 0 \qquad (65)$$

$$d_t + (ud)_x + (vd)_y = 0 \qquad (66)$$

where (u,v) is the fluid velocity in the lower layer, U is the magnitude of that velocity, (u_A,v_A) is the fluid velocity in the upper layer, V is the magnitude of the shear between the layers, $h(x,y)$ is topographic height, $d(x,y)$ is fluid depth, f is the Coriolis force (negative in the Southern Hemisphere), C_D and E are surface and interfacial drag coefficients, and P_x and P_y represent external pressure-gradient forces in the x and y directions. Subscripts x, y, t denote differentiation. The interfacial drag is the drag between the lower and upper layers. It is analogous to surface drag but unlike surface drag does not necessarily have a retarding effect. In the case of a fast-flowing upper layer, for instance, the interfacial drag could act to accelerate the lower layer.

It is these equations, without the drag terms, which are the basis of the well-known conservation of potential vorticity rule and this in turn provides a qualitative check upon the results. Before proceeding, the assumptions are made explicit.

The underlying assumptions are that a layer of fluid (usually thought of as water) is incompressible and of constant density; the layer has an aspect ratio (defined as that of the vertical to the horizontal scale) very much less than unity. The hydrostatic assumption (that the distribution of pressure with respect to height is unaffected by vertical motion in the fluid) is also invoked. Usually g is replaced by Eqn 12 ($g' = g\delta\theta/\theta_0$) for the case of a shallow homogeneous layer but, as shown earlier, it would seem reasonable to replace g according to Eqn 14 ($g' = 4N^2d/\pi^2$) in the case of a shallow continuously stratified layer.

Now consider a mountain range invariant in the north-south direction associated with a flow for which u_y, v_y and d_y are zero. In this case, the three equations reduce to

$$u_t + uu_x + g\,(h+d)_x - fv + \frac{C_D U u}{d} - P_x - EV\,(u_A - u) = 0 \tag{67}$$

$$v_t + uv_x + fu + \frac{C_D U v}{d} - P_y - EV\,(v_A - u) = 0 \tag{68}$$

$$d_t + (ud)_x = 0. \tag{69}$$

It is always possible to derive an energy equation from the two horizontal momentum equations. Since hydraulic jumps with energy losses are anticipated, it is clear that energy will not be conserved. For this reason, then, we shall work with the flux form of the momentum equations. So we add (Eqn 68) d to (Eqn 69) v, which gives

$$(vd)_t + (uvd)_x + fud + C_D U v - P_y d - EV\,(v_A - v) = 0 \tag{70}$$

and we add (Eqn 67) d to (Eqn 69) u, which yields

$$(ud)_t + (u^2 d)_x + \tfrac{1}{2} g\,(d^2)_x + gdh_x - fvd \tag{71}$$

$$+ C_D U u - P_x d - EV\,(u_A - u) = 0\ .$$

The three underpinning equations for the model are now therefore Eqns 69,70 and 71. This system of prognostic equations may be regarded as initial-value flux-conservation problems and solved numerically to second-order accuracy by using centred time and space differencing (Press et al. 1986). Parrett and Cullen used this type of technique; specifically, they used a variation of a staggered leapfrog scheme. However, their scheme of equations did not incorporate drag or external forces: this author found that with values of drag (greater than about 0.003), their technique was unstable, apparently due to mesh drifting. Baines and Leonard used a more sophisticated upwind differencing scheme. The method presented here is quite simple and is a variation of the Lax-Wendroff two-step scheme which is described in Press et al. (1986). It was found to be stable for the range of parameters tested. A pragmatic feature of this model is that at low resolution it is stable and will run in a semi-interactive mode on a desktop computer. The author and colleagues (professional weather forecasters) have trialled the software in a subjective fashion. Although ideally it needs accurate upstream data, the input of subjectively estimated upstream conditions gives results consistent with experience.

If we define m, n, ϕ, μ and λ as

$$\left.\begin{array}{ll} m \equiv ud & \mu \equiv mu \\ n \equiv vd & \phi \equiv nu \\ \lambda \equiv \dfrac{\delta t}{\delta x}\ , & \end{array}\right\} \qquad (72)$$

then provisional 'halfway' values of m, n and d are calculated from:

$$\begin{aligned} 2m^{t+\frac{1}{2}}_{j+\frac{1}{2}} = {} & m^t_{j+1} + m^t_j - \lambda(\mu^t_{j+1} - \mu^t_j) - \tfrac{1}{2}g\lambda(d^{t2}_{j+1} - d^{t2}_j) \\ & - \tfrac{1}{2}g\lambda(d^t_{j+1} + d^t_j)(h_{j+1} - h_j) + \tfrac{1}{2}\delta t f(n^t_{j+1} + n^t_j) \\ & - \tfrac{1}{2}\delta t C_D(Uu|^t_{j+1} + Uu|^t_j) + \tfrac{1}{2}\delta t P_x(d^t_{j+1} + d^t_j) \\ & + \tfrac{1}{2}\delta t E(V^t_{j+1}(u_A - u^t_{j+1}) + V^t_j(u_A - u^t_j)) \end{aligned} \qquad (73)$$

$$\begin{aligned} 2n^{t+\frac{1}{2}}_{j+\frac{1}{2}} = {} & n^t_{j+1} + n^t_j - \lambda(\phi^t_{j+1} - \phi^t_j) - \tfrac{1}{2}\delta t f(m^t_{j+1} + m^t_j) \\ & - \tfrac{1}{2}\delta t C_D(Uv|^t_{j+1} + Uv|^t_j) + \tfrac{1}{2}\delta t P_y(d^t_{j+1} + d^t_j) \\ & + \tfrac{1}{2}\delta t E(V^t_{j+1}(v_A - v^t_{j+1}) + V^t_j(v_A - v^t_j)) \end{aligned} \qquad (74)$$

$$2d^{t+\frac{1}{2}}_{j+\frac{1}{2}} = d^t_{j+1} + d^t_j - \lambda(m^t_{j+1} - m^t_j) \tag{75}$$

where m^t_j, n^t_j, ϕ^t_j, μ^t_j represent discrete values on a time-space grid.

Using these provisional values, updated values are calculated from the properly centred expressions:

$$\begin{aligned} m^{t+1}_j = {} & m^t_j - \lambda\left(\mu^{t+\frac{1}{2}}_{j+\frac{1}{2}} - \mu^{t+\frac{1}{2}}_{j-\frac{1}{2}}\right) - \frac{1}{2}g\lambda\left({d^{t+\frac{1}{2}}_{j+\frac{1}{2}}}^2 - {d^{t+\frac{1}{2}}_{j-\frac{1}{2}}}^2\right) \\ & - \frac{1}{2}g\lambda\left(d^{t+\frac{1}{2}}_{j+\frac{1}{2}} + d^{t+\frac{1}{2}}_{j-\frac{1}{2}}\right)\left(h_{j+\frac{1}{2}} - h_{j-\frac{1}{2}}\right) + \frac{1}{2}\delta t f\left(n^{t+\frac{1}{2}}_{j+\frac{1}{2}} + n^{t+\frac{1}{2}}_{j-\frac{1}{2}}\right) \\ & - \frac{1}{2}\delta t C_D\left(Uu|^{t+\frac{1}{2}}_{j+\frac{1}{2}} + Uu|^{t+\frac{1}{2}}_{j-\frac{1}{2}}\right) + \frac{1}{2}\delta t P_x\left(d^{t+\frac{1}{2}}_{j+\frac{1}{2}} + d^{t+\frac{1}{2}}_{j-\frac{1}{2}}\right) \\ & + \frac{1}{2}\delta t E\left(V^{t+\frac{1}{2}}_{j+\frac{1}{2}}\left(u_A - u^{t+\frac{1}{2}}_{j+\frac{1}{2}}\right) + V^{t+\frac{1}{2}}_{j-\frac{1}{2}}\left(u_A - u^{t+\frac{1}{2}}_{j-\frac{1}{2}}\right)\right) \\ & + \lambda\frac{\kappa}{\delta x}\left(m^t_{j+\frac{1}{2}} - 2m^t_{j-\frac{1}{2}}\right) \end{aligned} \tag{76}$$

$$\begin{aligned} n^{t+1}_j = {} & n^t_j - \lambda\left(\phi^{t+\frac{1}{2}}_{j+\frac{1}{2}} - \phi^{t+\frac{1}{2}}_{j-\frac{1}{2}}\right) - \frac{1}{2}\delta t f\left(m^{t+\frac{1}{2}}_{j+\frac{1}{2}} - m^{t+\frac{1}{2}}_{j-\frac{1}{2}}\right) \\ & - \frac{1}{2}\delta t C_D\left(Uv|^{t+\frac{1}{2}}_{j+\frac{1}{2}} + Uv|^{t+\frac{1}{2}}_{j-\frac{1}{2}}\right) + \frac{1}{2}\delta t P_y\left(d^{t+\frac{1}{2}}_{j+\frac{1}{2}} + d^{t+\frac{1}{2}}_{j-\frac{1}{2}}\right) \\ & + \frac{1}{2}\delta t E\left(V^{t+\frac{1}{2}}_{j+\frac{1}{2}}\left(v_A - v^{t+\frac{1}{2}}_{j+\frac{1}{2}}\right) + V^{t+\frac{1}{2}}_{j-\frac{1}{2}}\left(v_A - v^{t+\frac{1}{2}}_{j-\frac{1}{2}}\right)\right) \\ & + \lambda\frac{\kappa}{\delta x}\left(n^t_{j+\frac{1}{2}} - 2n^t_j + n^t_{j-\frac{1}{2}}\right) \end{aligned} \tag{77}$$

$$d^{t+1}_j = d^t_j - \lambda\left(m^{t+\frac{1}{2}}_{j+\frac{1}{2}} - m^{t+\frac{1}{2}}_{j-\frac{1}{2}}\right) + \lambda\frac{\kappa}{\delta x}\left(d^t_{j+\frac{1}{2}} - 2d^t_{j+\frac{1}{2}} + d^t_{j-\frac{1}{2}}\right) \tag{78}$$

where the final term in each is a numerical diffusion term. κ is the numerical diffusion coefficient and is chosen so that

$$\lambda\frac{\kappa}{\delta x} \ll 1. \tag{79}$$

Finally, it is known that a further stability criterion is

$$\lambda < \frac{1}{(u_{max} + \sqrt{g d_{max}})} \tag{80}$$

where subscript '*max*' refers to the maximum value.

Flow which is initially in synoptic balance (the external pressure-gradient force balancing the combined drag and Coriolis force prior to the introduction of topography) has P_x and P_y determined as

$$\left.\begin{aligned} P_x &= -fv_0 + \frac{C_D U_0 u_0 - EV_0 (u_A - u_0)}{d_0} \\ P_y &= -fu_0 + \frac{C_D U_0 v_0 - EV_0 (v_A - v_0)}{d_0} \end{aligned}\right\} \tag{81}$$

where subscript 0 refers to initial upstream conditions. For flow which is not initially in such a balance (e.g. a sea-breeze) then P_x and P_y are balanced against the drag in such a way that

$$\left.\begin{aligned} P_x &= \frac{C_D U_0 u_0 - EV_0 (u_A - u_0)}{d_0} \\ P_y &= \frac{C_D U_0 v_0 - EV_0 (v_A - v_0)}{d_0} . \end{aligned}\right\} \tag{82}$$

6.3 Comparison with other models

Four comparisons were made with results from the model of Houghton and Kasahara (1968), without rotation and or friction. With $\kappa\lambda/\delta x = 0.07$, the results were practically indistinguishable.

Parrett and Cullen (1984) used the same topography and initial conditions as Houghton and Kasahara, but included unbalanced rotation. Again, the results of their model when compared with QT model results were practically indistinguishable. A comparison against Baines and Leonard's (1989) two sets of plotted results also yielded very close agreement. These authors used asymmetric topography and an external force such that the unperturbed flow was in geostrophic balance. There is sufficient evidence therefore to accept the numerical veracity of the QT model.

6.4 Simulations using the QT model

An east-west cross-section (looking south) through the Mount Lofty Ranges was simulated by

$$\left.\begin{array}{ll} h = \dfrac{H}{1 + \dfrac{x^2}{a^2}} & \text{for } x > 0 \\ h = \dfrac{H}{1 + \dfrac{x^2}{b^2}} & \text{for} x \leq 0 \end{array}\right\} \quad (83)$$

with $H = 500\ m$, $a = 3\ km$ and $b = 15\ km$. Thus the flow is from left to right over an asymmetric ramp-shaped hill. Note that easterly and northerly wind components will be positive in this reference frame.

From Stull (1989), typical values of surface drag coefficient in neutral conditions over plains are about 0.002: over the sea, C_D is 0.0007. Raupach et al. (1991) have measured drag and associated parameters over Australian farmland, forest and city surfaces. According to Raupach (personal communication), a plausible value of C_D over the well-treed parts of the Mount Lofty Ranges and the built-up areas of the lee plains would be about 0.010. Some of the values cited by Stull for coniferous forests are even an order of magnitude greater! At night, decoupling would minimise C_D whereas surface heating during the day would maximise it.

The left and right end points were chosen sufficiently distant to avoid interference from reflected perturbations, nevertheless, zero-gradient boundary conditions were applied. The ratio $\kappa\lambda/\delta x$ was 0.06, where δx was between 500 and 700 m. In the results, only a windowed, or zoomed, section is shown.

6.4.1 Balanced synoptic flow – (Type I)

Experiments with a 'Type I' stream in geostrophic balance introduced to topography (with and without friction) were conducted. Parameters were chosen to simulate a homogeneous layer in synoptic balance beneath a 6°C subsidence inversion at 850 *hPa*. As 'reference' or standard synoptic conditions, $u_0 = 10\ m/s$, $v_0 = 0$, $g' = 0.2\ ms^{-2}$, $d_0 = 1500\ m$, $f = -8.3\text{x}10^{-5} s^{-1}$, $C_D = 0.002$ and $E = 0$ were taken. P_x and P_y are determined from Eqn 81. Note that, since two homogeneous layers were used, this model was essentially a conventional $1\frac{1}{2}$-layer model with drag and inertial effects included, however.

The results of a preliminary run (denoted R41) with f and C_D set to zero are shown in Fig. 41. (Run numbers and figure numbers correspond). The four panels show the evolution of the flow in terms of u,v and d at three-hourly intervals. The features of note are the two hydraulic jumps, the maximum wind of about 23 *m/s* which occurs just upstream of the leeward hydraulic jump, and its steady leeward movement. Although not shown, one-hourly 'snaps' illustrate this point quite clearly. Meanwhile, the windward flow speed decreases significantly downstream of the upstream jump as it propagates upstream.

A second run, R42, this time with $f = -8.3\text{x}10^{-5} s^{-1}$ for latitude 35°South, was performed. Compared with R41, the leeward jump accelerates leeward and appears stronger, whereas the windward jump decays and decelerates, eventually reaching a steady state (although on these panels only the region 100 *km* to windward is shown). The decelerated flow veers and the accelerated flow backs – in accord with potential vorticity conservation in the Southern Hemisphere.

Figures 41 to 49 – evolution of Type I flow with 'Witch of Agnesi' topography given by $H = 500\ m$, $a = 3\ km$, $b = 15\ km$, and preconditions of $u_0 = 10\ m/s$, $v_0 = 0\ m/s$, $d_0 = 1500\ m$, $g' = 0.2\ m/s^2$, $f = -83 \times 10^{-6} s^{-1}$, $C_D = 0.002$ and $E = 0.0$ unless noted otherwise.

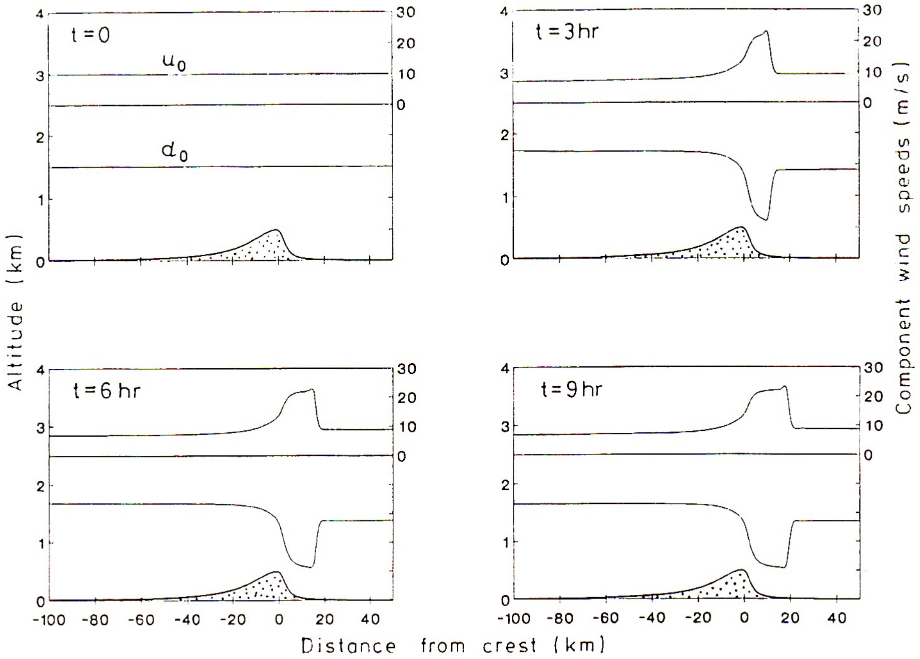

Fig. 41 The case in which $f = 0\ s^{-1}$, $C_D = 0$, in which transitional flow and downslope winds eventuate.

A third run, R43, which was used as the reference for all subsequent comparisons involving synoptically balanced flow, had the same preconditions as R42 except that $C_D = 0.002$. In comparison to R42, the motion of the jumps has been slowed and the maximum wind slightly decreased.

R44, with u_0 reduced to 5 *m/s*, exhibits a nontransitional flow. The stronger wind zone is confined to the crest region and there is no jump. R45, with d_0 raised to 2000 *m* and u_0 reset to 10 *m/s* yields similar results.

To investigate the effect of inversion strength, g' was set to 0.1 and 0.3 m/s^2 in runs R46 and R46, respectively. R46 has weaker maximum winds, but the jump has propagated further

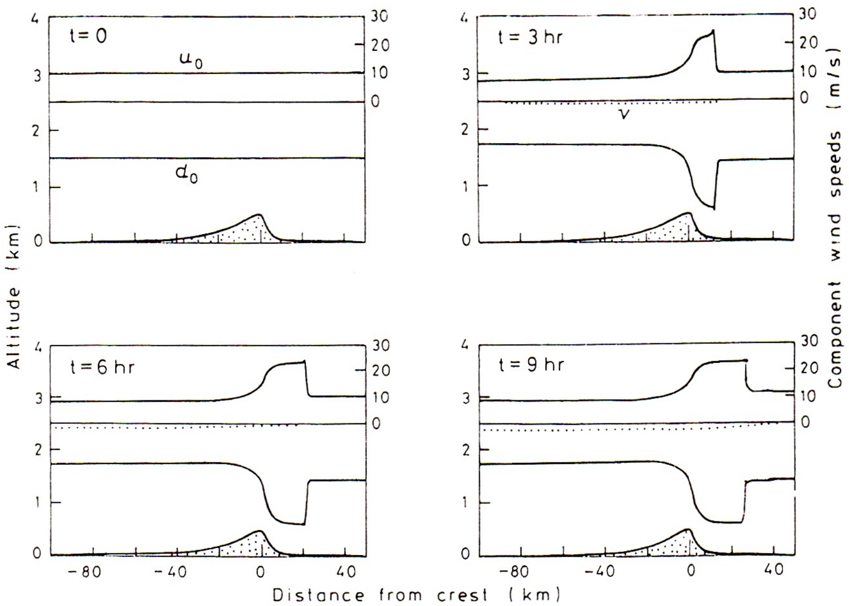

Fig. 42 The case in which $C_D = 0$ but $f = -83 \times 10^{-6} s^{-1}$. In this, the leeward jump is further leeward but the upstream jump is weakened and retarded.

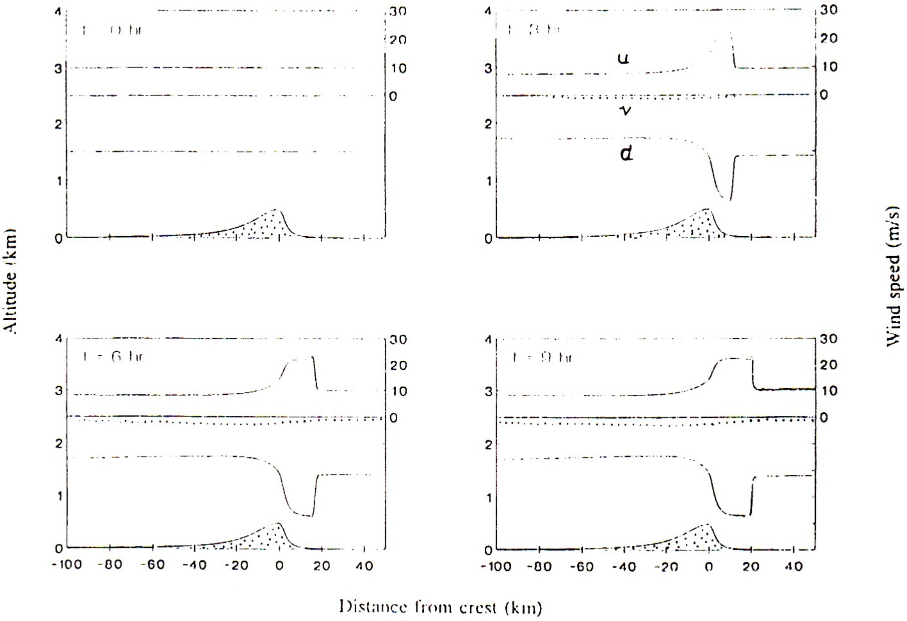

Fig. 43 The 'reference' preconditions for Type I flow.

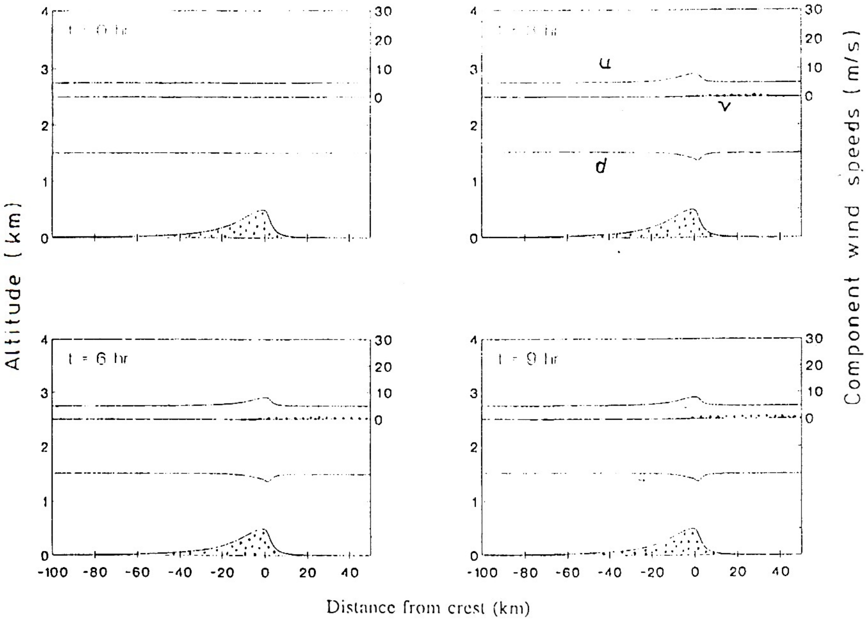

Fig. 44 Non-transitional flow for the reference conditions except that $u = 5\ m/s$.

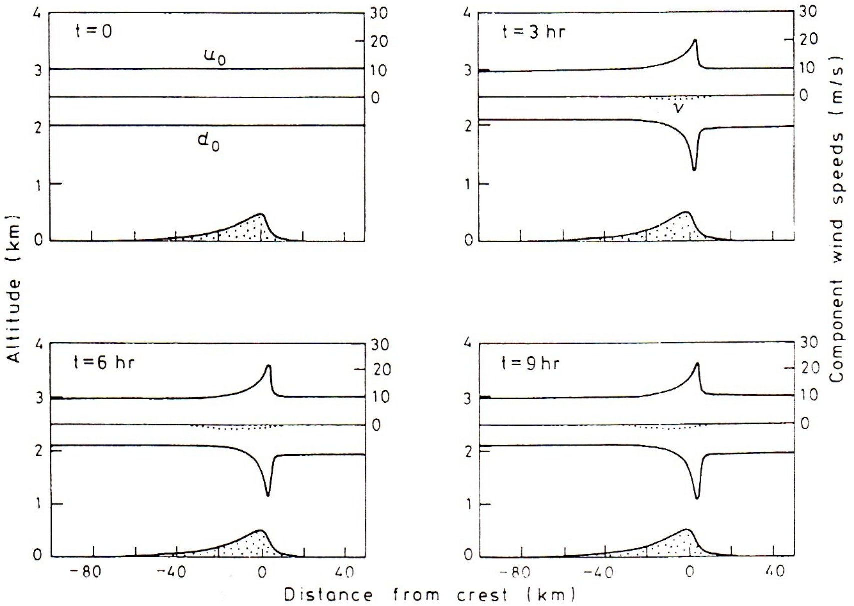

Fig. 45 Non-transitional flow for the reference conditions except that $d_0 = 2000\ m$.

leeward. R47 is nontransitional. It is therefore evident that increasing g' increases the maximum wind in the supercritical zone but decreases the likelihood of transitional flow. This latter run appears to simulate well the first case event described in section 3.2, where foothills suburbs experienced damaging winds and yet a few kilometres downstream the winds were light. Note, however, that modifying the conditions of R47 by lowering d_0 to 1000 *m* causes very strong downslope winds to propagate further leeward (though this run is not shown).

From the above experiments, it can be inferred that increasing u_0/d_0 acts to increase the likelihood of transitional flow, to increase the maximum wind and to push the leeward jump (if any) further leeward, thereby exposing a greater area of the lee plains to downslope winds. However, increasing g' increases the subsequent leeside wind speed maximum but decreases the leeward extent of strong winds.

Numerical modelling by Richard et al. (1989) and by Pitts and Lyons (1990) has shown that the inclusion of surface drag acts to delay and to weaken downslope winds. By comparing R42 and R43, it can be seen that the effect of surface drag is to weaken the maximum wind attained and to limit its leeward extent. Not only are these results intuitively reasonable, but they are also consistent with those of the sophisticated models. In run R48, the flow is initialised as in R43 but the value of C_D in the vicinity of the mountain is greatly increased. Ten kilometres either side of the crest, C_D is set to 0.01, in keeping with Raupach's estimate, and is then reduced to 0.002 with a single cosine step over a further ten kilometres. That is, the perturbation is now due to a hill which is rougher than the plains. The dramatic effect of having a relatively rough hill is evidenced by the weaker jump, the weaker wind maximum and the lesser leeward extent of the jump. This effect was further investigated by means of another run, R49, which was initially identical to R48, except that C_D was halved over the entire domain. Here it is seen that the wind maximum is greater and that the jump is located further leeward. Thus, surface drag acts to inhibit downslope wind maxima and to draw the strong wind zones back toward the crest.

It was conjectured that friction might account for the known ramp shape trigger effect, based on the assumption that a gentler lee slope would allow more time for the drag to dissipate energy from system. Several runs, not shown here, were made with reversed topography but, at least for the values of C_D used herein, there was nothing to support this conjecture.

6.4.2 Inertially unbalanced flow – (Type II)

Further experiments were performed, with a 'Type II' flow balanced only against drag but subject to topographic and inertial influence. A novel feature of these experiments was that the initial depth was set below the height of the ranges (that is, $d_0 < H$) and this was done to simulate a sea-breeze regime (or possibly a nocturnal inversion layer, or a shallow post-frontal layer). Layers such as these would be continuously stratified and therefore it is appropriate to determine g' from Eqn 14 as in the Q1½ model.

In this section, we use as 'reference' conditions a southerly sea-breeze of 8 *m/s* (v_0 = -8 *m/s*, $u_0 = 0$), depth 300 *m*, g' of 0.1 m/s^2 (roughly equivalent to a sea-breeze-layer 3 to 4°C cooler than the adiabatic environment) and C_D of 0.002 and $E = 0$. The flow is initially balanced by determining P_x and P_y from Eqn 82. The first run, R50, yields the extremely interesting result that the Coriolis force gradually 'slops' the cooler air over the hill in the form of a supercritical density current. Upstream, the layer tends to be roughly horizontal at an altitude of 600 *m*; a value not greatly in excess of H itself.

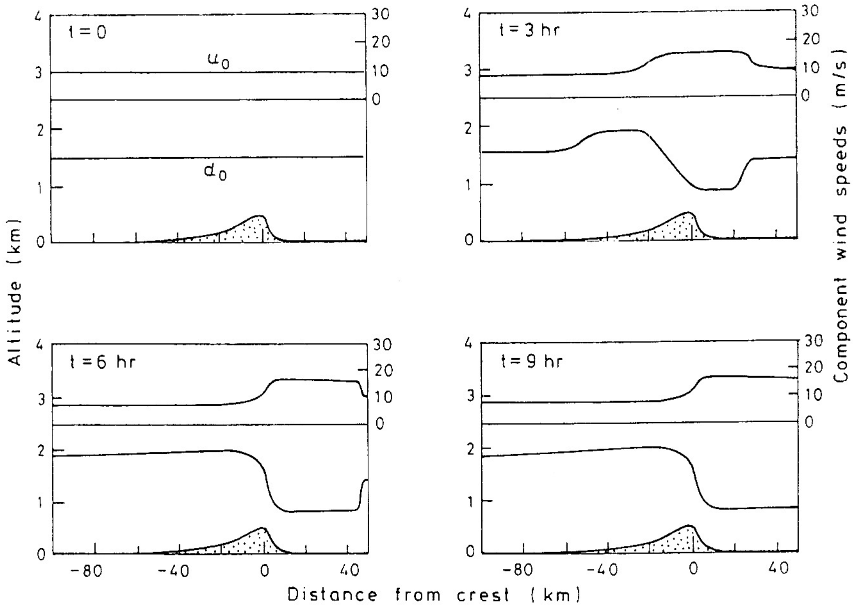

Fig. 46 Flow results for the reference conditions except that $g' = 0.1$ m/s^2. Note that the supercritical flow is more extensive than before, although maximum speeds are decreased.

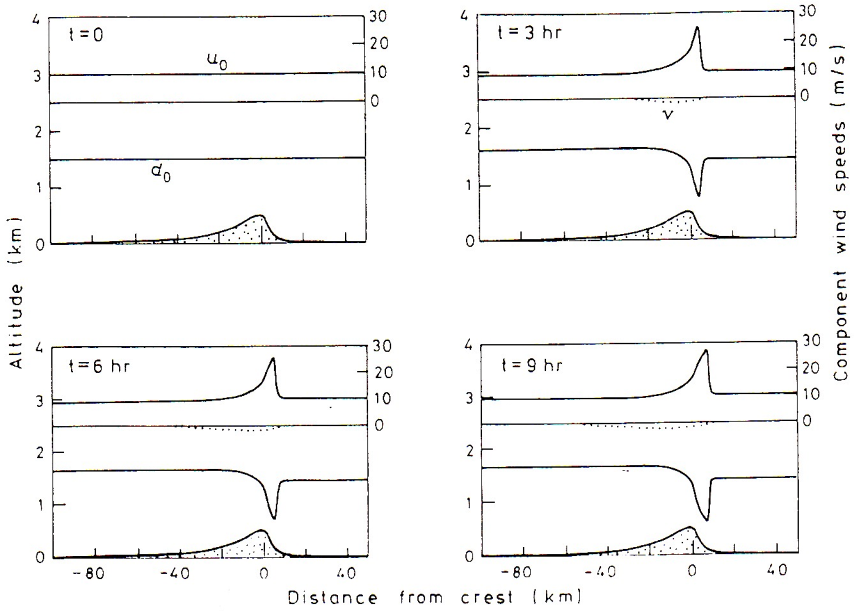

Fig. 47 Flow results for the reference conditions except that $g' = 0.3$ m/s^2. Note that the transitional flow is much less extensive, although maximum speeds are increased. This is equivalent to very strong gully-winds about the foothills with much weaker winds a few kilometres downstream.

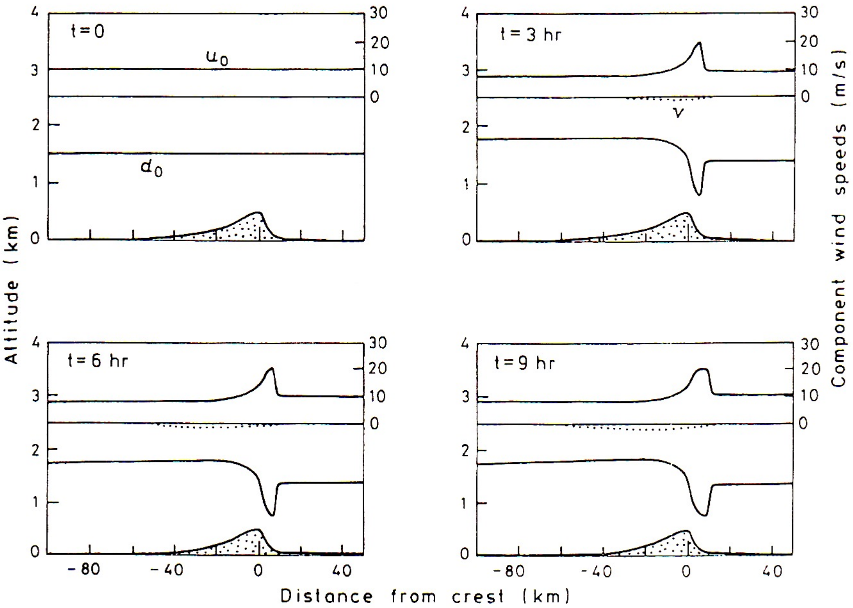

Fig. 48 Flow results for the reference conditions except that C_D over the hills region is increased to 0.01 (though C_D over the plains is held at 0.002). Note that the leeward jump is held back.

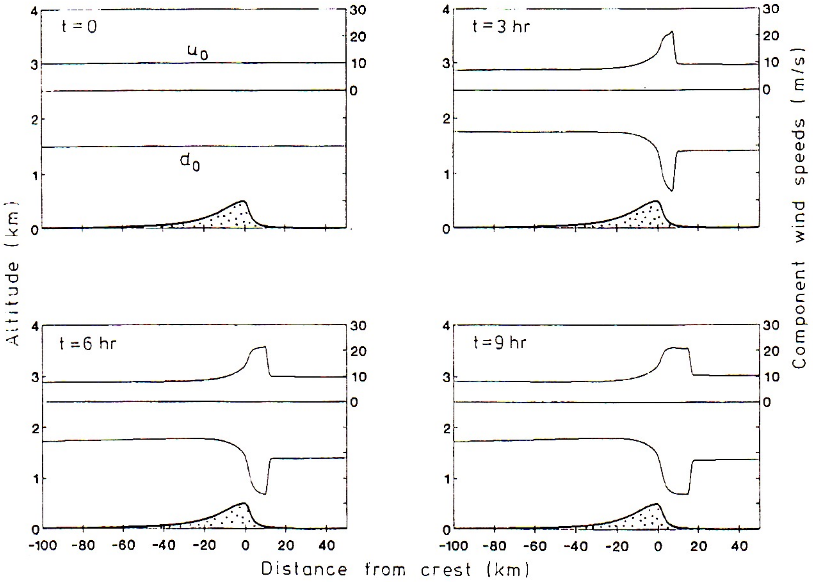

Fig. 49 Flow results for the reference conditions except that C_D over the hills region is increased to 0.005 (while C_D over the plains is held at 0.001). Note that the leeward jump is held back, but less so than in Fig. 48.

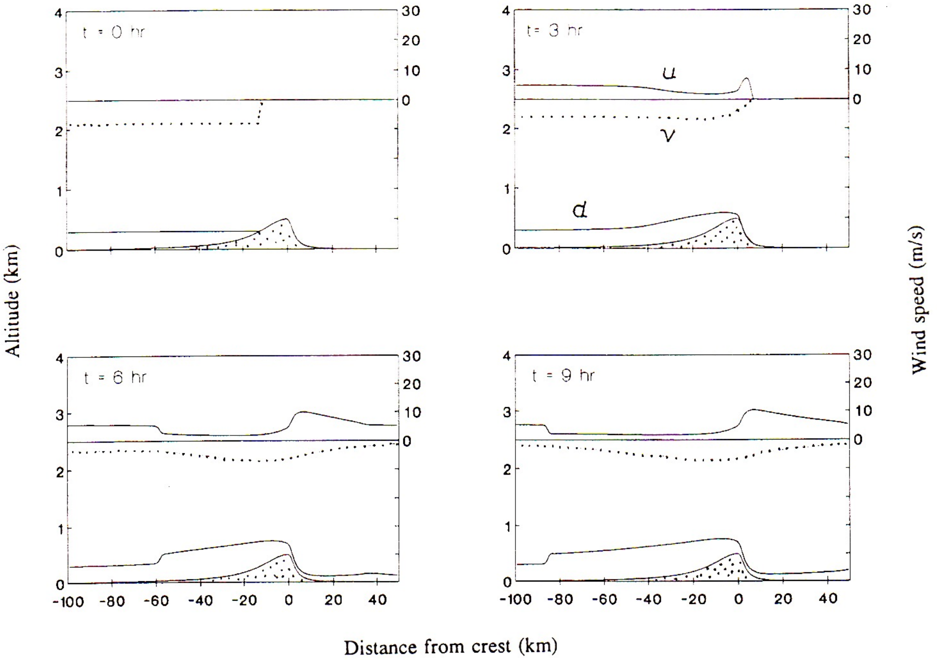

Fig. 50 Type II flow with initial conditions of a southerly of 8 *m/s*, d_0 = 400 *m*, g' = 0.1 *m/s*^{2} and C_D = 0.002. Note that this type of flow is associated with a sea-breeze from the Coorong area.

With v_0 = -4 *m/s*, there is a weaker and shallower gully-wind which occurs several hours later (Fig. 51). Thus, a weak sea-breeze leads to a weak or non-existent gully-wind. Obviously lower and smoother ranges will induce a gully-wind more easily than higher, rougher ranges. Runs performed for southerly sea-breezes simultaneously on *both* sides of the ranges gave similar results, but with a jump-like feature on the lee plain where the supercritical flow ran into the other sea-breeze. However, these are not shown here. The software as provided does not model this dual sea-breeze regime without a minor change to the source code.

As a point of conjecture, it was surmised that an interfacial drag increases the possibility of transitional flow. If the homogeneous upper layer were to flow from left to right (easterly) for synoptic reasons then interfacial drag between this layer and the lower cooler layer would produce upslope drag. In the Southern Hemisphere, a high-pressure ridge building to the south at night would be consistent with these preconditions.

It is difficult to estimate *E*, the interfacial drag coefficient, though on scales different to those of the gully-winds and for markedly more stable air, katabatic wind studies by Manins and Sawford (1979) show *E* to be of order 10^{-3}. It is stressed that the following run with a nonzero value of *E* is intended only as a basis of conjecture. For v_0 = -4 *m/s* and C_D = 0.002, it was shown that weak downslope winds occurred (Fig. 51). However, with interfacial drag operating in such a way that u_A = 15 *m/s* and *E* = 0.001, the spillover effect is greatly enhanced (see Fig. 52). This suggests that the interfacial drag may indeed be a significant factor in gully-wind formation.

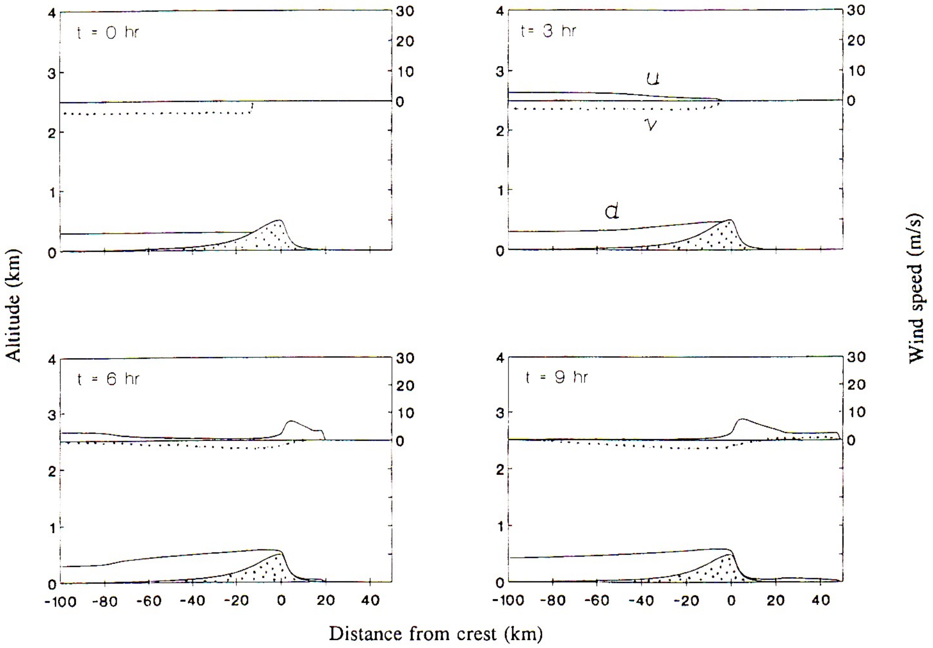

Fig. 51 Type II flow under the same conditions as for Fig. 50, except that $v_0 = -4$ *m/s*.

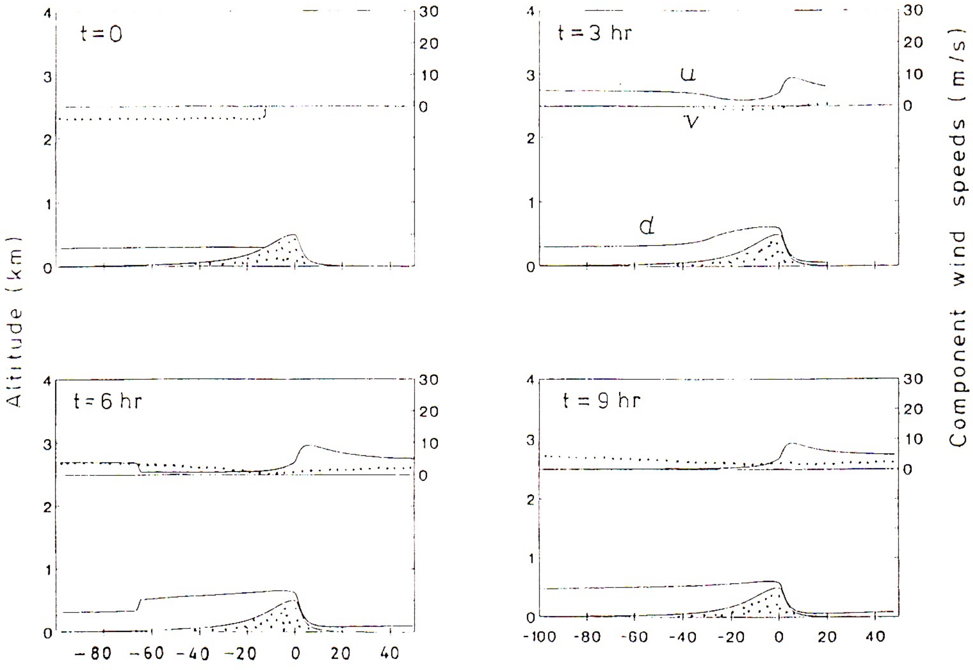

Fig. 52 Type II flow under the same conditions as for Fig. 51, except that $E = 0.001$.

6.5 Summary

Geostrophic (and frictionless) flow perturbed by topography behaves similarly to non-rotational flow except that the upstream jump is retarded while the downstream jump is accelerated leeward. Some veering and backing occurs due to the near-conservation of the vertical component of potential vorticity. With increasing friction, the leeward jump is reduced in strength and retarded, sometimes to a stationary position, and the maximum wind speed is significantly reduced. Presumably significant friction could inhibit the occurrence of downslope winds.

For inertially unbalanced flow, a range-parallel sea-breeze may turn sufficiently to spill over the crest in a shallow supercritical-layer. This effect is reduced and delayed by increasing surface drag, although the details of this have not been given herein. Not surprisingly, it is also enhanced by interfacial drag from a favourable upper wind, although this last finding is qualitative at best. In the Southern Hemisphere (where most of this study has focussed), the presence of topographic barrier with a quasi-meridional orientation tends to create a southerly jet on the eastern flank of the ranges. The Murray Mallee area to the east of the Mount Lofty Ranges is known to be prone to strong sea-breezes, so this is certainly a valid result in the South Australian case. Maybe, it could be regarded as a small scale version of the southeast Australian southerly buster.

Simulations, using realistic preconditions pertinent to the postulated archetypes, reveal that the model either reproduces or partially explains the main features of the Adelaide gully-wind. In particular, for light geostrophic wind situations, it appears that a sea-breeze spilling over in a shallow layer (~100 *m*) fits the acoustic sounder observations and balloon pilots' experience outlined in section 3.4.

The model has been incorporated as a menu-style software package for practical forecasting. Operational forecasters[3] have experimented with the model in a 'what if' mode and indicated to the author that its results are reasonably consistent with their experience. The reader is invited to carry out his/her own experiments using the copy of the software package provided with this thesis.

---

[3] The author, too, has many years operational weather forecasting experience.

CHAPTER 7

DISCUSSION AND CONCLUSIONS

7.1 Hydraulics versus waves

Until recently, the hydraulic theory was confined to one or two homogeneous layers. The work of Smith (S85 and SS87), Baines and Guest (1988) and Baines and Granek (1990) in both tank and numerical experiments has extended the applicability of the theory from homogeneous fluids to continuously stratified fluids. The steady-state model developed in Chapter 4 is in line with this approach. Recent literature (see sections 2.6 and 2.7) has expressed a preference for the hydraulic theory to explain the essential physics and nonlinear behaviour of downslope wind events. Notable exceptions are the work of Peltier and Clark (1977 and several later papers) (PC) and of Laprise and Peltier (1989a,b,c) (LP). LP present much numerical evidence in support of the nonlinear wave-amplification mechanism of PC.

For the Adelaide gully-wind and the bora, at least, the observed ratio of the height of decoupling to the mountain height is about two – much less than the value of about five predicted by PC. It seems that such low-level decoupling is therefore due to other reasons, e.g. subsidence inversion or a shear layer. This does not rule out the PC mechanism occurring for certain types of flow, e.g. possibly the chinook. For the Adelaide gully-wind there is evidence (although it is not documented) that much of the flow is on occasion channelled through the gullies and valleys. One of the author's professional colleagues has noted that gully-winds can often be heard flowing through a valley below his residence. Arakawa (1969) and Pettre (1982) have successfully used the concept of hydraulic flow through a valley to model downslope winds. It is difficult to see how PC's wave-amplification theory could easily accommodate the channelling effect.

The hydraulic model accounts for the postulated Type II gully-wind, where the primary mechanism is the Coriolis force 'slopping' a shallow dense layer up and over the ranges, possibly aided by drag from aloft.

7.2 Utility of the steady-state ($Q1^1/_2$) model

From Eqn 27 it is seen that maximum wind speeds of two to three times the upstream value are anticipated over the lee plains – a realistic result. Qualitatively, the model compares well with each of Smith (1985), Durran and Klemp (1987), Bacmeister and Pierrehumbert (1988) and PC and LPa,b,c. Detailed comparisons with DK in particular were very good. For instance, in the presence of an environmental critical-layer, both models were quite similar in predicting transitional flow. Drag predictions from $Q1^1/_2$ when compared to DK and BP were extremely good. In contrast, drag as calculated by S85 was about double the expected value. The splitting-streamline height of the steady-state model tended to be 10 to 15% higher than that of S85. Both $Q1^1/_2$ and S85 predict multiple higher altitude values of $\hat{d}_0$; a result validated by DK and BP. The disadvantages of both these hydraulic models are that N_0 and u_0 must be idealised as constant with height and that the existence of a critical mountain for which the transitional flow is self-initiated cannot be directly inferred. Baines and Granek's quantitative approach obviously has many of the advantages of both models and can be used with realistic upstream atmospheres and topography. Data from tank experiments by Rottman and Smith (1989) and numerical experiments by DK, BP and PC show that Q1½ is equally good at predicting $\hat{d}_0$ (Fig. 33).

An assumption in the model is that the hydraulically-active layer may be approximated by an equivalent homogeneous model and that the value of g' used for the equivalent layer is $4| \pi^2 N_0^2 d_E$. The overall utility of the model indicates the validity of this assumption.

The inclusion of some topographic effects, such as lower leeside plains and channelling between the major hills of a range, showed that valley mouths, especially those at relatively low elevation, are prone to chronic and severe downslope winds. This result is similar to Arakawa's (1969) observations of the hiroto-kaze in Japan and with many observations concerning the so-called extreme katabatics off the Antarctic and Greenland coasts.

With the remarkable exception of these extreme katabatics, a feature of all downslope winds is their gustiness in speed yet constancy of direction. Surge periods of 3 to 4 minutes have been reported for the bora, and lidar measurements of a chinook windstorm by Nieman et al. (1988) showed a tendency for periodicity of 4 minutes and 14 minutes. Resonant tuning was hypothesised between vertically and horizontally propagating waves (both of which have their oscillations in the vertical). Under this hypothesis directional fluctuations would not be anticipated – nor do they occur. Using the Q1½ steady-state model the consequent speed fluctuations were found to be of the order of 3 minutes and 15 minutes for large-scale downslope winds – both values being well supported by the observations. The internal waves could be initiated by topographic irregularities. Over ice, the lack of irregularities to initiate such waves could well account for the well-known constancy in the speed of the Antarctic katabatics.

7.3 Utility of the time-dependent (QT) model

Although this model is based on the shallow-water equations where the layers are usually assumed to be homogeneous, the results of the Q½ steady-state model and the good agreement with DK's results suggest an extension to the case of a continuously-stratified shallow layer. Thus, it may be used in model atmospheres where N_0 is constant with height.

The shallow-water equations incorporating *f*, *CD* and *E* were solved by a two-step Lax-Wendroff numerical scheme. The results are consistent with and anticipate many of the features of downslope winds in general and the Adelaide gully-wind in particular.

The primary output values of the model such as maximum wind speed, zone of strong winds and layer depth (or inversion height) as presented are realistic.

In simulating typical synoptic conditions expected for Type I Adelaide gully-winds (Figs 41 to 49), the resulting leeside inversion turns out to be at about 600 *m* with maximum winds in excess of 20 *m/s* and these results are consistent with the data presented in section 3.2. The appropriate comparison for these modelled maximum winds is the observed *gust* speed. This is because, although friction has been accounted for in a parameterised manner, the actual surface wind will be significantly less than the layer-mean. Air transferred from the mid-layer region to produce a gust at the surface will have a speed representative of the layer-mean. In section 3.3, a shallow post-frontal layer crossing the ranges (in synoptic balance) evolved into a gully-wind with downstream depth of ~550 *m*, leeside depth of ~300 *m* and upstream depth of ~600 *m*. A simulation (not shown) of this event also gave comparable values. In section 3.4 data from an acoustic sounder and private communication from an experienced balloon pilot both showed that the inversion could be as low as 60 to 200 *m*. Such small depths and the generally lower wind speeds are probably not explicable in terms of Type I behaviour; nor does it seem likely that the mechanism of PC is relevant here. They are, however, explicable in terms of Type II behaviour, which involves the inertial turning of a very shallow upstream layer $(d_0 < H)$. The Type II preconditions would apply to streams such as a sea-breeze-layer or a shallow post-frontal layer.

Figures 50 and 51 for Type II flow depict the evolution of this spillover due to Coriolis turning. With a weaker sea-breeze or greater surface drag, the spillover effect is delayed or prevented. In more speculative vein, however, it does seem that the effect of interfacial drag from a fast-moving upper layer would be adequate to help pull a shallow stable layer up hill even in the presence of surface friction. In all of these cases the subsequent leeside layer is of the order of 100 *m* deep, which is significantly shallower than those of Type I and yet quite consistent with the available observations.

The sensitivity of the occurrence of transitional flow and of the jump position to upstream velocity, inversion height or environmental critical-layer height, stability of the layer or strength of the inversion, mountain height, external pressure-gradient forces and surface drag all account for the marked spatial and temporal variability of the Adelaide gully-wind. The inclusion of non-zero C_D had the effect of bringing the jump back towards the crest. With C_D maximised during the day and minimised during the night, it is be expected that the Adelaide gully-wind, and downslope winds generally, would have a pronounced preference for occurring nocturnally. With C_D relatively high over the ranges, the gully-wind was inhibited. This finding is also consistent with the occurrence of stronger gully-winds in areas where the ranges are smoother and sparsely timbered.

For Type II flow, an intriguing result is the effect of variations in C_D and H, the mountain height. It is apparent that increasing C_D and/or H lessens the likelihood of the spillover, so that rougher and/or higher parts of the ranges could be untouched by the shallow layer whilst lower and/or smoother parts of the ranges are subject to a shallow layer moving cross-range. In such a case, it follows that there would be no downslope winds over the leeslopes of Mount Lofty itself, but downslope winds could be occurring on leeslopes further to the north and south. This may have been the situation for the nights of 2/3 and 3/4 February 1985 and 25/26 February 1991.

A pragmatic feature of the model is its use as a semi-interactive forecasting tool. The main input parameters of d_0, u_0 and g' may be estimated from synoptic data by experienced forecasters. Informal feedback from the author's colleagues indicates that the model outputs tend to correspond to their subjective expectations. A major problem is the correct specification of the initial or undisturbed conditions, since there are no upper-air data acquired routinely within 200-300 *km* upwind of the ranges. Therefore the model is difficult to either test or use in a thorough and objective fashion.

CHAPTER 8

FINAL REMARKS AND FUTURE DIRECTIONS

A simple steady-state hydraulic model of downslope winds was developed, presented and found to account for many of the observed features of downslope winds. As an extension of this steady-state model, a time-dependent quasi layer-and-a-half model was constructed, presented and also shown to account for several intriguing aspects of downslope winds and of the Adelaide gully-wind in particular.

Several unique postulates (concerning the steady-state model as presented, mountain drag, turbulence intensity and jump strength as related functions of the non-dimensional mountain height, a resonant tuning of gravity waves to account for the surging characteristic of downslope winds, a modelled valley effect, the evolution of a downslope wind due to inertial forcing, the way in which drag inhibits downslope winds during daylight, and the signature of a hydraulic jump 'written in the wind') were proposed and framed within current knowledge and theory in the literature. Also robust, interactive and operationally useful software was devised.

Not surprisingly there are still many fascinating questions to ask... and to answer. From an observational perspective, just how extensive are, for example, the Adelaide gully-winds, how far to the lee do they blow, what is their spatial variation and their association with surface features and conditions? The advent of automatic weather stations, loggers, computer power and techniques together with sophisticated and robust flying instrument packages (the aircraft operated by the Flinders Institute of Atmospheric and Marine Science) promises much in this area.

Noting the success of a tank model for the famous Spillane eddy in Melbourne, it is an obvious step to construct one for the Mount Lofty Ranges, especially if the results were to be compared with the data of the observational program envisaged above.

In hindsight, it is apparent that the direction shown by Baines and Granek (1989) has the potential to be the simplest possible, yet realistic, model of downslope winds. Its extension to time-dependency will almost certainly repay the effort. Meanwhile, there are many sophisticated mesomodel packages that will soon be easy to use on typical PCs and work stations (over the next 3 to 5 years). Prior to such numerical models being available to operational forecasters, it should be possible to extend the software provided with this thesis in two useful ways (but probably not simultaneously). Firstly, a time-dependent *multi-level* two-dimensional model would be relatively simple to construct. It would take longer to run of course (of the order of an hour rather than a few minutes), but would probably still be useful operationally. A second extension would be to an *x,y* plane, whilst retaining the $1^1/_2$-layer vertical structure (or further extended perhaps with $2^1/_2$, or possibly $3^1/_2$ layers).

All three programs are more general than just downslope wind studies. A host of questions relating to sea-breezes, early morning wind on the Adelaide plains, channelling and funnelling, fog advection and local eddies could be pursued.

REFERENCES

Arakawa, S. 1968. A proposed mechanism of fall winds and Dashi-kaze. *Pap. Met. Geophys., 19,* 69–99.

Arakawa, S. 1969. Climatological and dynamical studies on the local strong winds, mainly in Hokkaido, Japan. *Geophys. Mag., 34,* 359–425.

Ash, A. 1987. *Gliding News.* Aircraft Mag. of R. Aero. Soc. Aust., May, 11–17.

Atkinson, B. 1981. *Meso-scale atmospheric circulations.* Academic Press. Ch. 3, 91–105.

Bacmeister, J.T. and Pierrehumbert, R.T. 1988. On High-Drag States of Nonlinear Stratified Flow Over an Obstacle. *J. Atmos. Sci., 45,* 63–80.

Baines, P.G. and Hoinka, K.P. 1985. Stratified flow over two-dimensional topography in fluid of infinite depth: A laboratory simulation. *J. Atmos. Sci., 42,* 1614–30.

Baines, P.G. and Guest, F. 1988. The nature of upstream blocking in uniformly stratified flow over long obstacles. *J. Fluid Mech., 188,* 23–45.

Baines, P.G. and Granek, J. 1990. Hydraulic models of deep stratified flows over topography. In *The Physical Oceanography of Sea Straits,* L.J. Pratt (ed.), Dordrecht:Kluwer, 245–69.

Baines, P.G. 1987. Upstream blocking and airflow over mountains. *Ann. Rev. Fluid Mech., 19,* 75–97.

Baines, P.G. and Leonard, B.P. 1989. The effects of rotation on flow of a single layer over a ridge. *Q.Jl R. met. Soc., 115,* 293–308.

Bower, J.B. and Durran, D.R. 1986. A study of wind profiler data collected upstream during windstorms in Boulder, Colorado. *Mon. Weath. Rev., 102*, 592–602.

Boyer, D.L. and Tao, L. 1987. Impulsively Started, Linearly Stratified Flow over Long Ridges. *J. Atmos. Sci.,* 44, 23–42.

Brown, J.M. 1986. A decision tree for forecasting downslope windstorms in Colorado. *11th Conf. Weather and Forecasting,* Kansas City Met. Office, 83–88.

Bureau of Meteorology, 1971. *Climatic Survey South Australia, Region I.* Bur. Met., Australia.

Clark, T.L. and Peltier, W.R. 1977. On the evolution and stability of finite amplitude mountain waves. *J. Atmos. Sci., 34,* 1715–30.

Clark, T.L. and Peltier, W.R. 1984. Critical level reflection and the resonant growth of nonlinear mountain waves. *J. Atmos. Sci., 41,* 3122–34.

Colson, D.V. 1954. Meteorological problems in forecasting mountain waves. *Bull. Am. met. Soc., 35,* 363–71.

Durran, D.R. 1986a. *Mesoscale Meteorology.* Amer. Met. Soc. S. Ray (ed.), Ch. 20, 472–92.

Durran, D.R. 1986b. Another look at downslope windstorms. Part I: The development of analogs to supercritical flow in an infinitely deep, continuously, stratified fluid. *J. Atmos. Sci., 43,* 2527–43.

Durran, D.R. and Klemp J.B. 1987. Another look at downslope winds. Part II: Nonlinear amplification beneath wave-overturning layers. *J. Atmos. Sci., 44,* 3402–12.

Gill, A.E. 1982. *Atmospheric-Ocean Dynamics.* Academic Press. Ch. 8, 247–370.

Grace, W.J. 1991. Hydraulic jump in a fog bank. *Aust. Met. Mag., 44*, 205–9.

Grace, W.J. 1992. Modelling the downslope winds of Adelaide, South Australia. *CTAC 91* (Conf. proc. Computational Techniques and Applications 1991) (in press).

Grace, W.J. and Holton, I.C. 1988. A mechanism for downslope winds with special reference to the Adelaide gully wind. *Met. Note No. 179,* Bur. Met., Australia, 21 pp.

Grace, W.J. and Holton, I.C. 1990. Hydraulic jump signatures associated with Adelaide downslope winds. *Aust. Met. Mag., 38,* 43–52.

Hacker, J.M. and Schwerdtfeger, P. 1988. *The FIAMS Research Aircraft System Description.* (2nd edn) Flinders University of South Australia, 60 pp.

Hoinka, K.P. 1985. A comparison of numerical simulations of hydrostatic flow over mountains with observations. *Mon. Weath. Rev., 113,* 719–35.

Hoinka, K.P. and Rösler, F. 1987. The Surface Layer on the Leeside of the Alps during Foehn. *Meteor. Atmos. Phys., 37,* 245–58.

Holmes, N., Richmond, K. and Sanguineti, T. 1981. Studies of the Meteorology and dispersion characteristics of the Beverley area – Lake Frome, South Australia. *An Environmental Impact Study* available from Lang, Dames and Moore, Crows Nest NSW.

Holton, I.C. 1985. The Adelaide Gully wind and associated hazards to aviation. *Met. Note No. 166,* Bur. Met., Australia, 21 pp.

Holton, I.C. and Grace, W.J. 1989a. The Adelaide downslope winds. Part I Nowcasting Turbulence and Wind Shear. *Met. Note No. 186,* Bur. Met., Australia, 12 pp.

Holton, I.C. and Grace, W.J. 1989b. The Adelaide downslope winds. Part II Nowcasting Wind Speed. *Met. Note No. 188,* Bur. Met., Australia, 16 pp.

Houghton, D. and Kasahara, A. 1968. Nonlinear Shallow Fluid Flow Over an Isolated Ridge. *Comms of Pure and App. Math.* XXI, 1–23.

Humphreys, W.J. 1929. *Physics of the Air.* McGraw Hill, 159 pp.

Kingsborough, L.S. 1967. *The horse tramways of Adelaide 1875-1907.* Libraries Board of South Australia, 175 pp.

Klemp, J.B. and Durran, D.R. 1987. Numerical Modelling of Bora Winds. *Meteor. Atmos. Phys., 36,* 215–27.

Klemp, J.B. and Lilly, D.K, 1975. The dynamics of wave induced downslope winds. *J. Atmos. Sci., 32,* 320–39.

Küttner, J. 1939. Moazagotl und Föhnwelle. *Beit. Phys. freien Atmos., 25,* 79–114

Küttner, J. 1958. The rotor flow in the lee of mountains. *Schweiz. Aero. Rev., 33,* 208–15.

Laprise, R. and Peltier, W.R. 1989a. Notes and Correspondence. On the structural characteristics of steady finite-amplitude mountain waves over bell-shaped topography. *J. Atmos. Sci., 46,* 586–95.

Laprise, R. and Peltier, W.R. 1989b. The linear stability of nonlinear mountain waves: Implications for the understanding of severe downslope windstorms. *J. Atmos. Sci., 46,* 545–64.

Laprise, R. and Peltier, W.R. 1989c. The structure and energetics of transient eddies in a numerical simulation of breaking mountain waves. *J. Atmos. Sci., 46,* 565–85.

Lighthill, J. 1978. Waves in Fluids. Cambridge Univ. Press. Ch 2,3, 89–283 and Epilogue, 437–69.

Lilly, D.K. and Klemp, J.B. 1979. The effects of terrain shape on nonlinear hydrostatic mountain waves. *J. Fluid Mech., 95,* 241–61.

Lilly, D.K. and Zipser, E. 1972. The Front Range windstorm of 11 January 1972 – a meteorological narrative. *Weatherwise, 25,* 56–63.

Long, R.R. 1953. Some aspects of the flow of stratified fluids I. A theoretical investigation. *Tellus, 5,* 42–58.

Long, R.R. 1954. Some aspects of the flow of stratified fluids II. Experiments with a two fluid system. *Tellus, 6,* 97–115.

Lopez, P. and Howell, W.E. 1967. Katabatic winds in the equatorial Andes. *J. Atmos. Sci., 24,* 29–35.

Mahoney, A.R., McAlister, L.G. and Pollard, J.R. 1973. The remote sensing of wind velocity in the lower troposphere using an acoustic sounder. *Bound. Lay. Met., 4,* 155–67.

Marsh, L. 1987. Towards an understanding of the Adelaide Gully Wind. *Met. Note No. 175,* Bur. Met., Australia, 32 pp.

Miles, J.W. and Huppert, H.E. 1969. Lee waves in a stratified flow. Part IV: Perturbation approximations. *J. Fluid Mech., 35,* 497–525.

Nicholls, J.M. 1973. The airflow over mountains Research 1958-72. *WMO Tech. Note 127,* 73 pp.

Nieman, P.J., Hardesty, R.M., Shapiro, M.A. and Cupp, R.E. 1988. Doppler Lidar Observations of a Downslope Windstorm. *Mon. Weath. Rev., 116,* 2265–75.

Parrett, C.A. and Cullen, M.J.P. 1984. Simulation of hydraulic jumps in the presence of rotation and mountains. *Q.Jl R. met. Soc., 110,* 147–65.

Pedlosky, J. 1987. *Geophysical Fluid Dynamics.* (2nd edn) Springer-Verlag, 59–62.

Peltier, W.R. and Clark, T.L. 1979. The evolution and stability of finite-amplitude mountain waves. Part II: Surface wavedrag and severe downslope windstorms. *J. Atmos. Sci., 36,* 1498–1529.

Pettre, P. 1982. On the problem of violent valley winds. *J. Atmos. Sci., 39,* 542–54.

Pielke, R.A. 1984. *Mesoscale Meteorological Modeling.* Academic Press, 473–82.

Pitts, R.O. and Lyons, T.J. 1989. Airflow over a two-dimensional escarpment. I: Observations. *Q. Jl R. met. Soc., 115,* 965–81.

Pitts, R.O. and Lyons, T.J. 1990. Airflow over a two-dimensional escarpment. II: Hydrostatic Flow. *Q. Jl R. met. Soc., 116,* 363–78.

Press, W.H., Flannery, B.P., Teukolsky, S.A. and Vetterling, W.T. 1986. *Numerical Recipes.* Cambridge Press, 631–5.

Queney, P. 1948. The Problem of Air Flow over Mountains: A Summary of Theoretical Studies. *Bull. Am. met. Soc., 29,* 16–25.

Raupach, M.R., Antonia, R.A. and Rajagopalan, S. 1991. Rough-wall turbulent boundary layers. *App. Mech. Rev., 44,* 1–25.

Richard, E., Mascart, P. and Nickerson, E.C. 1989. The Role of Surface Friction in Downslope Windstorms. *J. App. Met., 28,* 241–51.

Rottman, J.W. and Simpson, J.E. 1989. The formation of internal bores in the atmosphere: A laboratory model. *Q. Jl R. met. Soc., 115,* 941–63.

Rottman, J.W. and Smith, R.B. 1989. A laboratory model of severe downslope winds. *Tellus, 41A,* 401–15.

Scinocca, J.F. and Peltier, W.R. 1989. Pulsating Downslope Windstorms. *J. Atmos. Sci., 46,* 2885–914.

Scorer, R.S. 1949. Theory of Waves in the Lee of Mountains. *Q. Jl R. met. Soc., 75,* 41–56.

Scorer, R.S. 1978. *Environmental Aerodynamics.* Elliswood Horwood, England. Ch. 5.

Smith, R.B. 1985. On Severe Downslope Winds. *J. Atmos. Sci., 42,* 2597–603.

Smith, R.B. 1987. Aerial Observations of the Yugoslavian Bora. *J. Atmos Sci., 44,* 269–97.

Smith, R.B. and Sun, J. 1987. Generalized Hydraulic Solutions Pertaining to Severe Downslope Winds. *J. Atmos. Sci., 44,* 2934–39.

Stull, R.B. 1989. *An Introduction to Boundary Layer Meteorology.* Kluwer Academic, Ch. 7. 251–91.

Suzuki, S. and Yabuki, K. 1956. The Airflow Crossing over the Mountain Range. *Geophys. Mag., 27,* 273–91.

Van Burgel, J.L. 1984. Strong easterly airflow over the Darling Scarp. *M.Sc. Thesis.* Western Australian Inst. Tech. Library, 46 pp.

Vergeiner, I. 1971. An operational linear lee wave model for arbitrary basic flow and two-dimensional topography. *Q. Jl R. met. Soc., 97,* 30–60.

Yoshimura, M.M. 1976. Synoptic and Aerological Climatology of the Bora Day. In *Local Wind Bora,* M.M. Yoshino (ed.), Uni. Tokyo Press, 99–111.

Yoshino, M.M. 1976. *Local Wind Bora.* Uni. of Tokyo Press, 289 pp.

APPENDIX A

Derivation of transitional flow conditions

As in Fig. A1, consider two-dimensional flow of water of depth $d(x)$ over an obstacle of height $h(x)$ and maximum height of H at $x = 0$. The flow is from left to right in the positive x direction. The layer velocity is $u = u(x)$ and is constant with height. Differentiation with respect to x is denoted by subscript x. Subscripts 0 and c denote upstream and crest values, respectively.

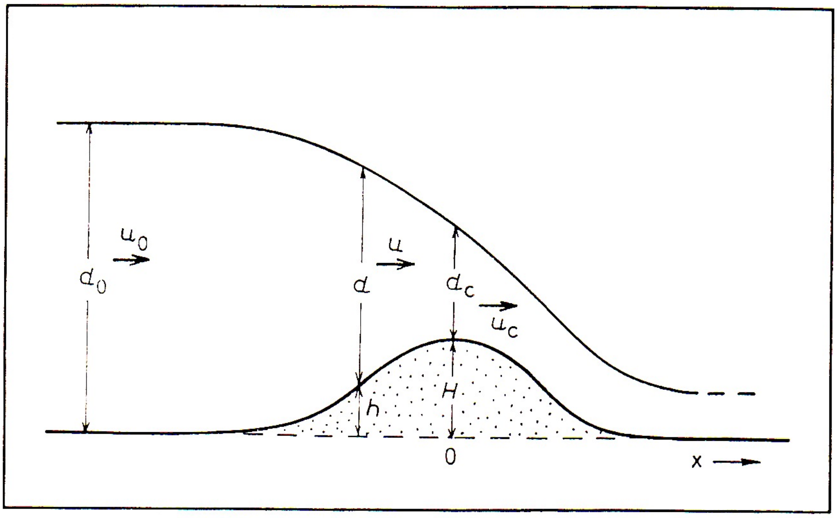

Fig. A1 Schematic diagram of transitional flow over an obstacle.

The continuity and momentum equations may be expressed as

$$\left.\begin{aligned} (ud)_x &= 0 \\ uu_x + g\,(d+h)_x &= 0 \end{aligned}\right\} \qquad \text{(A1)}$$

eliminating u_x between the equations of A1 and using

$$F^2 = \frac{u^2}{gd} \qquad \text{(A2)}$$

then yields

$$d_x = \frac{h_x}{F^2 - 1}\,. \qquad \text{(A3)}$$

Equation A3 shows that for $h_x > 0$ and $F < 1$ then $d_x < 0$ and hence $u_x > 0$. That is, subcritical 'windward' flow is accelerated. Similarly, supercritical leeward flow is accelerated. To have acceleration on both sides of the obstacle it is apparent that there must be a transition from $F < 1$ to $F > 1$. Assuming that $d(x)$ is a smooth function (in the sense that its first derivative exists and is continuous everywhere), we can show from the first equation of A1 that u_x/u must be continuous and hence that $u(x)$ is likely to be smooth (unless any discontinuities in u_x and u which may occur happen to coincide and to cancel each other out, which is fairly unlikely from a physical point of view). If the topographic function $h(x)$ is also smooth, it can be shown from A3 that $F(x)$ must be everywhere continuous. Since the latter must take all values during its transition from $F < 1$ to $F > 1$, it follows then that there must exist some point at which $F = 1$.

Since $h_x = 0$ at the crest of the mountain, the condition for transitional flow is therefore that $F_c = 1$. As $F = 1$ at $x = x_c$, application of L'Hôpital's rule to A3 will show that

$$d_x(x_c) = \frac{h_{xx}(x_c)}{2F_x(x_c)}, \tag{A4}$$

which is finite for the kind of topography considered. Integrating Eqns A1, we find that

$$\left.\begin{aligned} u_0 d_0 &= u_c d_c \\ \frac{u_0^2}{2g} + d_0 &= \frac{u_c^2}{2g} + d_c + H \end{aligned}\right\} \tag{A5}$$

and substituting A2 into A5 gives

$$\left.\begin{aligned} F_0^2 + 2\left(1 - \frac{H}{d_0}\right) &= \frac{d_c}{d_0}(F_c^2 + 2) \\ &= 3\frac{d_c}{d_0}. \end{aligned}\right\} \tag{A6}$$

But from A2,

$$d_c = \frac{u_c^2}{g} \tag{A7}$$

and thus,

$$\frac{d_c}{d_0} = \frac{u_c^2}{gd}. \tag{A8}$$

From A5 then,

$$u_c = u_0\frac{d_0}{d_c}. \tag{A9}$$

Together, A8 and A9 yield

$$F_0^2 = \left(\frac{d_c}{d_0}\right)^3 . \tag{A10}$$

Substituting A10 into A6 gives

$$F_0^2 - 3F_0^{2|3} + 2\,(1 - \frac{H}{d_0}) = 0. \tag{A11}$$

For a homogeneous fluid overlaid by a much deeper one it may be shown that the above derivation is valid except that g is to be replaced by the modified gravity under the Boussinesq approximation (Baines, 1987).

APPENDIX B

Derivation of steady-state jump conditions

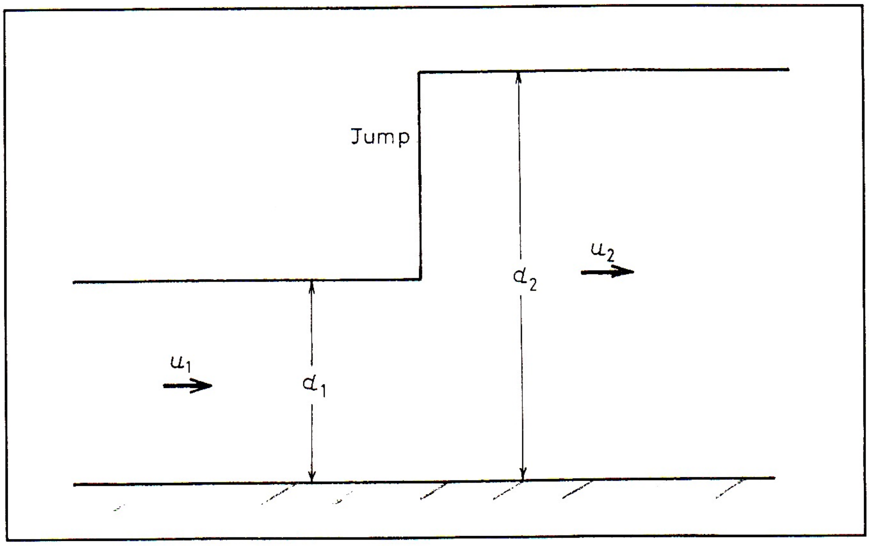

Fig. B1 Schematic diagram of an idealised hydraulic jump.

Consider steady-state two-dimensional flow of water with a stationary hydraulic jump as in Fig. B1. With subscripts 1 and 2 denoting pre- and post-jump conditions, respectively, then the continuity equation may be expressed as

$$u_1 d_1 = u_2 d_2 = m. \tag{B1}$$

By equating the momentum flux change across the jump to the pressure force across it, then it is evident that

$$u_1^2 d_1 - u_2^2 d_2 = \frac{1}{2} g(d_2^2 - d_1^2) . \tag{B2}$$

Eliminating u_1 and u_2 between the three equations in B1 and B2 easily yields:

$$m^2 \frac{d_2 - d_1}{d_1 d_2} = \frac{1}{2} g(d_2^2 - d_1^2) . \tag{B3}$$

Discarding the trivial solution of $d_1 = d_2$, we find that the remaining root of B3 satifies

$$\frac{m^2}{gd_1^3} = d_2\frac{d_2 + d_1}{2d_1^2} \tag{B4}$$

from which it follows that

$$\frac{d_2}{d_1} = \frac{1}{2}\sqrt{1 + F_1^2} + \frac{1}{2}. \tag{B5}$$

Again, the substitution of modified gravity, g' for g, in the above equations may be made in the case of a shallow layer of homogeneous fluid overlaid by a deeper homogeneous layer.

APPENDIX C

Derivation of steady-state mountain drag

The drag force, *r*, exerted by the mountain to change airflow from what it would have been otherwise, is the difference in the combined momentum flux and pressure force acting on the changed layer (that is, below altitude, d_0, along which $p = p_0*$) between upstream and downstream sites (see e.g. S85; and indeed, the derivation given here closely follows S85, including nomenclature).

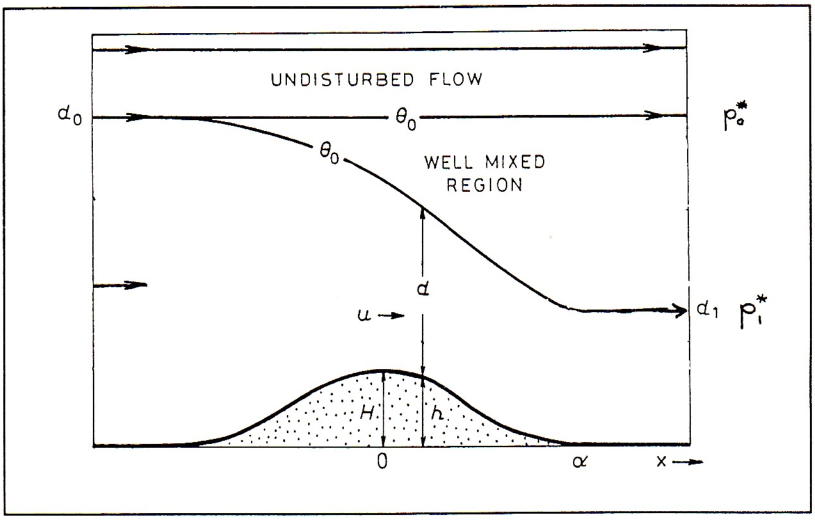

Fig. C1 Schematic diagram of homogeneous fluid crossing a two-dimensional obstacle.

As in Fig. C1, consider a deep homogenous layer of density ρ_c overlaying a relatively shallow homogenous layer of density, ρ. The term *PF* (horizontal pressure force per unit width normal to the flow) at upstream site 0 in the active layer is

$$PF_0 = p_0{*}\,d_0 = \frac{1}{2}\rho g d_0^2. \tag{C1}$$

Similarly, at a lee side site

$$PF_1 = p_1{*}\,\mathrm{d}_1 + \frac{1}{2}\rho g d_1^2 \tag{C2}$$

where (from the hydrostatic equation) we have

$$p_1^* = p_0^* + \rho_c g\,(d_0 - d_1)\,. \tag{C3}$$

The momentum flux, *MF*, at each site is

$$MF_0 = \rho u_0^2 d_0 \qquad \text{(C4)}$$

$$MF_1 = \rho u_1^2 d_1$$

Finally, the drag, *r*, is calculated from

$$r = (PF_0 - PF_1 - \Gamma) + (MF_0 - MF_1) \qquad \text{(C5)}$$

where Γ denotes the pressure force on the layer from the mixed region, and is given by

$$\Gamma = p_0^* \ (d_0 - d_1) + \frac{1}{2}\rho_c g (d_0 - d_1)^2 \ . \qquad \text{(C6)}$$

Now remembering that

$$\hat{s} = \frac{d_0}{d_1} = \frac{u_1}{u_0} \qquad \text{(C7)}$$

and that

$$g' = g\frac{\rho_c - \rho}{\rho} \qquad \text{(C8)}$$

$$= g\frac{\theta - \theta_c}{\theta_c}$$

then, after some manipulation, C5 reduces to

$$r = \frac{1}{2} g (\rho - \rho_c) \ (d_0^2 - d_1^2) \ - \rho u_0^2 d_0 (\hat{s} - 1) \qquad \text{(C9)}$$

$$r = \frac{1}{2} \ g' \rho \, (d_0^2 - d_1^2) \ - \rho u_0^2 d_0 (\hat{s} - 1) \, .$$

Now if we define non-dimensionalised drag as

$$\hat{r} = r\frac{N_0^2}{\rho u_0^3} \qquad \text{(C10)}$$

it follows that

$$\hat{r} = \frac{2}{\pi^2}\hat{d}_0^3 (1 - \frac{1}{\hat{s}^2}) + \hat{d}_0 (\hat{s} - 1) \qquad \text{(C11)}$$

represents the non-dimensional drag for continuously stratified flow over an obstacle. Since $\hat{s}$ and $\hat{d}_0$ are functions of $\hat{H}$, then so too is $\hat{r}$.

PUBLICATIONS

GRACE, W.J. 1991. Hydraulic jump in a fog bank. *Aust. Met. Mag. 44,* 205-9.

GRACE, W.J. 1992. Modelling the downslope winds of Adelaide, South Australia. CTAC 91 (*Conf. proc. Computational Techniques and Applications 1991*) (in press).

GRACE, W.J. and HOLTON, I.C. 1990. Hydraulic jump signatures associated with Adelaide downslope winds. *Aust. Met. Mag., 38,* 43-52.

SOFTWARE

Files

1 *GULLY.EXE*

2 *EGAVGA.BGI*

Place both files into a common directory, A:, say. Then type 'GULLY' and enter. The program is then reasonably self-evident. Use the ESC key to obtain a menu.

All three publications and a disc containing the software file are in the back-cover jacket.*

---

* Applies to original set of theses copies only. Software and publications are available from the author c/- Bureau of Meteorology, PO Box 421, SA, 5071 or e-mail w.grace@bom.gov.au